2013-06

Method for VAWT placement on a complex building structure

Taylor, Katharin C.

Monterey, California: Naval Postgraduate School

NAVAL POSTGRADUATE SCHOOL

MONTEREY, CALIFORNIA

THESIS

METHOD FOR VAWT PLACEMENT ON A COMPLEX BUILDING STRUCTURE

by

Katharin C. Taylor

June 2013

Thesis Advisor: Anthony J. Gannon
Co-Advisor: Garth V. Hobson

THIS PAGE INTENTIONALLY LEFT BLANK

REPORT DOCUMENTATION PAGE

Form Approved OMB No. 0704-0188

1. AGENCY USE ONLY ***(Leave blank)***	**2. REPORT DATE** June 2013	**3. REPORT TYPE AND DATES COVERED** Master's Thesis

4. TITLE AND SUBTITLE
METHOD FOR VAWT PLACEMENT ON A COMPLEX BUILDING STRUCTURE

5. FUNDING NUMBERS

6. AUTHOR(S) Katharin C. Taylor

7. PERFORMING ORGANIZATION NAME(S) AND ADDRESS(ES)
Naval Postgraduate School
Monterey, CA 93943-5000

8. PERFORMING ORGANIZATION REPORT NUMBER

9. SPONSORING /MONITORING AGENCY NAME(S) AND ADDRESS(ES)
Office of Naval Research (ONR)
875 N Randolph St
Arlington, VA 22217

10. SPONSORING/MONITORING AGENCY REPORT NUMBER

11. SUPPLEMENTARY NOTES The views expressed in this thesis are those of the author and do not reflect the official policy or position of the Department of Defense or the U.S. Government. IRB Protocol number ____N/A____.

12a. DISTRIBUTION / AVAILABILITY STATEMENT
Approved for public release;distribution is unlimited

12b. DISTRIBUTION CODE

13. ABSTRACT (maximum 200 words)

This thesis is part of a larger project that will demonstrate the feasibility of powering a commercially sized 7.5-ton cooling system. Excess cooling will be stored thermally using ice. This system has the potential to be used in military bases to reduce energy costs and fossil fuel consumption. A scaled down version would be suitable for data centers and forward operating bases where the transport of fuel can be costly and dangerous. The system will be built and operated at the Turbopropulsion Laboratory (TPL) of Naval Postgraduate School. This thesis concentrates on the choice and location of wind turbines used to power the cooling system.

A simulation of Building 216, which is the planned site of the cooling system, was performed. A wind flow analysis found that optimum placement of the wind turbines is at the front of the south end of the building. The method for placing the wind turbines is outlined and applicable to other structures. Vertical Axis Wind Turbines (VAWTS) were found to be the most suitable for site location. A transient analysis of the VAWTS was necessary to accurately simulate their performance. This supported the selection of a three-bladed helical VAWT design. Further simulations of wind turbine separation showed some beneficial effects of close spacing.

14. SUBJECT TERMS Commercial cooling system, vertical axis wind turbines, horizontal axis wind turbines, computational fluid dynamics (CFD)	**15. NUMBER OF PAGES** 155
	16. PRICE CODE

17. SECURITY CLASSIFICATION OF REPORT	**18. SECURITY CLASSIFICATION OF THIS PAGE**	**19. SECURITY CLASSIFICATION OF ABSTRACT**	**20. LIMITATION OF ABSTRACT**
Unclassified	Unclassified	Unclassified	UU

NSN 7540-01-280-5500

Standard Form 298 (Rev. 2-89)
Prescribed by ANSI Std. 239-18

THIS PAGE INTENTIONALLY LEFT BLANK

Approved for public release; distribution is unlimited

METHOD FOR VAWT PLACEMENT ON A COMPLEX BUILDING STRUCTURE

Katharin C. Taylor
Ensign, United States Navy
B.S, United States Naval Academy, 2012

Submitted in partial fulfillment of the
requirements for the degree of

MASTER OF SCIENCE IN MECHANICAL ENGINEERING

from the

NAVAL POSTGRADUATE SCHOOL
June 2013

Author: Katharin C. Taylor

Approved by: Anthony J. Gannon, Research Assistant Professor
Thesis Advisor

Garth V. Hobson, Professor
Thesis Co-Advisor

Knox Millsaps
Chair, Department of Aerospace and Mechanical Engineering

THIS PAGE INTENTIONALLY LEFT BLANK

ABSTRACT

This thesis is part of a larger project that will demonstrate the feasibility of powering a commercially sized 7.5-ton cooling system using wind power. Excess cooling will be stored thermally using ice. This system has the potential to be used in military bases and data centers to reduce energy costs and fossil fuel consumption. A scaled down version would be suitable for forward operating bases where the transport of fuel can be costly and dangerous. The system will be built and operated at the Turbopropulsion Laboratory (TPL) of Naval Postgraduate School. This thesis concentrates on the choice and location of wind turbines used to power the cooling system.

A simulation of Building 216, which is the planned site of the cooling system, was performed. A wind flow analysis found that optimum placement of the wind turbines is at the front of the south end of the building. The method for placing the wind turbines is outlined and applicable to other structures. Vertical Axis Wind Turbines (VAWTS) were found to be the most suitable for site location. A transient analysis of the VAWTS was necessary to accurately simulate their performance. This supported the selection of a three-bladed helical VAWT design. Further simulations of wind turbine separation showed some beneficial effects of close spacing.

THIS PAGE INTENTIONALLY LEFT BLANK

TABLE OF CONTENTS

LIST OF FIGURES

LIST OF TABLES

THIS PAGE INTENTIONALLY LEFT BLANK

LIST OF ACRONYMS AND ABBREVIATIONS

TPL	Turbopropulsion Laboratory
NPS	Naval Postgraduate School
HAWT	Horizontal Axis Wind Turbine
VAWT	Vertical Axis Wind Turbine
CFD	Computational Fluid Dynamics
TSR	Tip Speed Ratio
FNMOC	Fleet Numerical Meteorology and Oceanography Center
UGE	Urban Green Energy

THIS PAGE INTENTIONALLY LEFT BLANK

ACKNOWLEDGMENTS

I would like to thank my advisors, Dr. Anthony Gannon and Dr. Garth Hobson, for their guidance and support throughout this thesis. I would like to thank Harriett, an intern at the Turbopropulsion Laboratory, for her guidance on running some of the initial simulations. Additionally, I would like to thank CDR Scott Drayton, who provided insight and guidance throughout the entirety of the thesis. Finally, I would like to thank my sister, Ellie Taylor, for her support.

THIS PAGE INTENTIONALLY LEFT BLANK

I. INTRODUCTION

A. MOTIVATION

The leadership of the United States of America realizes the importance of developing renewable energy for purposes of national security. President Barack Obama has pledged continued support for renewable energy advancement [1]. Additionally, the Navy is determined to power 50% of its shore based installations from renewable energy by the year 2020 [1]. In following with this decision, the Naval Postgraduate School (NPS) is developing a renewable energy facility to support its energy curriculum program. NPS will demonstrate the feasibility of powering a commercially sized 7.5-ton cooling system. Excess cooling will be stored thermally using ice. This application has the potential to be extended to military bases and data centers that have high-energy costs. A scaled down version would be suitable for forward operating bases where the transport of fuel can be costly and dangerous. This thesis focuses on various multidisciplinary aspects of installing wind turbines on existing structures. The wind flow around the structure must be analyzed to determine the location of highest velocity flow, which is the optimum location for the wind turbines. A wind turbine suitable for the site conditions must be selected. It is important to examine how the separation distance between wind turbines affects their performance. Finally, supporting structures for the wind turbines must be designed.

Vertical Axis Wind Turbines (VAWTS), as opposed to Horizontal Axis Wind Turbines (HAWTS), have been selected for the project. The rooftop application was selected to imitate urban locations, where there is limited space for wind turbines. Rooftops are widely applicable for the installation of wind turbines, because this is unused space on existing buildings. Ideally rooftops are thought to be the best locations as there are fewer obstructions further from the ground, resulting in higher wind flow for the wind turbines to extract power. There may be potential for placement on the sides of buildings and surrounding locations, but that was not investigated here.

1. Wind Turbine Designs: Horizontal Axis versus Vertical Axis

The predominant wind turbine designs are horizontal axis wind turbines (HAWTS) and vertical axis wind turbines (VAWTS). HAWTS have an axis of blade rotation perpendicular to the structure and parallel with the ground. Typical HAWT examples of various sizes are shown in Figure 1.

Figure 1. Horizontal axis wind turbines. From [1].

VAWTS have curved or straight blades with an axis of rotation parallel to the structure and perpendicular to the ground. Some typical examples are shown in Figure 2.

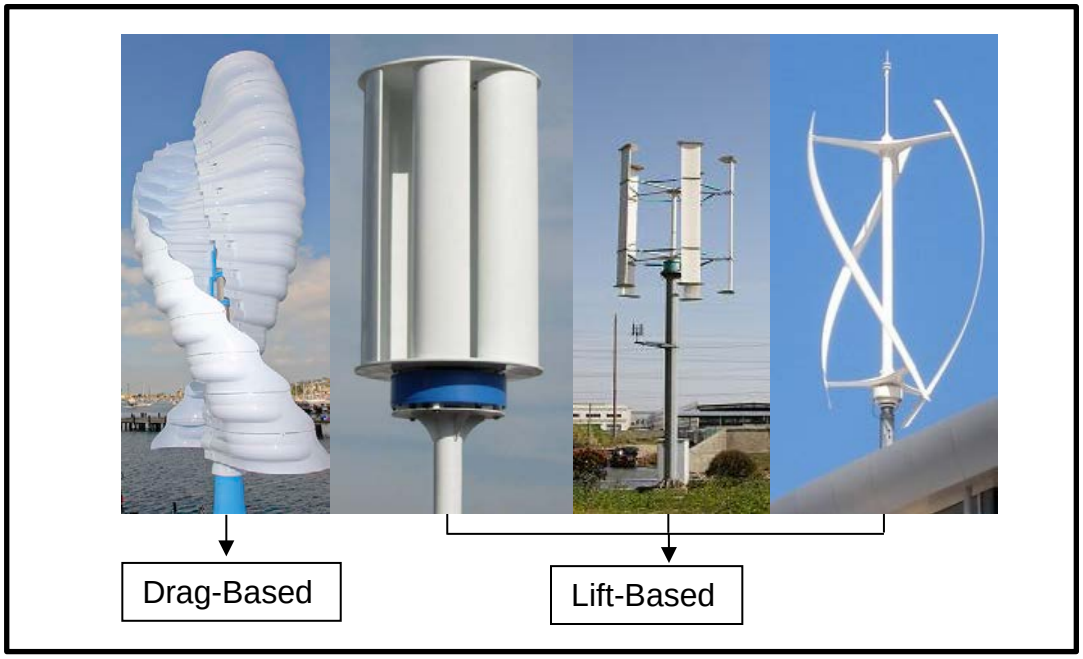

Figure 2. Vertical axis wind turbines. From [3].

There are numerous VAWT designs including lift-based, drag-based, and a combination of lift and drag-based designs. Traditional VAWTS are lift-based designs. In lift-based designs the motion of the turbine rotor is driven by the lift forces on the blades. Conversely, drag-based designs are when the resultant force on the blade is approximately in the same direction as its motions. Examples of each type are noted in Figure 2. Various drag-based and combination drag and lift VAWT designs are currently under development [4].

In comparison with HAWTS, there is little published research regarding the design optimization of VAWTS. The development of VAWTS was initially abandoned because it was thought that they were highly inefficient in comparison with HAWTS. It was originally perceived that VAWTS had structural and bearing loading issues [4]. In the recent past, VAWTS have gained attention because their relatively simple design presents certain advantages. VAWTS are omnidirectional: they can capture wind from all directions without having to change their orientation to face the oncoming wind [4]. VAWTS appear to have little power loss during short wind gusts [2]. This is useful if the wind profile changes from the top to the bottom of the wind turbine, which is likely on a building.

Recent research also suggests that VAWTS have a better response to unsteady and turbulent wind flows where similarly sized HAWTS may not attain similar performance [4]. VAWTS potentially attain higher performance than HAWTS in skewed flow and therefore are better suited for the roof top environment [5]. Additional research indicates VAWTS have lower acoustic emissions, making them even more suited for urban settings [6]. The gearbox and generator of VAWTS can conveniently be located on the ground, unlike HAWTS, so production and service costs are potentially lower [6].

Disadvantage of VAWTS come at the expense of decreased efficiency due to the drag on the blade opposing the wind flow at low tip speed ratios (TSRS). Additionally, there is greater aerodynamic complexity for VAWTS since loading is unsteady and highly nonlinear [6]. Certain VAWT blades are difficult to manufacture [2]. Additionally, intrinsic torque ripple affects the power output and there are challenges associated with poor starting torque from the wind flow at low speeds (the “cut-in” velocity”) [2].

Until recently, simulating these wind turbines has been very difficult to do, because of lack of computing power. Computational VAWT research requires transient simulations, which are computationally intensive. Advanced equipment and software is required and it can take days to solve basic problems. Quite possibly, this is why there is such little design research about VAWTS. With the improvement of computing power, the use of Computation Fluid Dynamics (CFD) has proven a viable means for design investigation. CFD is becoming more cost effective than other testing methods. Typical methods for testing the performance of wind turbines include wind tunnel measurements and analytical methods, such as the vorticity transport model [7]. Wind tunnel testing can be difficult to conduct, because it requires large wind tunnels. Modern CFD packages are relatively simple to use and are becoming ever more accurate. CFD has become more popular for improving engineering models and verifying final designs [4]. CFD is also very good at comparing design changes.

2. Previous Research

Commercial cooling systems powered by rooftop wind turbines have never been proven. A master’s thesis from the University of Colorado in the 1970’s investigated a

small-scale wind powered cooling system intended for use in underdeveloped villages [8]. The concept, while appearing sound, has lain idle until now.

The installation of vertical axis wind turbines on a roof top building was investigated at the University of Florence in Florence, Italy [5]. The k-epsilon model was used for their CFD simulations. They determined that the k-epsilon model most closely matched wind tunnel data. Additionally, they found that VAWTS have better performance than HAWTS in skewed flow and therefore are better suited for the roof top environment. The "performance improvement due to the effects of skewed flow can also lead to a reduction in the minimum cut-in speed, thus extending the operating range of the rotor and increasing the energy harvesting for the low-wind conditions" [5]. The study determined that the slope angle of the building influences the performance of the turbines: small inclination angles of approximately 8-10 degrees improve the flow conditions on the roof top. This is significant as it means small changes to a roof may yield significant improvements to the wind flow and increase the power output of the wind turbines.

B. PURPOSE

The purpose of this thesis focuses on the application of the vertical axis wind turbines onto the rooftop of the Turbopropulsion Laboratory (TPL). Wind power is a commercialized and developed renewable energy technology. Wind turbines harness the kinetic energy from the wind and convert it into electrical power. A limitation of wind turbines is that they produce intermittent power. The power output of wind turbines is primarily influenced by the amount of available wind, the effect of wind gusts, and the distance of the wind turbines from the ground [2].

C. OBJECTIVE

The objectives of this thesis are:

1. To find the optimum placement of the wind turbines.

2. To determine the best wind turbines for the application.

3. What is the optimum number of blades of a VAWT?

4. What should be the design of the beam support structures for the wind turbines?

5. How does the separation distance between wind turbines affect their performance?

A numerical CFD approach was the primary means of investigation to find the optimum solution to these problems. CFD was used to perform a wind flow analysis around the TPL, research the optimum number of blades of a VAWT, and investigate how the separation distance of wind turbines affects their performance. The design of the beam support structures was done using a classical approach for the initial phase and was verified using a Finite Element Analysis (FEA). The thesis begins with a wind flow analysis, progresses to a wind turbine design investigation, discusses the design of the supporting beams, and finishes with an investigation concerning the spacing between wind turbines.

II. WIND FLOW ANALYSIS

A. MOTIVATION

Wind turbines perform better in locations with high velocity wind flow. High velocity wind has more kinetic energy for wind turbines to extract and convert into unregulated AC electrical power. The roof of the TPL is a complex building shape: its shape obstructs wind flow in certain areas. This makes it difficult to determine the optimum location to place the wind turbines. The goal of the wind flow analysis was to determine the best location to place the wind turbines on the roof of the TPL. This approach is applicable to any building.

B. OVERVIEW

Weather data from Fleet Numerical Meteorology and Oceanography Center (FNMOC) was used to determine the velocity and orientation of prevailing winds at the TPL. CFD simulations were used to investigate the wind flow over the building. The simulations provided insight into the locations of unobstructed, higher velocity wind flow. From these results, in addition to practical space requirements and site limitations, a specific location was selected for the placement of the VAWTS.

Description of Building 216: A complex Building Structure

Building 216 at the NPS TPL is the location of the renewable energy research facility. It is located inside the grounds of the Monterey Pines Golf Course and it is northwest of the Monterey airport. The elevation is about 257 feet and it lies approximately one mile from the coast [9].

Figure 3 is an aerial image of Building 216. Building 216 was an engine testing laboratory made from 15-18 inches of solid concrete walls. The roof is flat. It has ample space so practical adjustments can be made for the installation of the wind turbines. With a few rearrangements, there is sufficient space to the south of the building for the cooling system and chiller units. Additionally, there is ample space for the possible addition of more wind turbines and solar panels in future years.

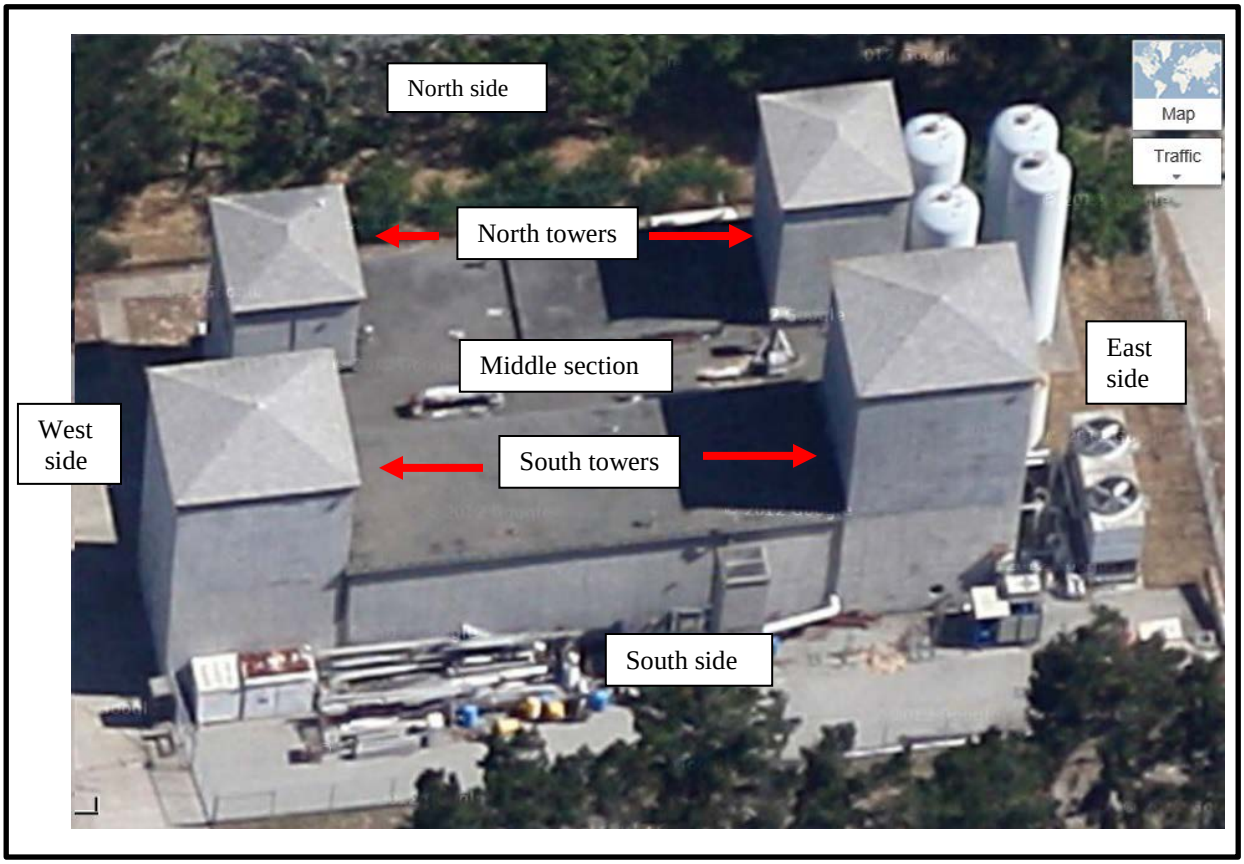

Figure 3. Aerial image of Building 216. After [10].

Figure 4 shows possible locations of the various energy facility components. As noted, the roof of Building 216 is a relatively complex shape when compared to open ground: the corners of the building have second story "towers," which obstruct the wind flow. Although the roof is flat, the south end of the building is about 5 feet higher in elevation then the north side. This could potentially increase the wind velocity received by the south end of the building due to a pressure buildup from the fluid flow being compressed to a smaller area as it flows over the ledge. However, it makes construction on the roof slightly more challenging. Of additional importance, the wind turbines must be placed below the elevation of the highest second story tower, which is about 8.84 m (29 ft.) from the base of the flat section of the roof. Building 216 is located on a flight path to the Monterey airport.

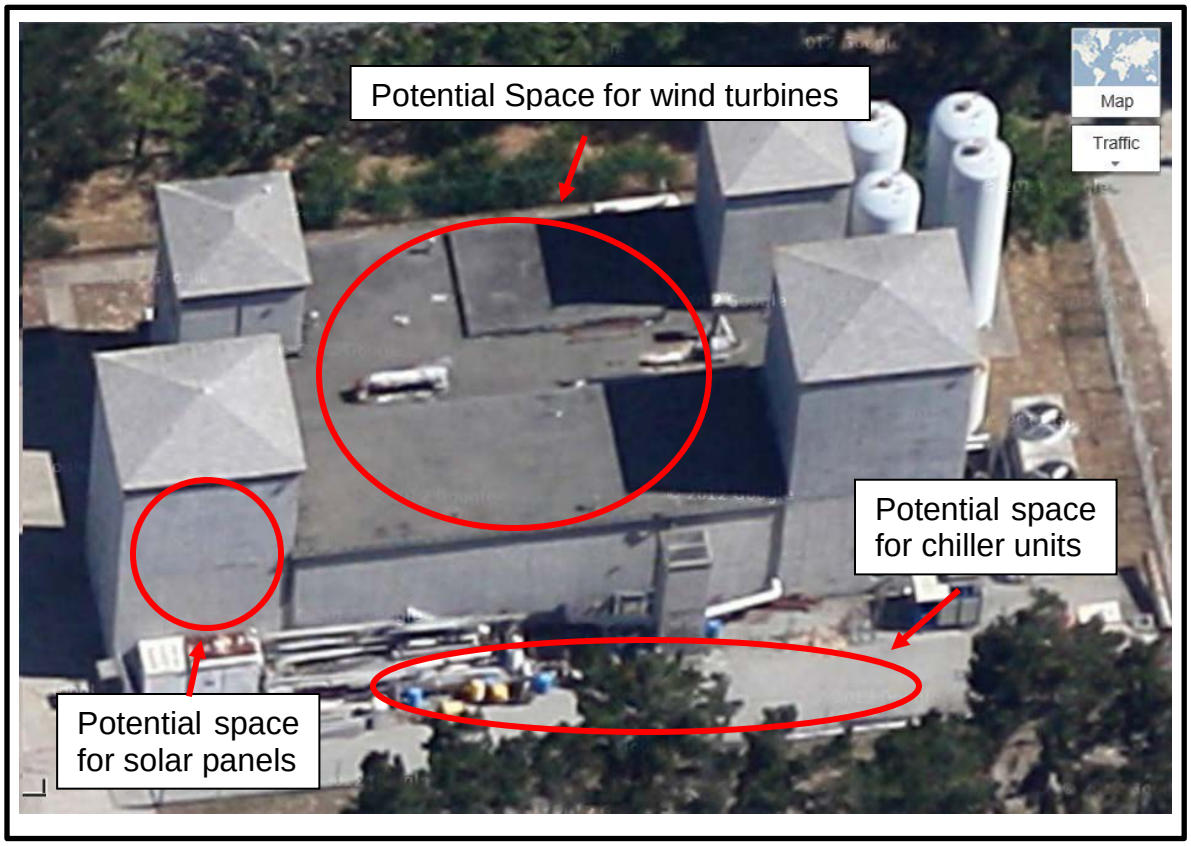

Figure 4. Potential locations for components of Renewable Energy Facility. After [10].

C. WIND FLOW DATA FOR MONTEREY

Data from Fleet Numerical Meteorology and Oceanography Center (FNMOC) was used to determine the direction and velocity of the prevailing wind. FNMOC has years of recorded data from a measuring station at the Monterey Peninsula Airport, which is located less than a mile from Building 216. FNMOC provided 282,000 observations of wind speed and direction in a spreadsheet. A sample of these observations is provided in Appendix A.

Figure 5 illustrates the annual wind rose for Monterey from 1980 until 2012, courtesy of FNMOC [11]. According to the data in Appendix A and the wind rose in Figure 5, prevailing winds come from the west at an average wind speed of 5.77 mph or 2.58 m/s. The majority of wind speeds range from 2 m/s-8 m/s. The median wind speed is 6.00 mph or 2.68 m/s.

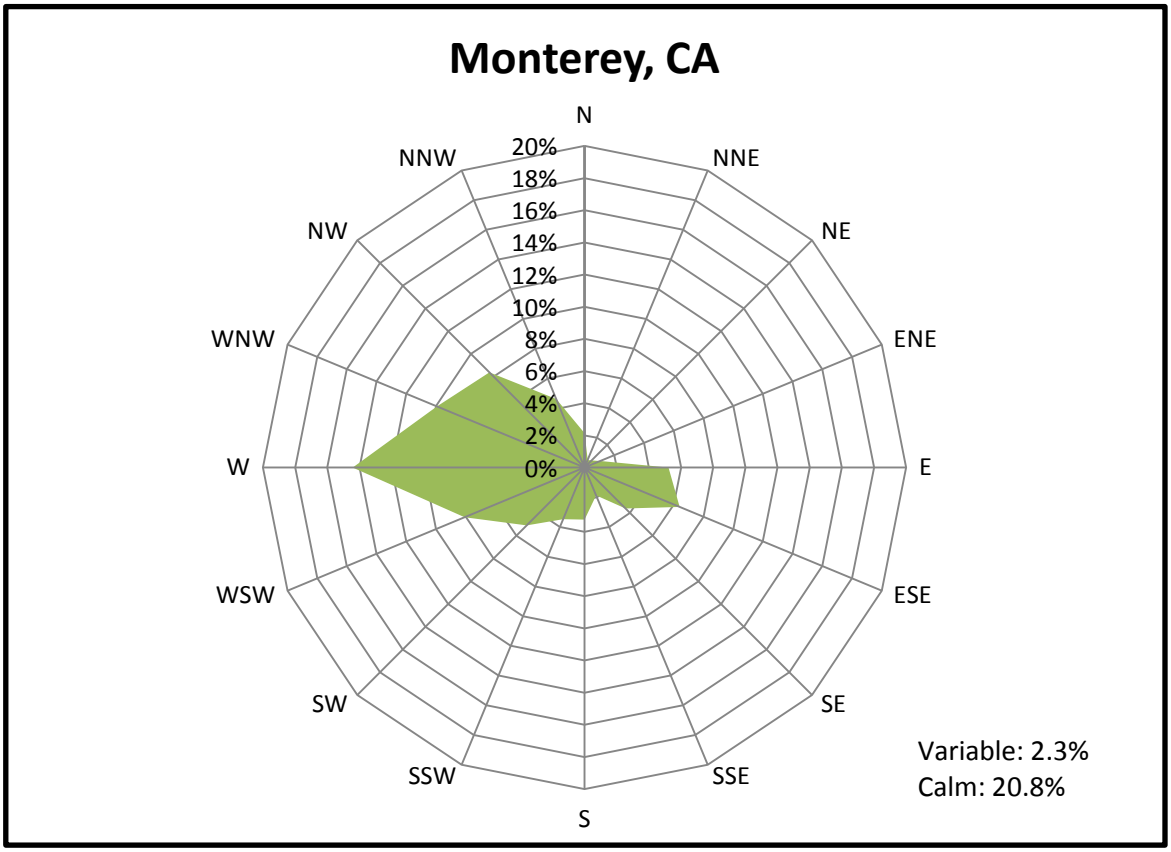

Figure 5. Wind Rose data for Monterey, CA. From [11].

Figure 6 illustrates a diagram of the prevailing wind flow across Building 216. The wind velocity will be reduced on the west side of the roof, since the prevailing wind hits the west towers almost directly. The direction the wind hits Building 216 is not ideal. However, existing structures may not always have the ideal orientation to prevailing winds.

Figure 6. Prevailing wind direction across Building 216. After [10].

Orientation of the Monterey Airport Runway

The orientation of the airport runway in relation to Building 216 provided guidance about the direction of the prevailing wind. Airport runways are designed so that they are oriented parallel to the direction of predominant wind flow.

By comparing the angle of orientation of the runway to Building 216, it was affirmed that the prevailing wind direction is from the west at about a 30 degree angle from the horizontal orientation of Building 216, as illustrated in Figure 7. It was necessary to determine this 30 degree angle to use as an appropriate orientation for the control volume surrounding Building 216 for the CFD simulations.

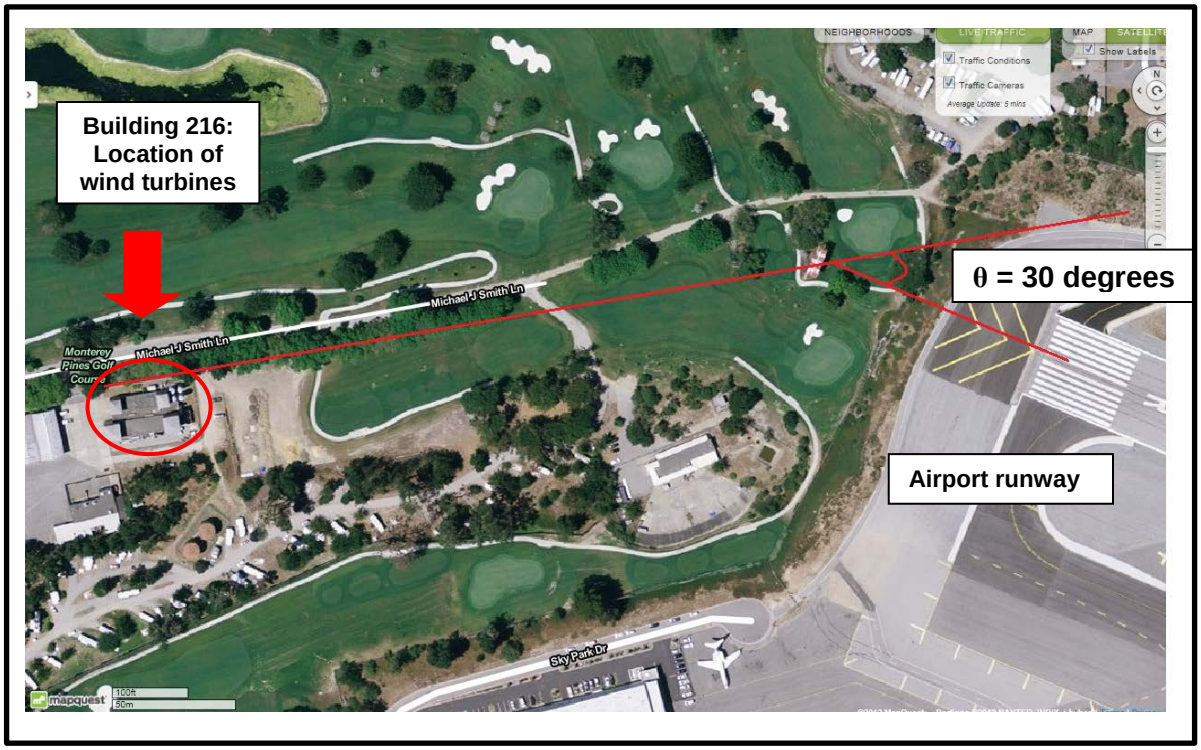

Figure 7. Orientation of the Monterey Airport runway in relation to Building 216. After [10].

D. DESCRIPTION OF CFD SIMULATION

ANSYS CFX was used for the CFD simulations. A design of Building 216 was created in Solidworks. Additionally, a control volume was created and oriented at a 30 degree angle from Building 216 to represent the direction of the prevailing wind. The control volume was approximately three times the length of Building 216 on either side. The model was imported into ANSYS CFX for analysis. Figure 8 displays the Solidworks model of Building 216 and the control volume inserted into ANSYS CFX.

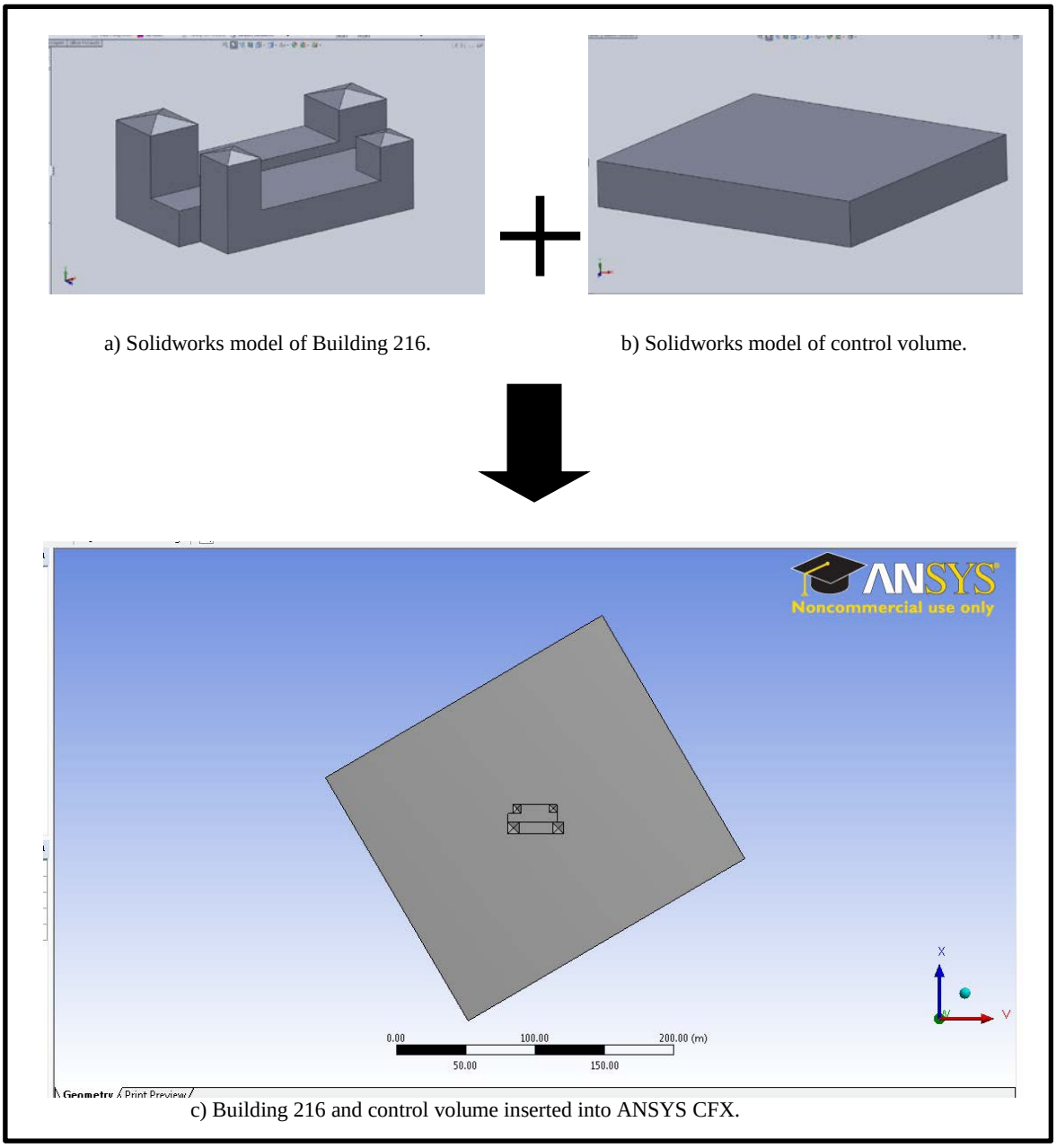

a) Solidworks model of Building 216.

b) Solidworks model of control volume.

c) Building 216 and control volume inserted into ANSYS CFX.

Figure 8. Solidworks model of Building 216 and the control volume inserted into ANSYS CFX.

Using ANSYS CFX, an appropriate mesh was created to ensure accurate results. Appendix B shows the mesh details. The mesh number of nodes was approximately 170,000 and number of elements was approximately 580,000. The mesh is displayed in Figure 9.

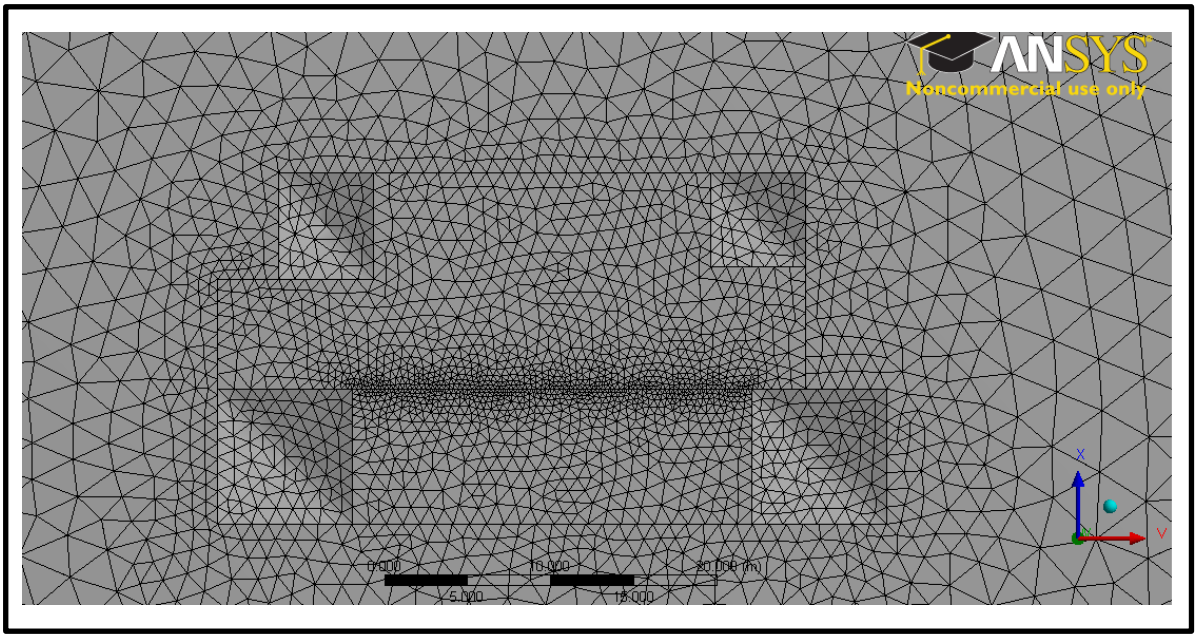

Figure 9. Mesh for ANSYS CFX analysis.

A steady-state simulation was performed assuming that the air was an ideal gas. Figure 10 shows the inlet and outlet boundary conditions.

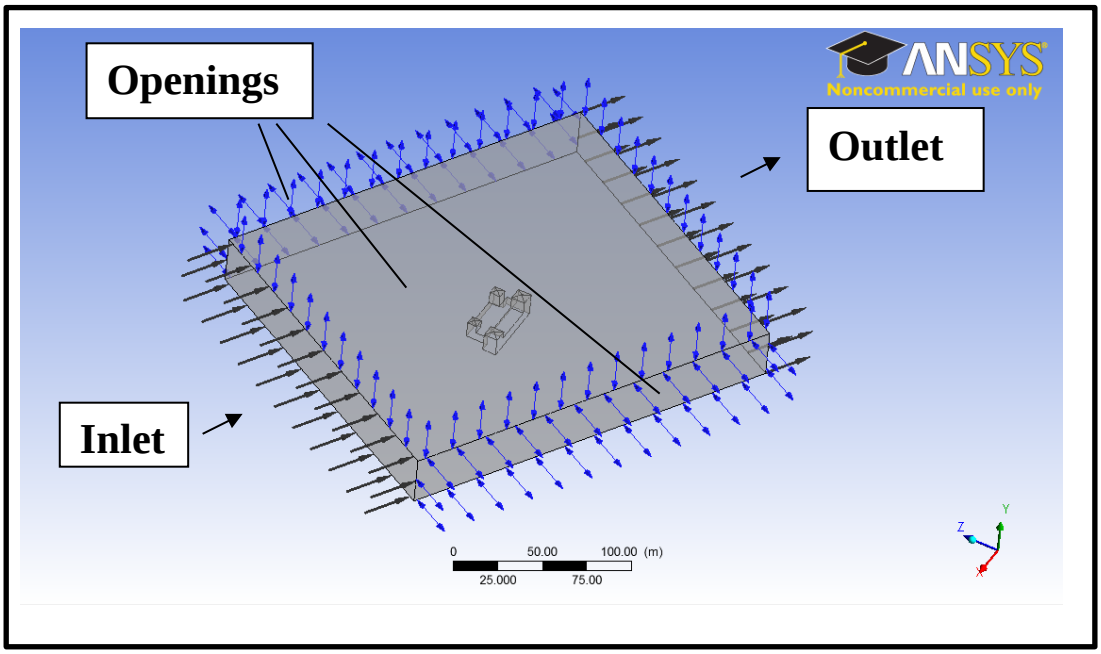

Figure 10. Set-up in ANSYS CFX.

The sides and top of the boundary were defined as openings, where air could enter and exit. From the FNMOC data, the median wind velocity in Monterey is 2.68 m/s with the majority of wind speeds ranging from 2m/s to 8 m/s. For this reason, a series of simulations were conducted where the "inlet" wind velocity was 3 m/s, 4 m/s, and 5 m/s. The results presented are for the 4 m/s simulations, which is just above the typical cut-in speed for most wind turbines. The numerical model settings specific to CFX are displayed in Table 1.

Target Final Residual	0.00001	
Algorithm	Steady State	
Boundary Conditions	Top,Bottom,Sides	Opening: Entrainment
	Inlet	Air Ideal Gas, Velocity: 3-5 m/s
	Outlet	Relative Pressure: 0 kPa

Table 1. Numerical Model Settings for Wind Flow Analysis.

Complete descriptions of the ANSYS CFX specifications are listed in Appendix C.

E. RESULTS OF CFD SIMULATION

Building 216 presents difficulties for the placement of the wind turbines, because of its complex shape. The goal is to place the wind turbines at the location of highest wind velocity where they are most likely to be over their cut-in speed, which for most wind turbines lies somewhere between 3 m/s and 4 m/s. Figure 11 illustrates velocity vectors across the southern roof of Building 216.

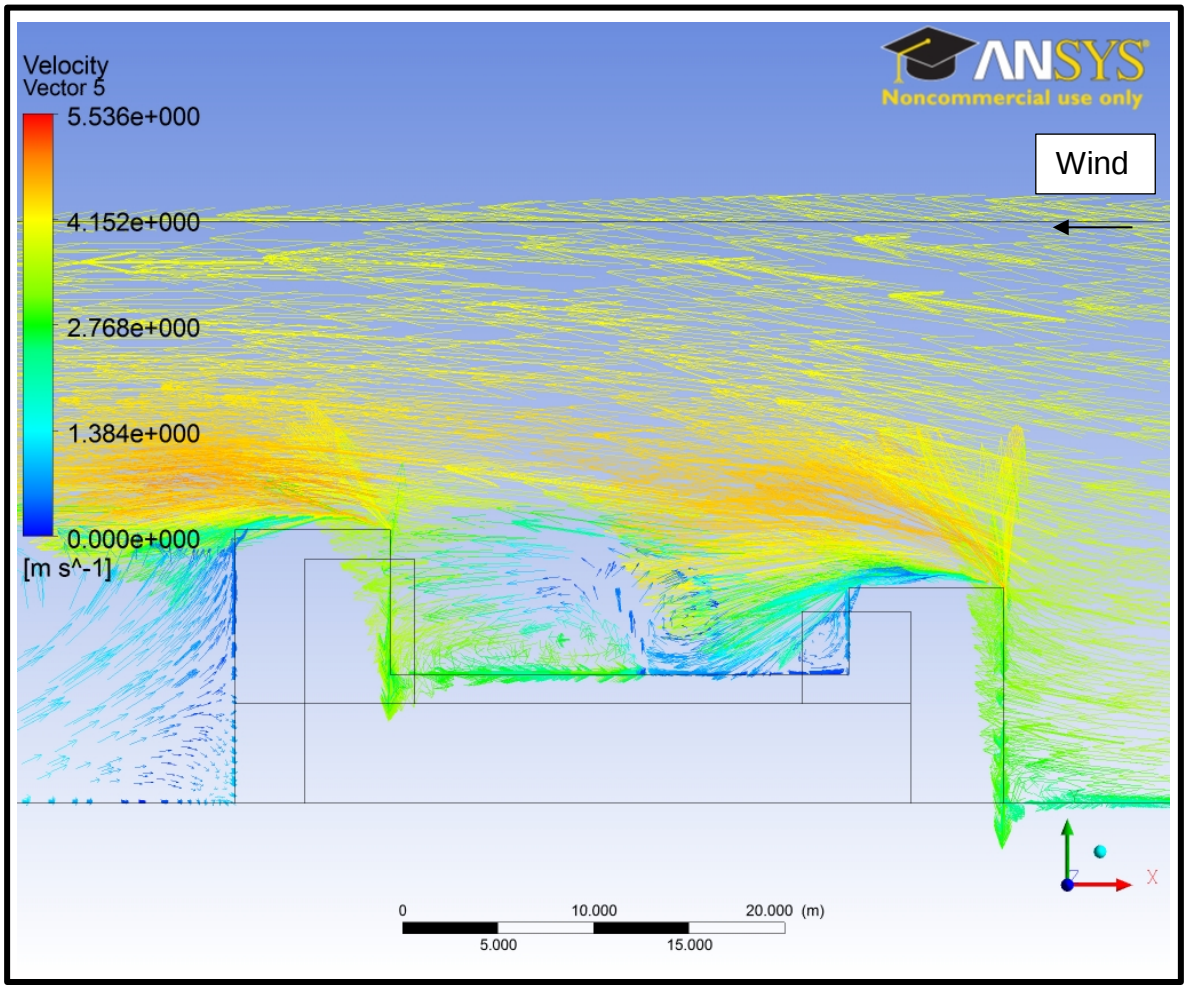

Figure 11. Velocity streamlines across Building 216.

Results affirm that the dominant wind flow hits the second story towers at an angle which heavily obstructs the wind flow, creating an area of nearly zero velocity adjacent to the towers. Average wind flows from the west present a significant challenge to achieving high velocities on the roof. Additionally, flat roofing is not optimal for fluid flow: the airflow is stopped and must recirculate around the edges. The edges cause the fluid flow to separate from the roof early on, leading to undesirable low velocity air flow.

Using ANSYS CFX, a series of velocity plans were taken across Building 216 to determine the areas of low velocity wind flow. The inlet wind speed for all velocity planes depicted is 4m/s, which is a reasonable expectation for wind conditions at the location and above the cut-in speed of the wind turbines. Figure 12 displays a series of

velocity planes across Building 216 labeled A-D. The velocity planes in Figure 12 are placed to effectively illustrate the fluid flow characteristics around the building.

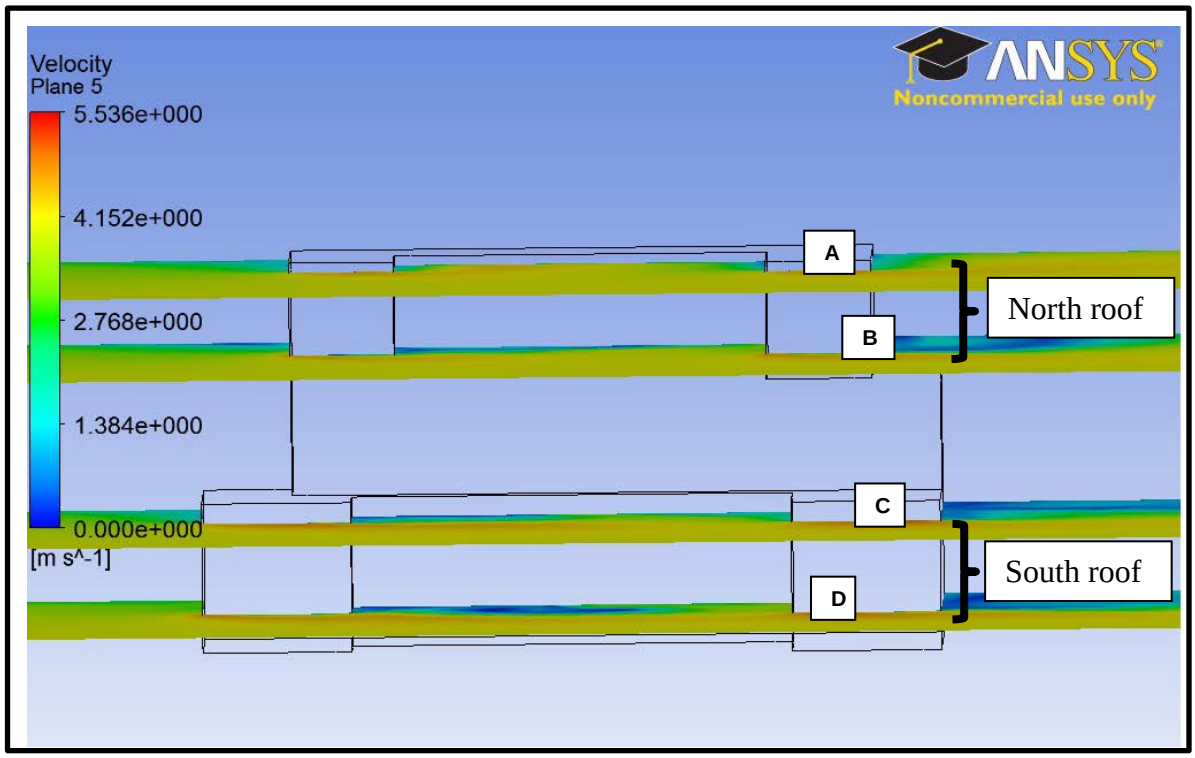

Figure 12. Velocity planes across Building 216 in ANSYS CFX.

Figure 13 displays the wind flow across plane "A", which is at the northern edge of the north roof. It is the least obstructed area of flow across the building. The flow velocity increases as it travels over the roof of the second story levels. The wind reaches almost zero velocity in the corners of the roof adjacent to the second story levels.

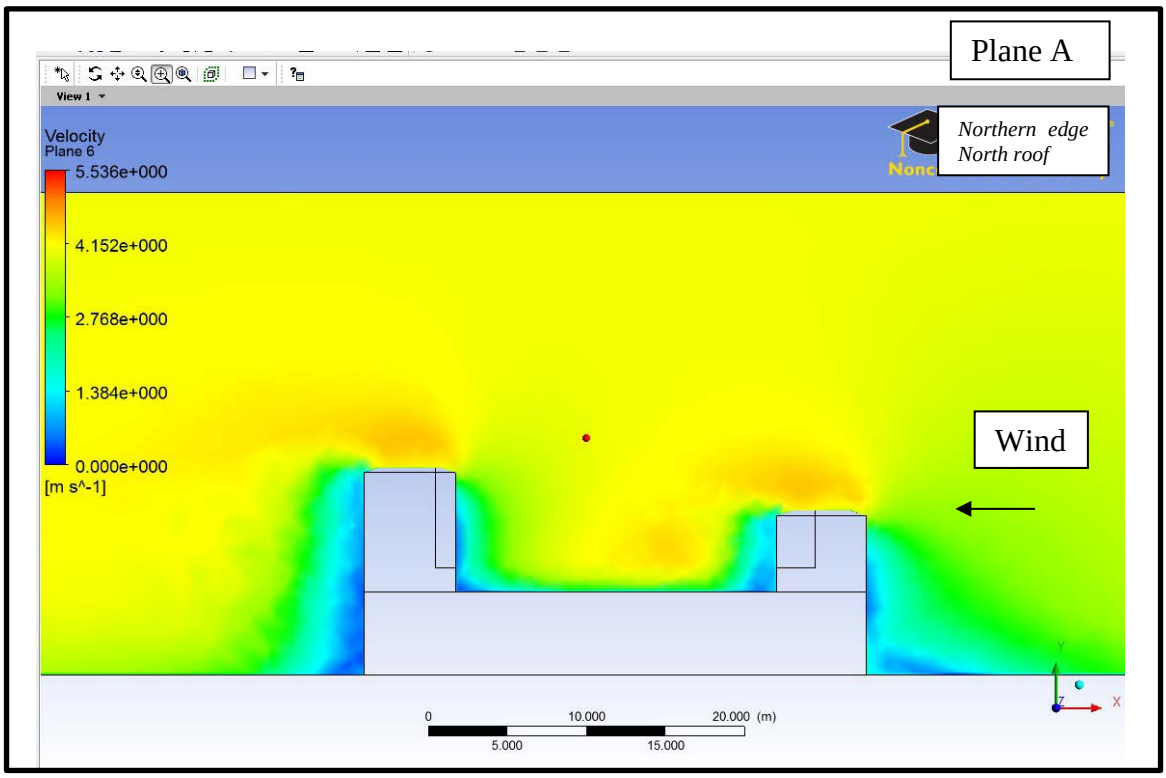

Figure 13. Velocity Plane "A" located at northern edge of Building 216.

Figure 14 depicts the differences in the wind flow on the southern edge of the north roof, in velocity plane "B." Velocity plane "B" demonstrates that the wind flow is more obstructed. Intuitively this makes sense, because the second story towers are a greater obstacle for the wind based on the angle of attack of the wind. A suitable location for the wind turbines according to Figure 14 is on the left hand side of the roof away from the low velocity flow on the right hand side.

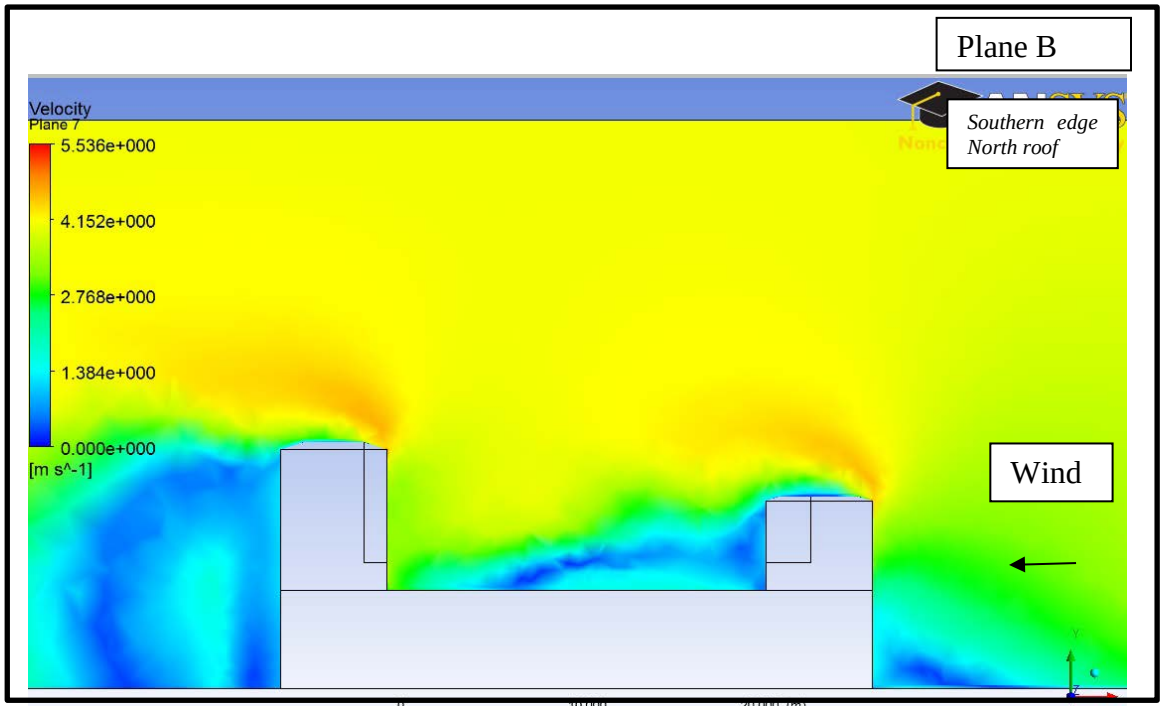

Figure 14. Velocity Plane B.

The wind flow on the north side of the building is higher in velocity then the south side. Figure 15 illustrates the velocity planes on the south roof, which are denoted as velocity planes “C” and “D” from Figure 10. Comparison between Figures 15 (a) and (b) illustrate that the wind flow is more obstructed further south, where the second story towers have a greater effect on the wind. Figure 15 (a) displays a large area on the right hand side of the roof with low wind velocity. However, on the left hand side there is an area with higher velocity wind flow. The left hand side could be a potential location for the wind turbines. Figure 15 (b) is on the southern edge. It illustrates a complex wind flow profile and larger area of low velocity wind flow extending 3/4th of the way along the distance of the roof.

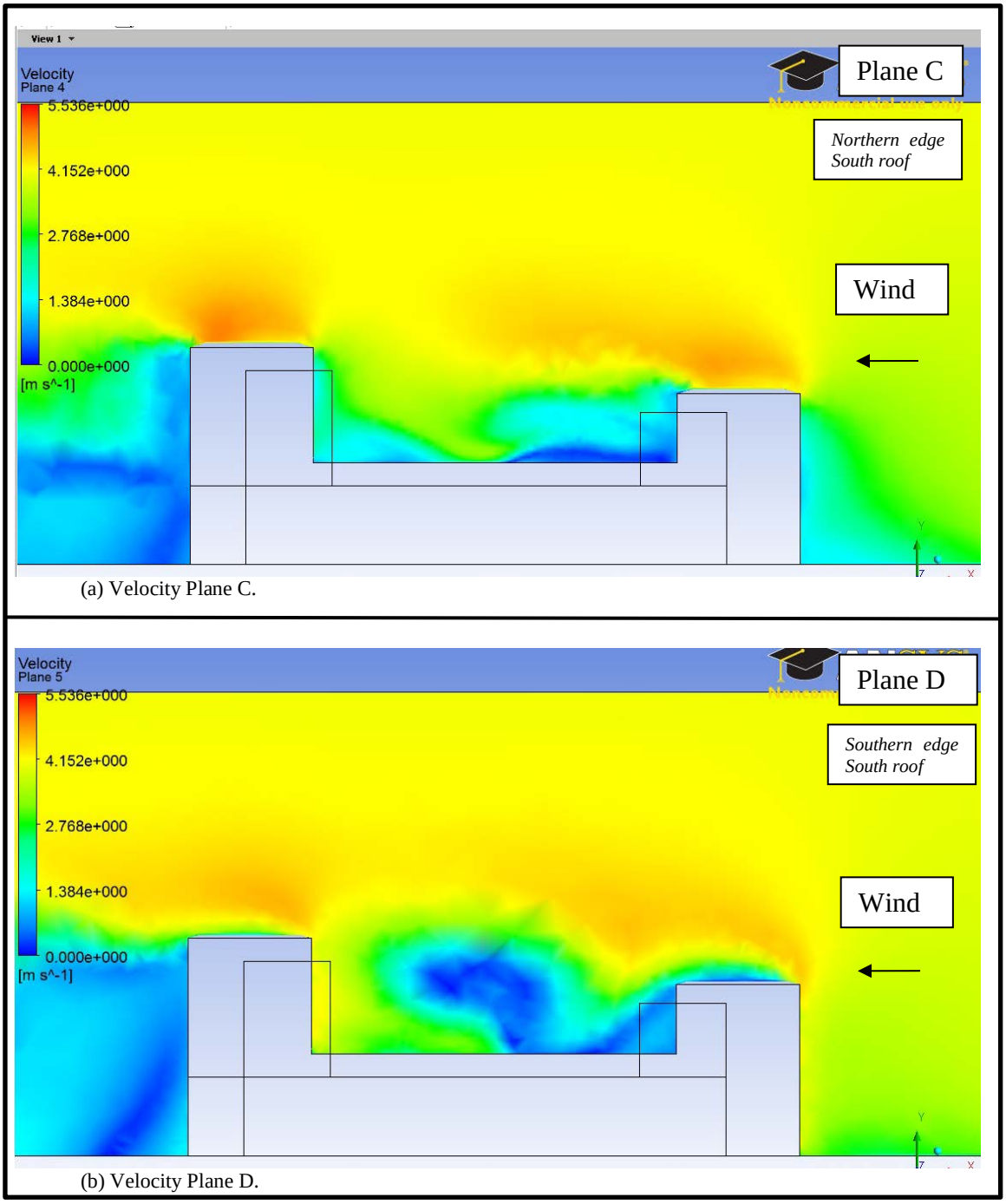

(a) Velocity Plane C.

(b) Velocity Plane D.

Figure 15. Velocity planes at south end of building.

A summary of the findings from the velocity planes is illustrated on an aerial view of Building 216 in Figure 16. Note that the reference frame for the direction of prevailing wind has reversed: in Figure 16 the wind approaches from the left hand side of the figure, while in Figures 13-15 the wind approaches from the right side of the figure.

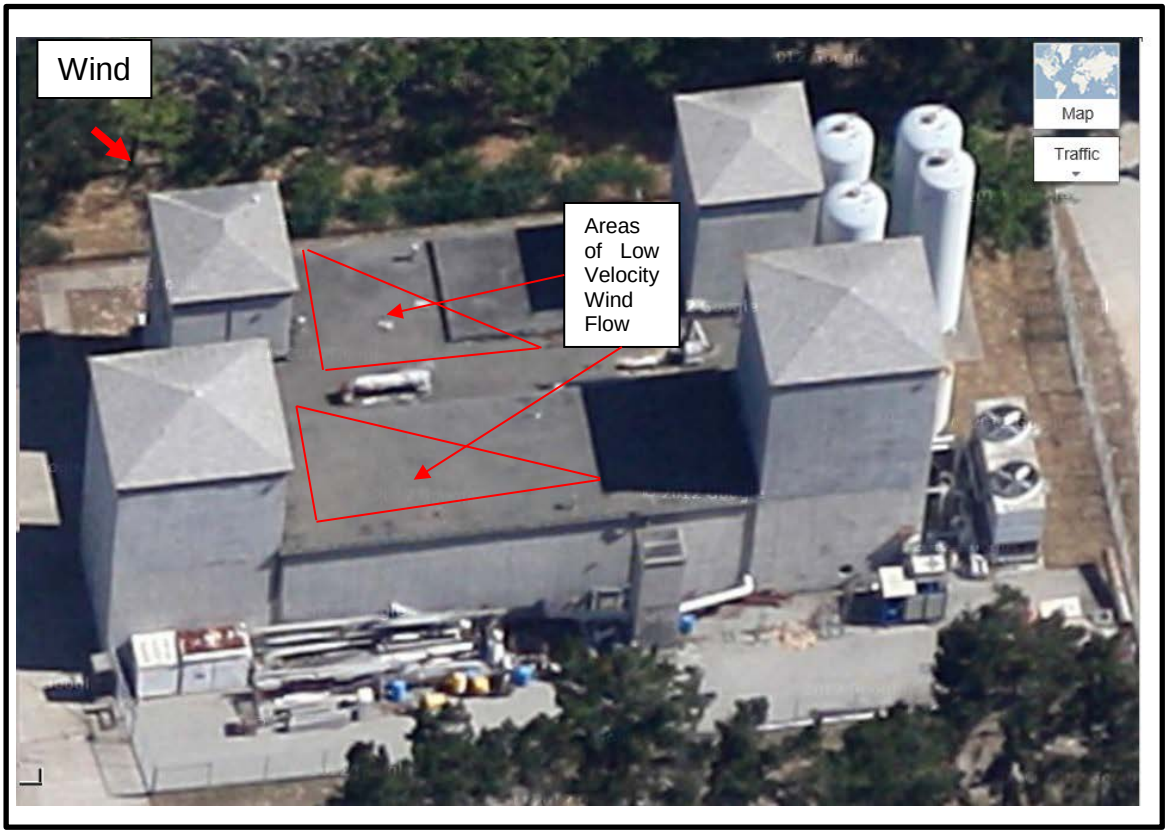

Figure 16. Areas of low velocity wind flow on roof of Building 216. After [10].

To summarize the findings of the wind flow analysis across Building 216, the wind flow is significantly impeded by the presence of the second story towers. The areas of low velocity wind flow make physical sense based off the wind's angle of attack on the towers. Figures 13 and 14 indicate that the highest velocity wind flow is on the north roof of the building. However, construction cannot be completed on the north roof. The north roof is physically restricted by various intakes and a removable slab. The slab is part of an engine test cell inside Building 216. There is more ground-level space for the support structures and cooling systems adjacent to the south roof. Wind flow is of high importance for the placement of the wind turbines, but other factors must also be taken into consideration. Although the north roof appears to have better wind flow, the south roof is the best option for the placement of the wind turbines due to spacing and

installation considerations. Figure 17 illustrates the selected location for the wind turbines on the south roof of Building 216.

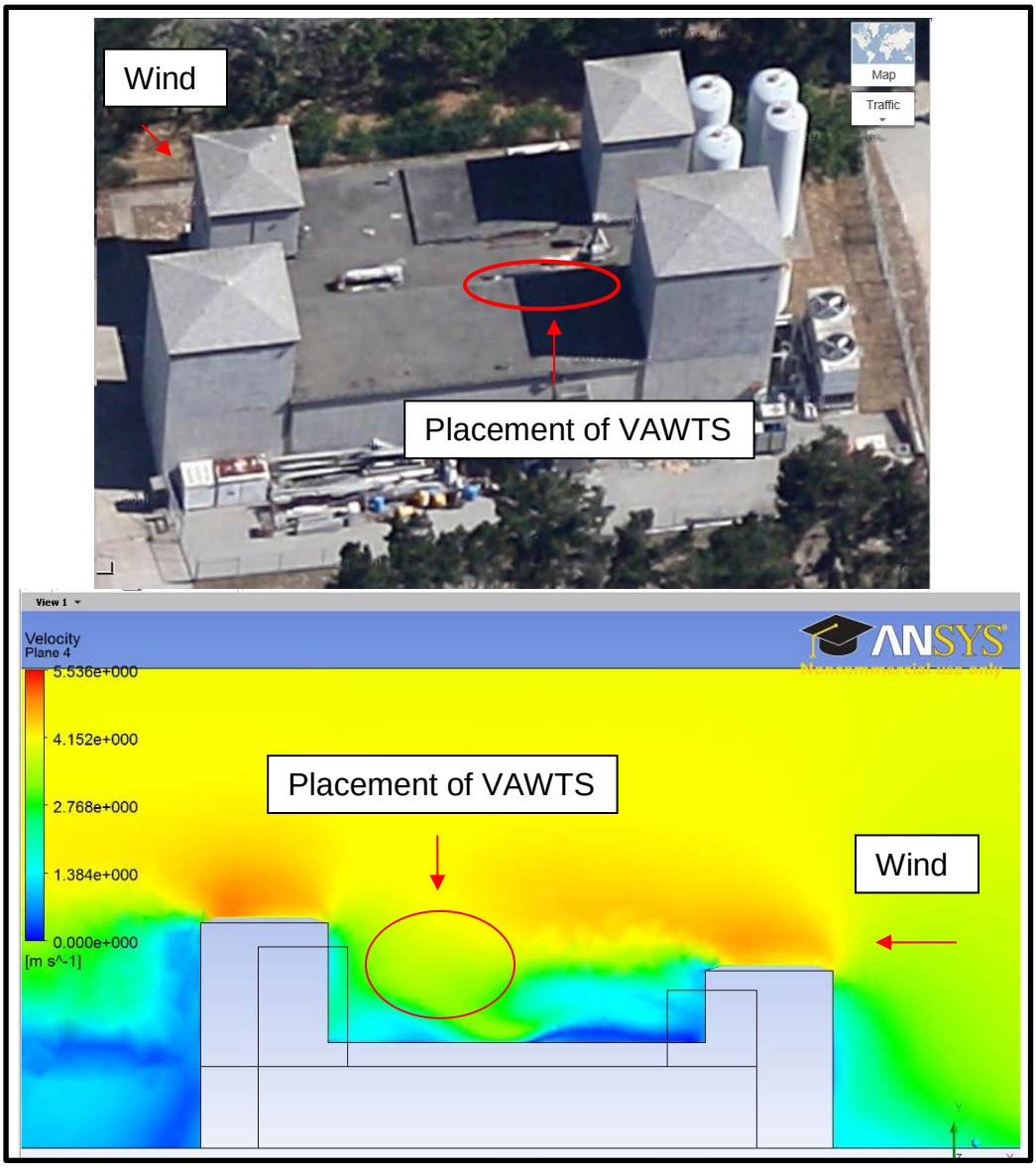

Figure 17. Selected site location for placement of VAWTS. After [10].

Implication of wind profile results on the selection of the wind turbines

As mentioned in the introduction, previous research suggests the use of VAWTS is best for rooftop applications, because VAWTS are omni-directional and they can capture skewed wind flow [5]. The wind profile supports the decision to use VAWTS for the NPS renewable energy facility.

F. SUMMARY OF GENERAL APPROACH

The general approach for a wind flow analysis is summarized below. This process is applicable to any building.

- Make an approximate Solidworks model of the building.
- Find representative wind data from the region.
- Analyze the Solidworks model using numerical CFD simulations.
- Determine the areas of high velocity wind flow.
- Examine the areas of high velocity wind. Ensure there are no physical or other restrictions at those locations.
- Determine the best location for the wind turbines.

THIS PAGE INTENTIONALLY LEFT BLANK

III. WIND TURBINE DESIGN ANALYSIS

A. MOTIVATION FOR VAWT DESIGN INVESTIGATION

Compared with HAWTS, there is little published research about the optimization of VAWTS. There are many VAWT designs but again there appear to be few publications comparing their performance and efficiency. The purpose of the design investigation is to evaluate different VAWT designs and research how their performance is affected by close spacing. It is advantageous to place as many wind turbines as close together as possible, because space is often limited. These results helped justify the selection and positioning of the VAWTS for the NPS renewable energy facility. Ultimately, the future goal of the NPS renewable energy facility is to design and manufacture its own VAWTS. For this reason, a significant portion of this thesis is devoted to optimizing VAWTS.

B. VAWT BLADE NUMBER OPTIMIZATION

1. Motivation

Conventional VAWTS have three blades. Speculation suggests manufacturers initially constructed VAWTS with three blades because the most efficient HAWTS have three blades. Three blades are structurally balanced. However, HAWTS and VAWTS are structurally different: the most efficient design of one may not be the most efficient design of the other. The research question to be addressed is what is the optimum number of blades of a VAWT?

2. Overview

VAWTS with two, three, six, and eighteen blades were analyzed in the CFD program, ANSYS CFX. The wind velocity was held constant while the tip speed ratio (TSR) varied. Transient simulations were performed to capture the blade effects at different moments in time. The simulations were 2-D. The torque on the blades was calculated. Results displayed that the torque was highly alternating. The power coefficient was calculated and plotted against the TSR. This illustrated the performance

of each wind turbine design. These results, as well as availability limitations, supported the selection of a three-bladed helically shaped VAWT for the site location.

3. Methodology

A cross-section of a VAWT was created in Solidworks. The wind turbine thickness was 10 cm. The thickness was small so that 2-D simulations were possible. Figure 18 illustrates a 3-D wind turbine represented as a 2-D simulated slice.

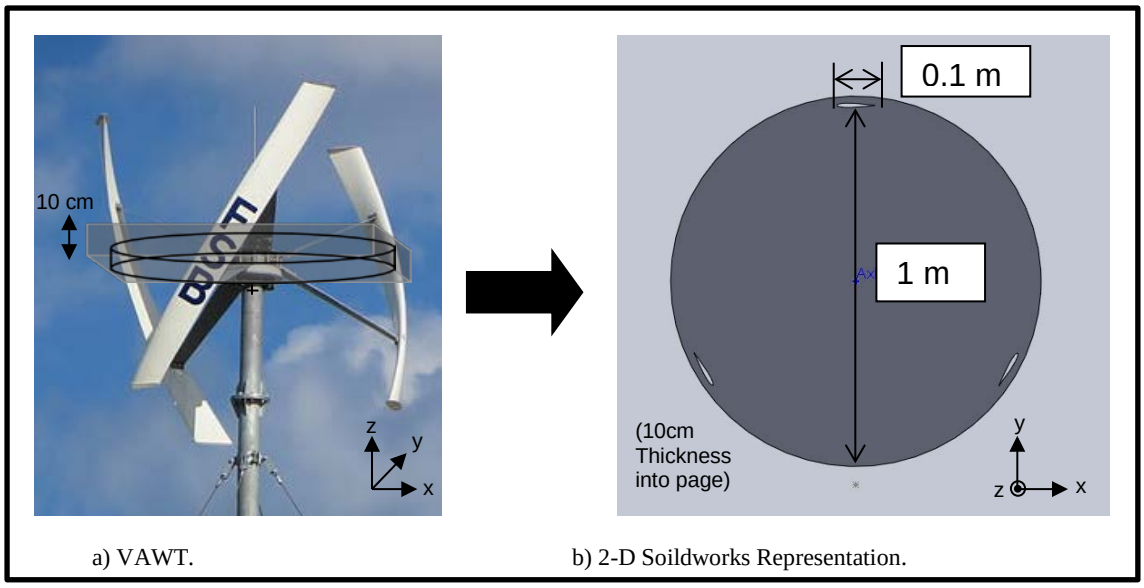

a) VAWT. b) 2-D Soildworks Representation.

Figure 18. Two-dimensional Wind Turbine representation. After [3].

NACA0012 airfoil was used as the blade shape. NACA0012 is a standard and widely used airfoil. The use of the airfoil was instructed in private communication [12]. NACA0012 airfoils have a maximum thickness of 12% at 30% chord [13]. Figure 19 displays the airfoil.

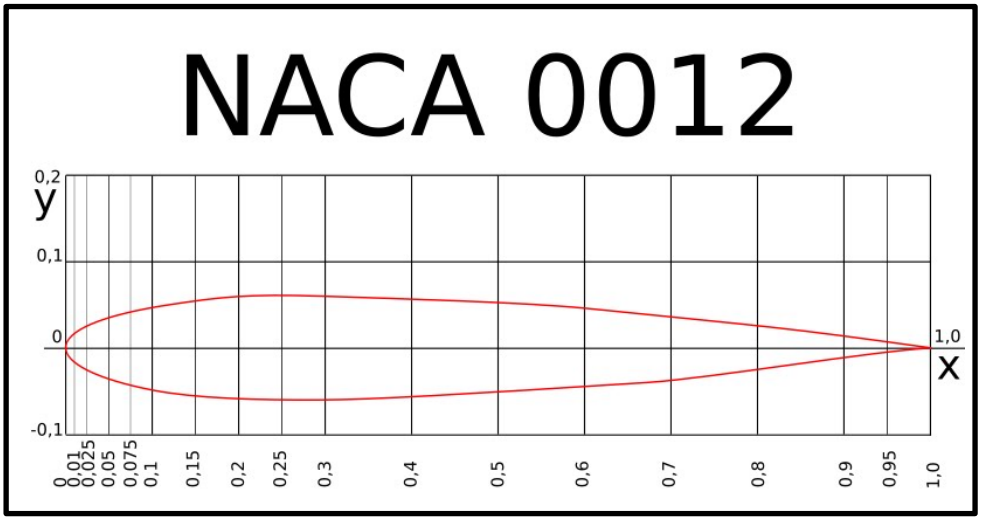

Figure 19. NACA0012 Airfoil. From [13].

The number of blades of each VAWT varied from two, three, six and eighteen in the numerical simulations. The blades were oriented around a center axis and had a rotor diameter of one meter. The chord of the blade was ten centimeters. Figure 20 shows the VAWT models. The VAWTS were placed inside a large rectangular control volume. The control volume was at a minimum 1.5 times the rotor diameter on either side of the rotor.

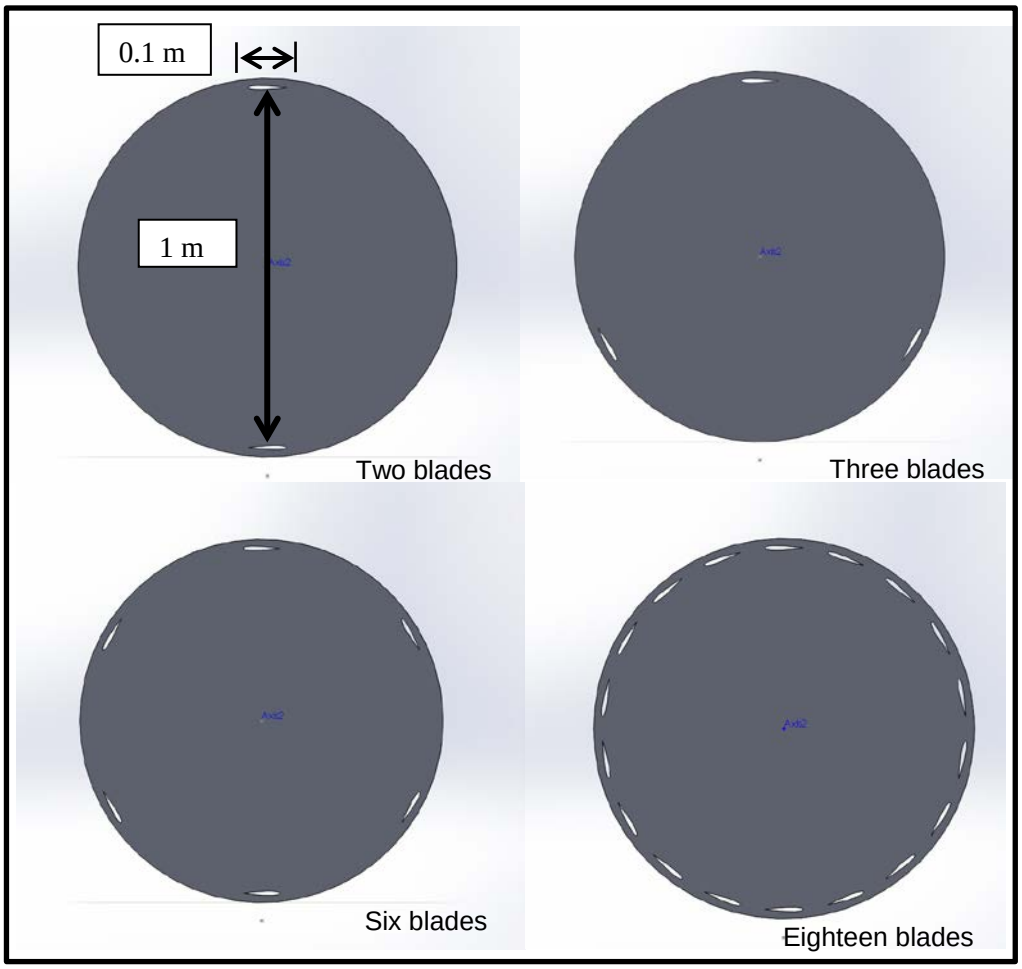

Figure 20. VAWTS with 2, 3, 6, and 18 blades.

Figure 21 illustrates the wind turbine and control volume in ANSYS CFX.

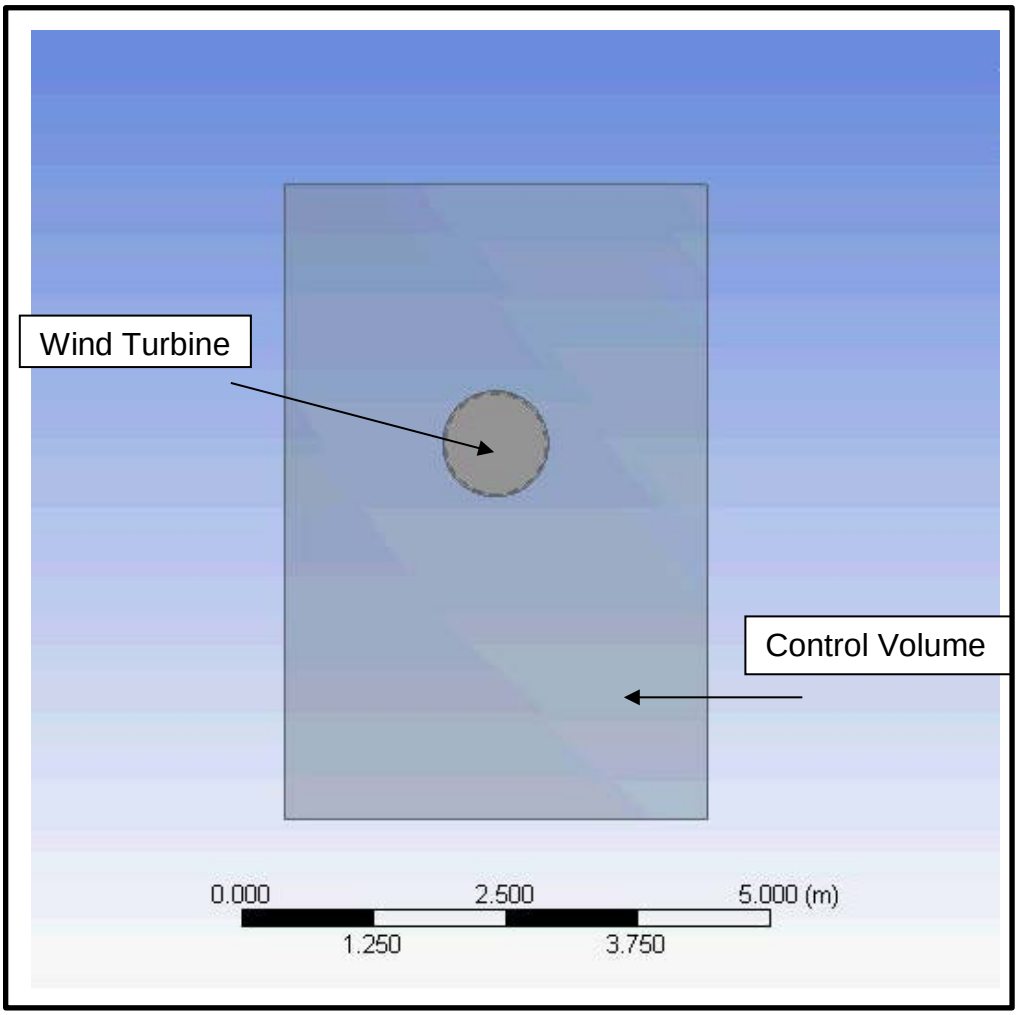

Figure 21. Wind turbine rotor and control volume in ANSYS CFX.

The mesh for the VAWT simulations was "fine," which is the smallest sizing option available in the ANSYS CFX program. The mesh had approximately 220,000 nodes and 100,000 elements for each wind turbine design. The mesh was approximately the same size for each VAWT simulation. The mesh elements were concentrated around the curved surfaces of the blades and rotor, as illustrated in Figure 22. Refer to Appendix D for mesh details.

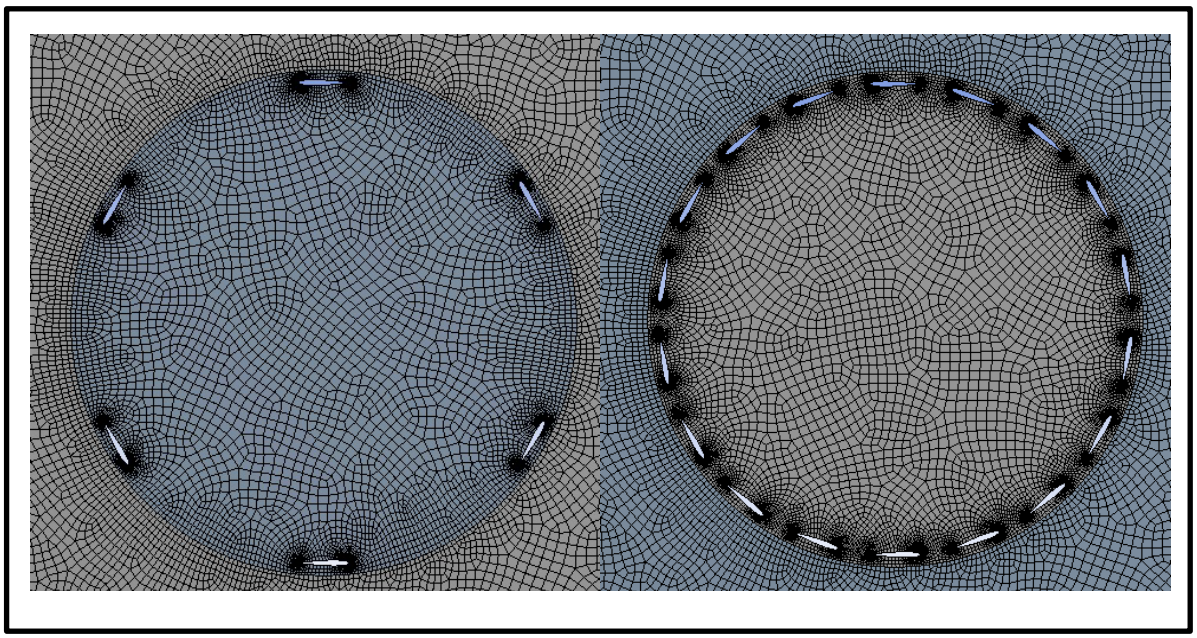

Figure 22. Mesh of 6 and 18-bladed wind turbines.

As the flow through the VAWT's was unsteady, transient CFD simulations were necessary. The rotational speed of the rotor varied while the "inlet" wind velocity was held constant. The boundary type on the rotor was a "no slip wall." The top and bottom boundaries of the control volume were "openings", which physically represent that the wind turbines operate in free air. The "symmetry" boundaries on the sides allowed for 2-D simulations. Table 2 illustrates the numerical model settings.

Numerical Model Settings	
Analysis Type	Transient, 2D
Turbulence Model	k- epsilon
Target Residual	1E -4
Transient Scheme	Second order backward Euler
Degree-stepping	One degree of rotation per time-step
Boundary Conditions	Inlet: air ideal gas, velocity 4 m/s
	Outlet: average static pressure 0 kPa
	Sides: symmetry boundaries
	Top/ bottom: opening with entrainment
	Rotor: No slip wall

Table 2. Numerical Model Settings for wind turbine blade number investigation.

Figure 23 displays the ANSYS CFX simulation set up.

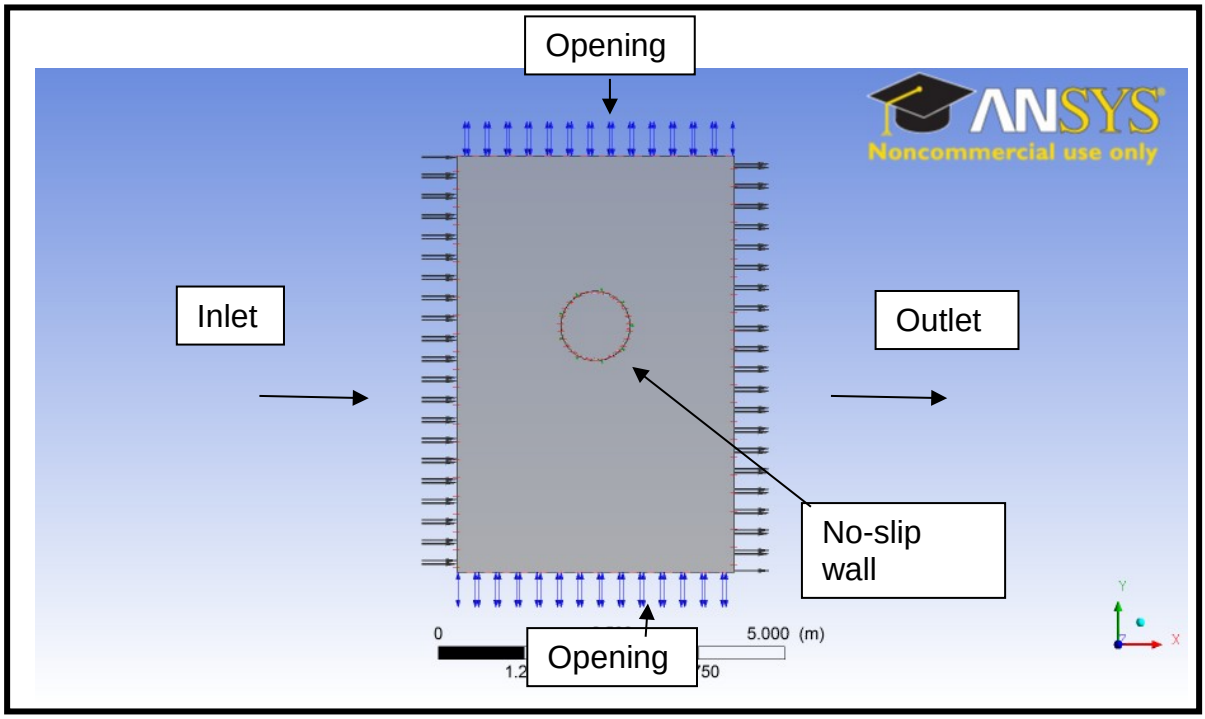

Figure 23. Set up of single rotor analysis in ANSYS CFX.

The inlet wind velocity was 4 m/s. This velocity is significant because it is above the average VAWT cut-in speed. Additionally, 4 m/s is within the range of Monterey winds. The simulations were timed so that a total of 6 rotor revolutions would occur per simulation. Previous simulations at the TPL have determined that approximately 6 revolutions provide accurate results for rotating machinery [12]. The rotor speed was based off the selected tip speed ratio for the simulation, an inlet velocity of 4 m/s, and the area of the rotor. The degree stepping was held constant so that there was one degree of rotation per time-step. ANSYS CFX calculated the torque during each time-step during the transient analysis for each VAWT blade design. The torque vector from all time-steps was exported into Microsoft Excel for data analysis. The specifics of the ANSYS CFX simulations are provided in Appendix E.

The turbulence model for the simulations was the standard two equation k-epsilon model. It is the most widely used turbulence model and it is highly accurate for VAWT

simulations [5] [14]. It is the default turbulence model in ANSYS CFX. Previous research concluded that the k-epsilon equations, compared with other turbulence methods, most closely modeled wind tunnel data [5].

4. Data analysis

The CFD simulations calculated the torque per time-step on the blades. The "time-step" was a function of the time required for 6 rotor revolutions and the TSR. The "torque" and "time-step" values were exported into Microsoft Excel for data analysis. Using Excel, the average torque was calculated. The angular velocity was set as an input. The power could be calculated from the average torque and angular velocity using Equation 1, where P is the power and ω is the angular velocity:

$$P = T\omega \qquad [1]$$

The Power Coefficient (C_p) is a non-dimensional parameter, which is used in wind turbine analysis to quantify how efficiently a wind turbine converts wind energy into mechanical power, refer to Equation 2 below [15].

$$C_p = \frac{P}{0.5\,\rho_{air} A\ V^3} \qquad [2]$$

$\boldsymbol{\rho}$ is the density of air, $\boldsymbol{A}$ is the frontal area of the wind turbines (the thickness multiplied by the diameter), and $\boldsymbol{V}$ is the air velocity or wind speed.

The Tip Speed Ratio (TSR) is the ratio between the rotational speed of the tip of the wind turbine blade and the velocity of the wind [15]. It is a non-dimensional quantity useful for wind turbine performance analysis. Refer to Equation 3 where $\boldsymbol{R}$ is the turbine radius.

$$TSR = \frac{\omega R}{V} \qquad [3]$$

Plotting the C_p versus TSR provides a good indicator of the wind turbine performance, and was used to evaluate the different VAWT designs.

5. Results of VAWT blade number investigation

The two-bladed wind turbine has the best overall performance: it attained the highest C_p and produced power over the largest range of TSRs. It's followed by, in decreasing order of performance, the three-bladed, six- bladed, and eighteen-bladed wind turbines. Figure 24 illustrates the power curves for each VAWT design. Note that the data did not violate the Betz limit, of a C_p of 0.593. The Betz limit is the maximum amount of power that a wind turbine can extract from the kinetic energy of the wind [15]. The detailed data for Figure 24 is in Appendix F.

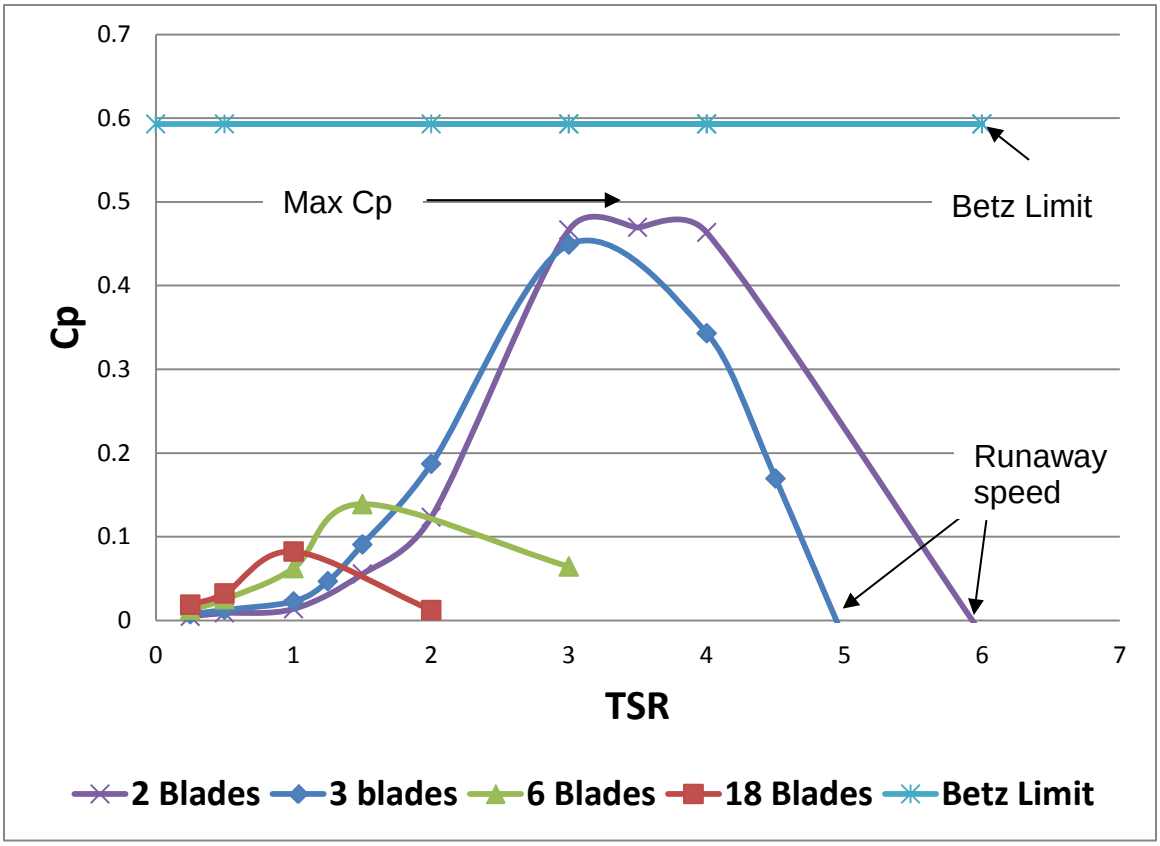

Figure 24. TSR versus C_p.

The two-bladed wind turbine reached a maximum C_p of approximately 0.47 at a TSR of 3.5. The three-bladed wind turbine reached a maximum C_p of about 0.45 at a TSR of 3. The max C_p was 4% less for the three-bladed wind turbine. The two-bladed wind turbine produced power over a TSR range of 0.25 to 6. However, the generated power was so small at low TSRs that the usable power range occurred at TSRs from 1.25 to 6. The three-bladed VAWT produced power at TSRs of 0.25 to 5. The usable power range was from 1.25 to 5. The three-bladed VAWT had a lower usable power range then the two-bladed VAWT.

The three-bladed wind turbine had a lower "runaway speed". The runaway speed is the unloaded rotor speed. A lower runaway speed is advantageous. It is annotated in Figure 24 and is the location where C_p is zero. For the three-bladed VAWT, the runaway speed occurred at a TSR of 5 and for the two-bladed VAWT was at a TSR of 6. However, at low TSRs from 1.25 to 2.9, the three-bladed wind turbine had a higher C_p. At a TSR of 2, the three-bladed VAWT outperformed the two-bladed by 41%. Both the two-bladed and three-bladed VAWTs had low starting torques.

A three-bladed VAWT may have potential structural advantages in comparison with a two-bladed VAWT. Three blades are more structurally balanced, which means there are less blade vibrations and the rotation is smoother. However, a two-bladed design is potentially worth further investigation.

The six and eighteen-bladed wind turbines had higher performance at lower TSRs from 0.25 to 1.75. The eighteen-bladed wind turbine had the highest C_p at a TSR of 1 and generated power from TSRs of 0.4 to 1.8. The nine-bladed wind turbine had the best C_p at a TSR of 1.5 and generated power from a TSR of 0.4 to 3. Although the nine and eighteen-bladed wind turbines performed better at low TSRs, they did not produce much power. The maximum C_p of the two-bladed VAWT was about four times the maximum C_p of the eighteen-bladed VAWT.

The torque versus number of revolutions for a three-bladed VAWT at a TSR of 0.25 is shown in Figure 25. The torque is highly alternating and unsteady.

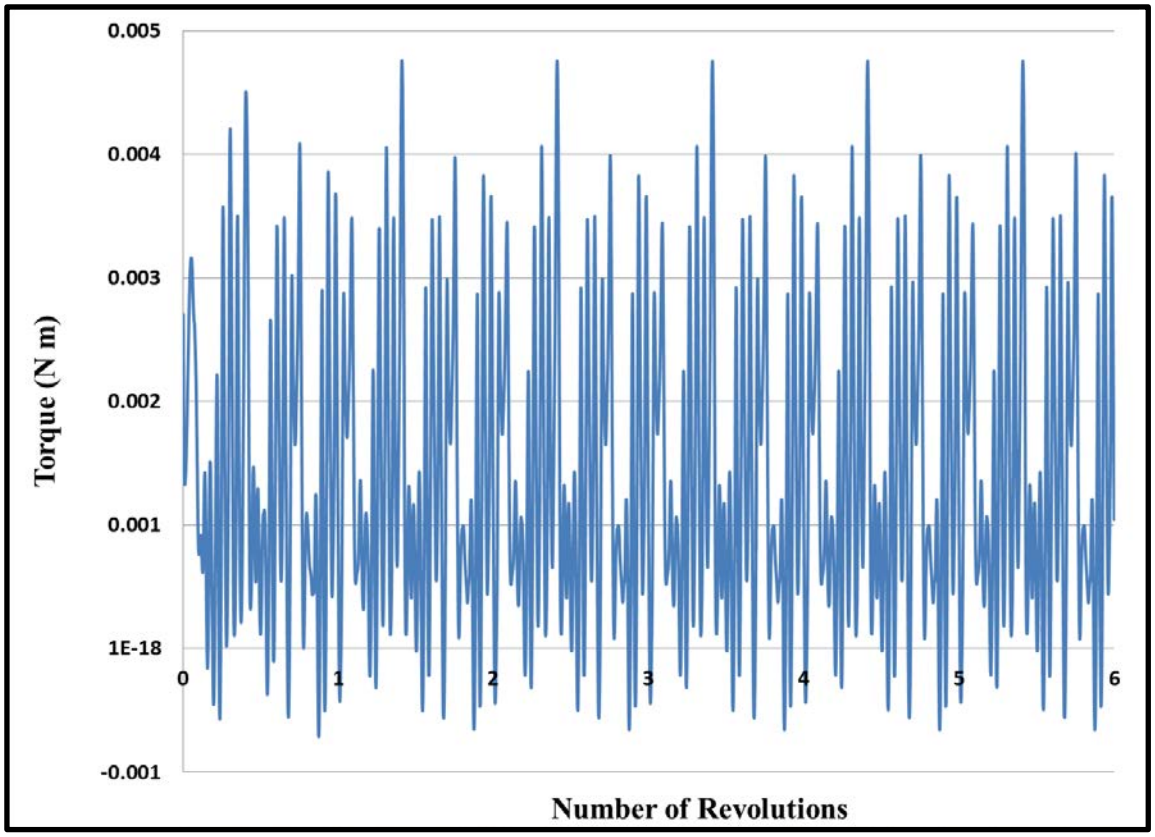

Figure 25. Torque versus number of revolutions for 3-bladed VAWT at TSR 0.25

The torque versus number of revolutions for a three-bladed VAWT at a TSR of 1 is illustrated in Figure 26. The torque has become more consistent at a higher TSR and the mean torque is at a higher value. The torque is an alternating sinusoidal shape. The results display the torque on the blades when the VAWT generates usable amounts of power.

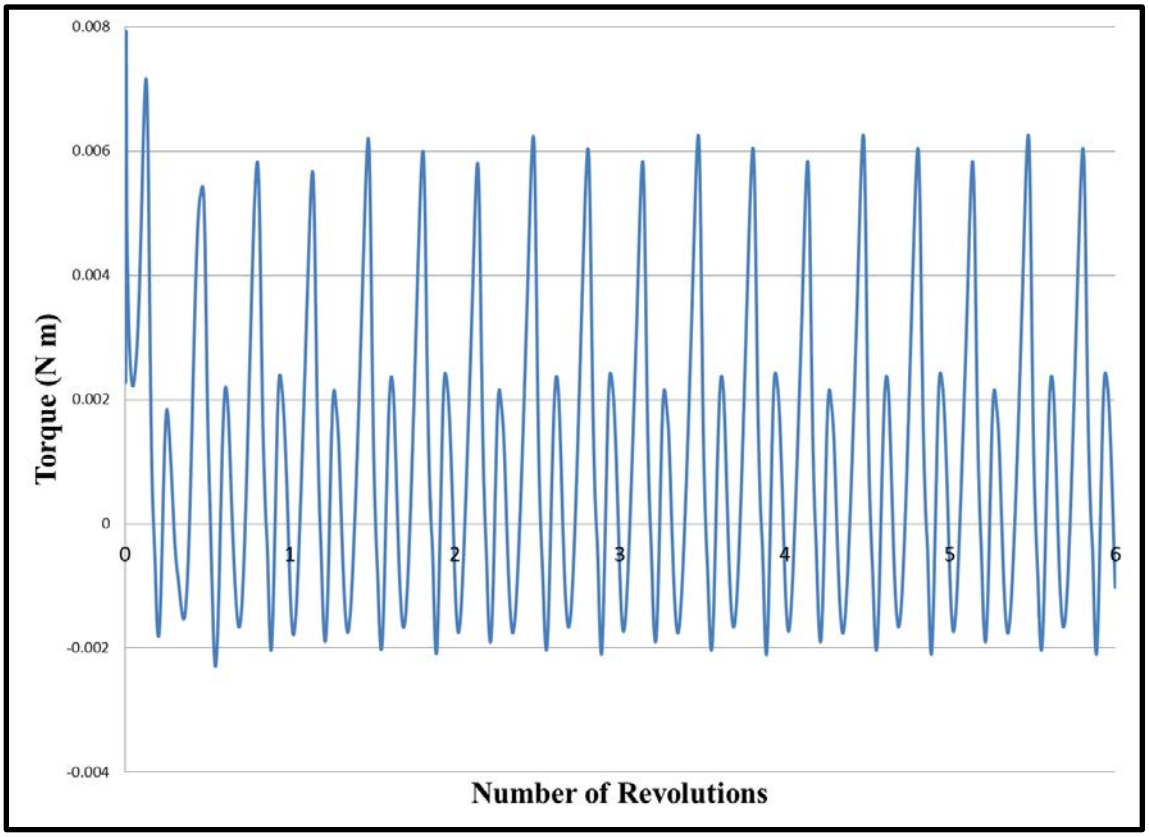

Figure 26. Torque versus number of revolutions for 3-bladed VAWT at TSR 1.

Figure 27 shows the torque versus number of revolutions of the 3-bladed VAWT at a TSR of 4. Notice the curve is more consistent then Figures 25 and 26. The torque alternates more smoothly at a higher TSR. This demonstrates that a smoother and more consistent torque is analogous to higher power generation: the C_p at a TSR of 4 was greater than the C_p's at TSRs of 0.25 and 4.

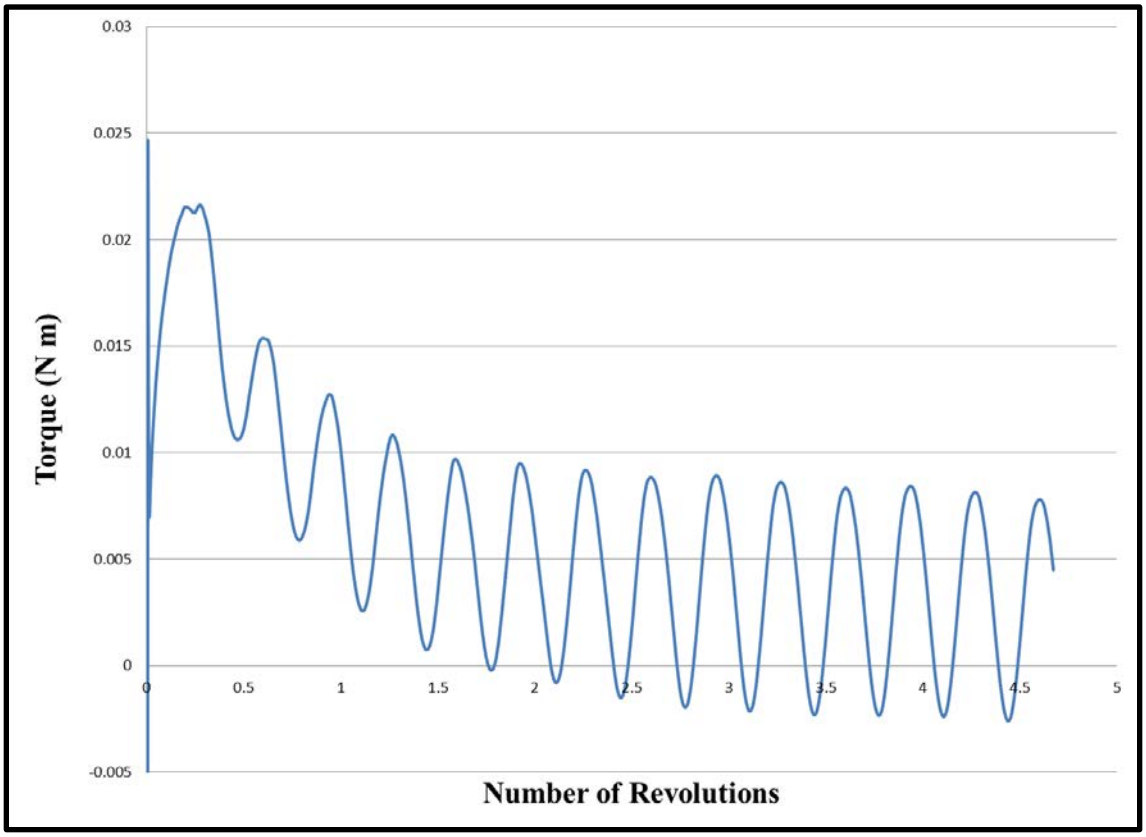

Figure 27. Torque versus number of revolutions for 3-bladed VAWT at TSR 4.

Selection of a Helical Blade Design

Each of the results presented in Figures 25, 26, and 27 represent the torque on a straight bladed VAWT. However, if the blades are helically shaped, the total torque would be the sum of the individual torques produced along each straight section of the blade. At each straight section of the blade the torque would represent something similar to what is represented in Figure 27 for a straight blade. The sum of the straight sections of the blade would be the sum of a series of torque curves shaped like that of the single blade results. The resulting torque curve would be a constant line, which represents a more constant output torque.

A straight blade and a helical blade are displayed in Figure 28.

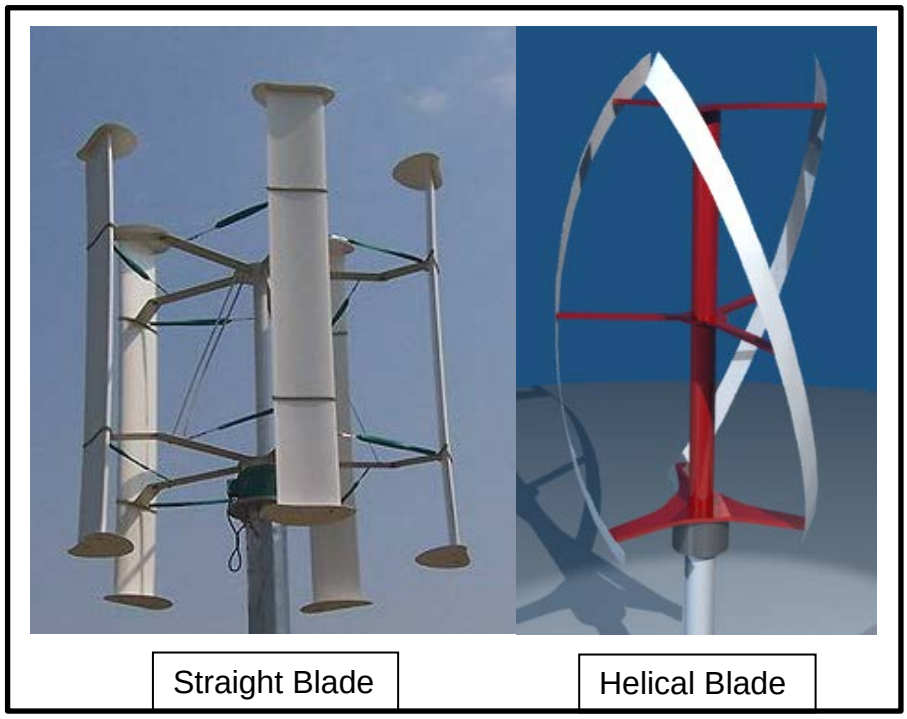

Figure 28. Straight-Bladed versus Helical Blade. From [3].

The constant torque output for a helical blade concept is illustrated in Figure 29. It shows the phase lag of each section.

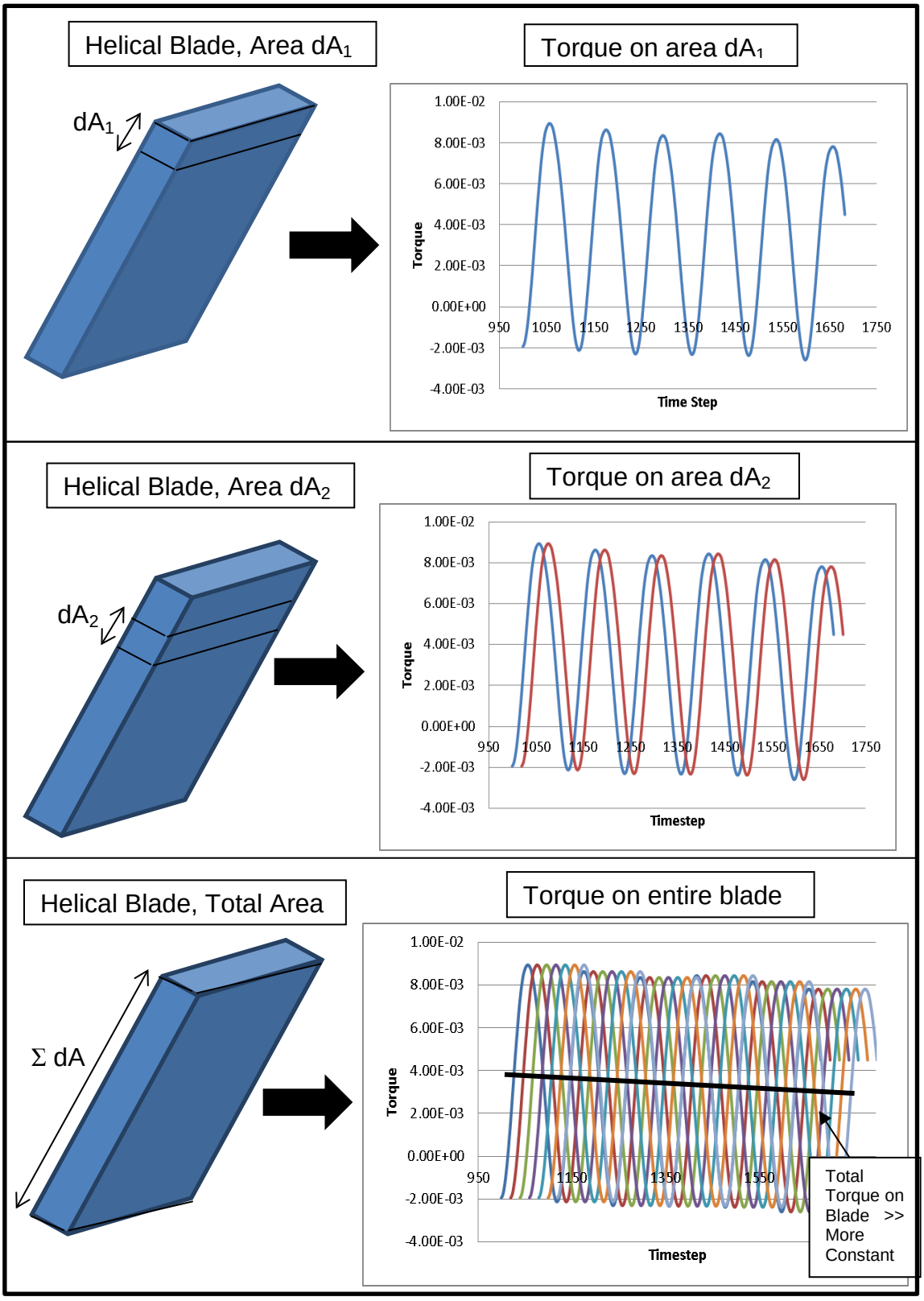

Figure 29. Helical Blade Design.

6. Velocity profiles

To visualize wind flow through the two, three, six and eighteen-bladed wind turbines, velocity contours were created using ANSYS CFX. Figures 30, 31, 32, and 33 illustrate the fluid flow through the wind turbines. The blades are rotating counter clockwise in each figure. The velocity profiles in the figures are at a TSR that correspond to the VAWTS maximum C_p. This TSR represents the desired operating condition for the VAWT.

Figure 30 demonstrates the velocity profile of the two-bladed VAWT at a TSR of 3.5, which produced its maximum C_p of 0.47.

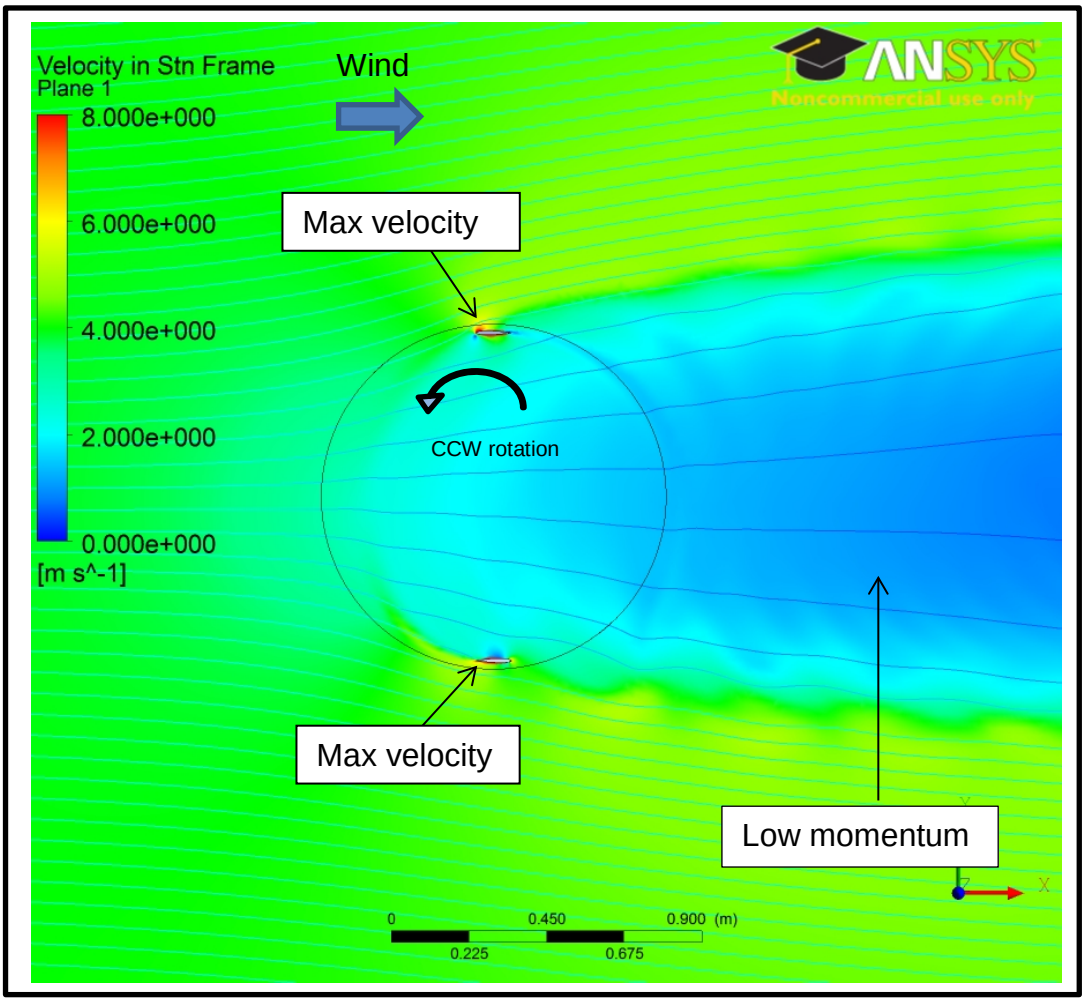

Figure 30. Velocity profile 2-bladed VAWT at TSR 3.5

The low momentum flow is evident behind the two-bladed VAWT. The maximum velocity occurs on the blade sections that directly capture the wind: the upper tip of the top blade and the tail end of the lower blade.

Figure 31 shows the velocity profile of the three-bladed VAWT at a TSR of 3, it had a maximum C_p of 0.45.

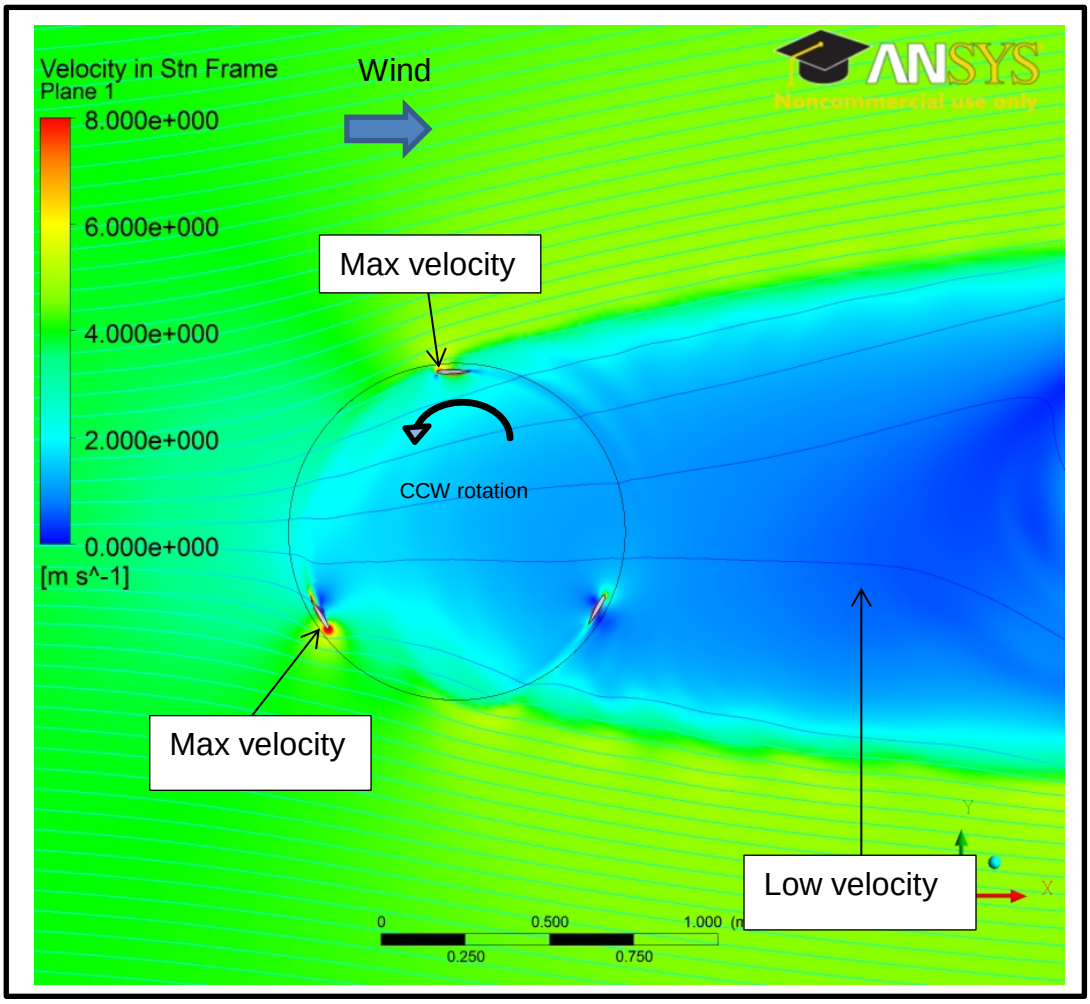

Figure 31. Velocity profile 3-bladed VAWT at TSR 3

The turbine wake appears to be less uniform then the two-bladed wind turbine wake and it has lower velocity flow. With more blades there is more fluid mixing. The max velocity occurs at the blades on the left and top of the VAWT, which is where the blades

are most exposed to the wind flow. On the right hand side the blade is not directly capturing the wind flow.

Figure 32 illustrates the velocity profile for the six-bladed VAWT at a TSR of 1.5. Its C_p was 0.14.

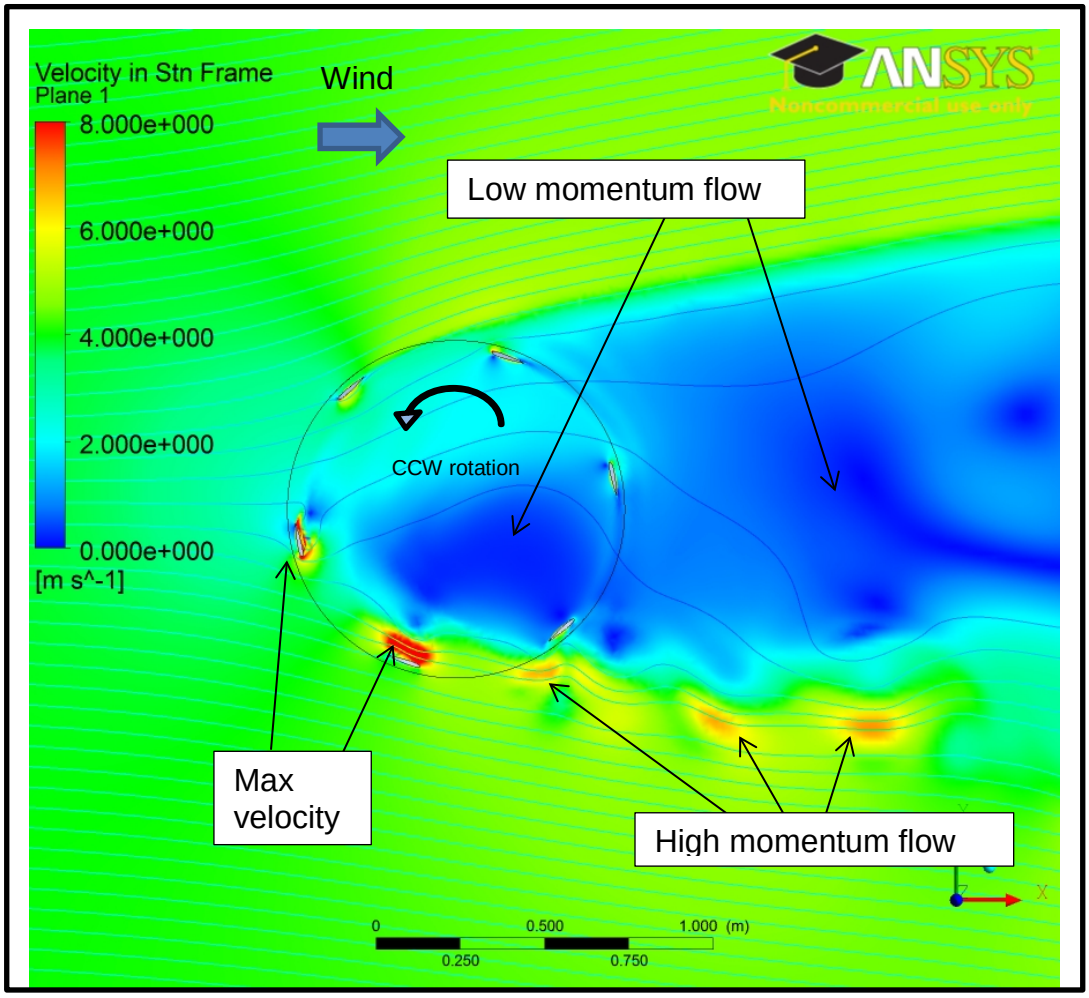

Figure 32. Velocity profile 6-bladed VAWT at TSR 1.5

The velocity profile varies significantly from the previous figures. Six blades create a more complex velocity profile. Notice the max velocity is on the blades located at bottom left. The high blade velocity contributes to a high velocity wake behind the VAWT on the bottom. Directly above the location of high velocity on the lower blade, there is a large

area of almost zero velocity flow within the turbine. The flow momentum in the wind turbine wake is lower than the two and three-bladed VAWTS.

Figure 33 displays the 18-bladed VAWT at a TSR of 1, which had a C_p of 0.082.

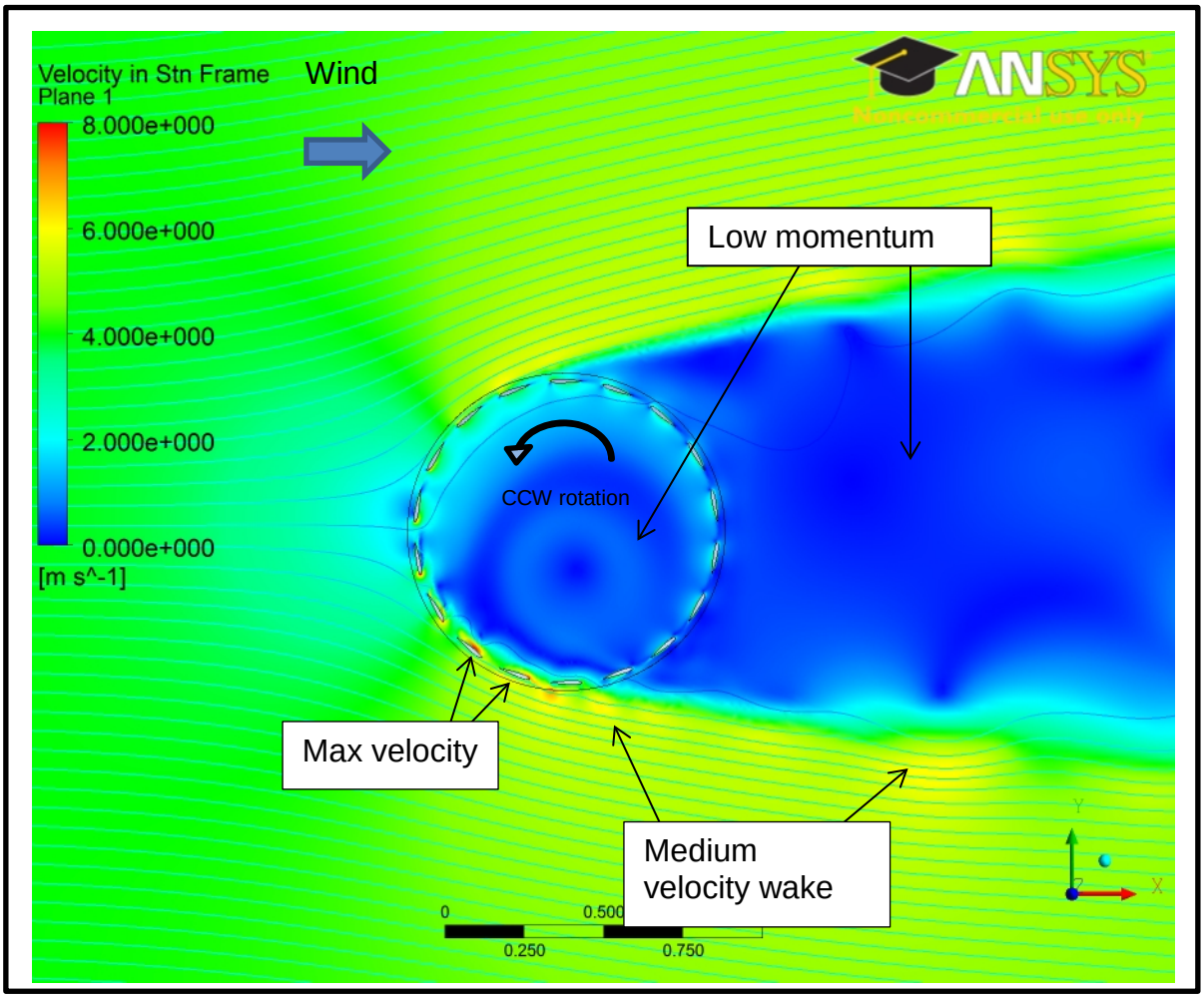

Figure 33. Velocity profile 18-bladed VAWT at TSR 1.

Notice the majority of the fluid flow through the wind turbine and in its wake is low velocity fluid flow. There appears to be high velocity flow on the blades located at the lower left of the turbine. Notice the medium velocity wake on the bottom. However, the majority of the fluid flow has low momentum. With more blades, there is less momentum in the wake. The data supports the observation that less downstream momentum corresponds to a lower C_p.

C. VAWT SELECTED FOR SITE LOCATION

The results show that a two-bladed VAWT has the highest performance. However, no manufactured two-bladed VAWTS were found. A three-bladed VAWT also performs well and is commercially available. A helical blade design can potentially output a constant torque. For these reasons a three-bladed helical VAWT was desired for the site location. There are very few three-bladed VAWTS with helical blades. The only one that could be found through local US distributors is manufactured by Urban Green Energy (UGE), who have multiple VAWTS with power ratings from 200W to 10 kW. UGE's 4kW VAWTS were selected because they are small enough to be installed on the roof top of Building 216. Additionally, they produce reasonable amounts of power. Two of UGE's 4 kW VAWTS are planned to be purchased at the time of writing. Dimensional drawings of UGE 4kW VAWTS are displayed in Appendix G. Figure 34 displays UGE's 4 kW VAWT.

Figure 34. UGE 4kW VAWT. From [16].

The cut-in wind speed for the UGE 4kW wind turbine is 3.5 m/s. Average Monterey winds are between 2 m/s and 8 m/s. The cutout wind speed is 30 m/s. Wind speeds this high are extremely unlikely to occur in Monterey. The power curves for UGE's 4kW VAWTS are displayed in Figure 35.

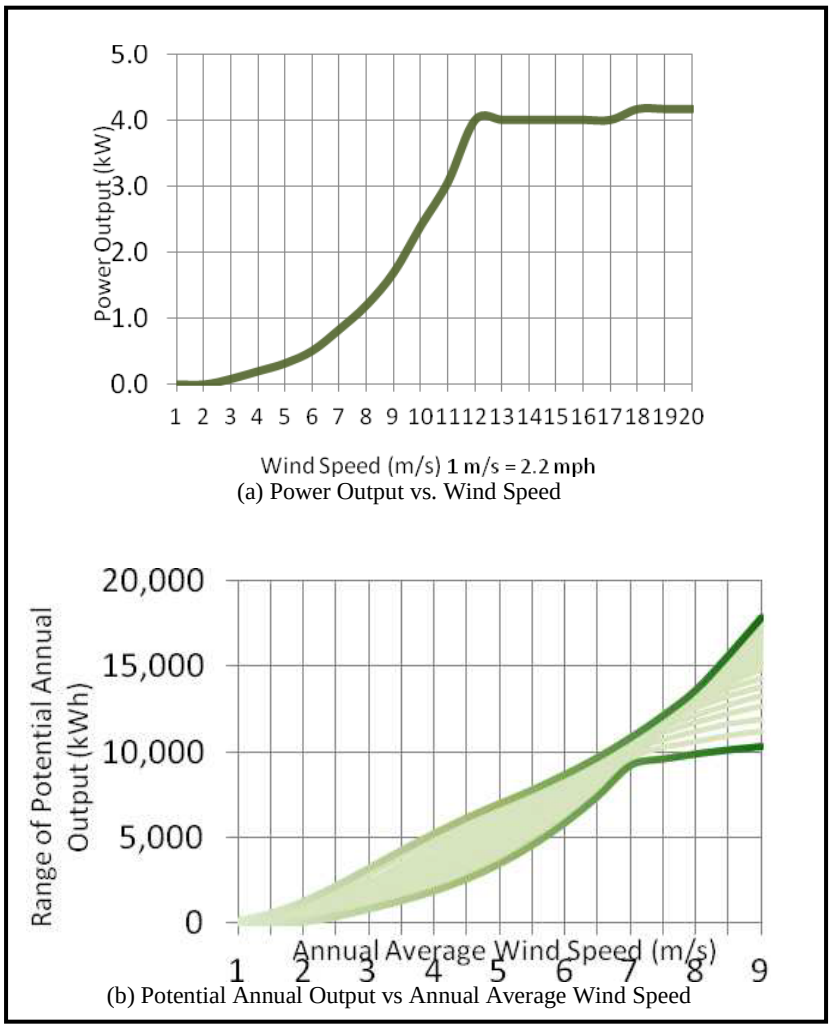

Figure 35. Power Curves for UGE 4kW Wind Turbine. From [17].

In another NPS thesis, these figures were analyzed to estimate the power output of the wind turbines at the TPL. Based off average wind speeds at the TPL, the expected annual power output is 1277.4 kW hr per year per wind turbine [18]. With two wind turbines, the total estimated power is 2554.8 kW hr per year.

D. DUAL ROTOR ANALYSIS

1. Motivation

It is common for multiple wind turbines, as opposed to a single wind turbine, to be installed in an array. Often it is desirable to fit many turbines in small land areas to derive maximum power from the space available. For these applications, it is important to understand how the separation distance between multiple wind turbines affects their

performance. Similar studies have taken place for HAWTS [19]. However, there has not been similar published research for VAWTS. The goal of this analysis was to determine how the separation between VAWTS affects their power output, which is useful for the placement of the wind turbines on the roof of Building 216. Additionally, the analysis sought to determine how three, six, and nine-bladed wind turbines were affected by spacing differences.

2. Overview

Dual rotor VAWTS were analyzed using CFD. The rotors were the same design as the 2-D VAWTS used in the single rotor analysis described in the previous section. The number of blades varied from three, six, and nine. The separation distance between the wind turbines varied from 0.4m, 0.1m, and 0.01m. The inlet wind velocity was a constant 4 m/s and the TSR was approximately 0.5. ANSYS CFX calculated the torque on the VAWTS for each simulation.

3. Methodology

The methodology was similar to that described in section III-B for the single rotor analysis. Instead of creating single 2-D rotors in Solidworks, dual vertically stacked 2-D rotors were used. The separation distance between the dual rotors varied from 0.01m, 0.1m and 0.4m.

Figure 36 illustrates the dual rotors and the spacing between them.

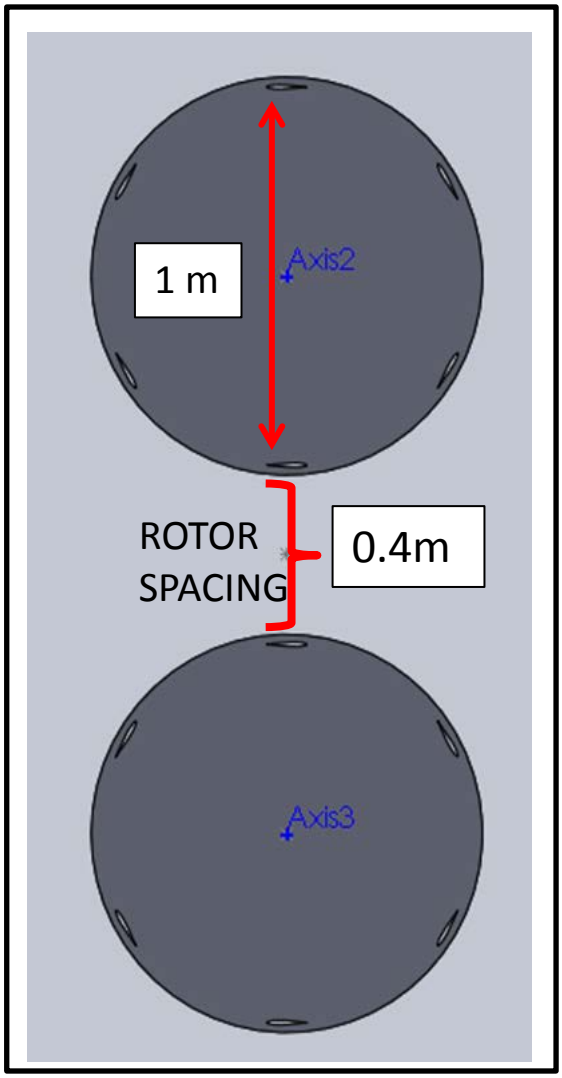

Figure 36. Rotor spacing.

The rotors were analyzed using the CFD program, ANSYS CFX. The TSR was set at approximately 0.5. The inlet wind velocity was 4 m/s. Dual VAWTS with three, six, and nine blades were analyzed with separation distances between the rotors of 0.4m, 0.1m, and 0.01m. The computational mesh was similar to that of the single rotor simulations. The mesh elements were concentrated around the curved surfaces of the blades and in-between the dual rotors. It was important to make sure there were enough mesh elements in-between the closely spaced rotors for accurate results. The mesh is illustrated in Figure 37.

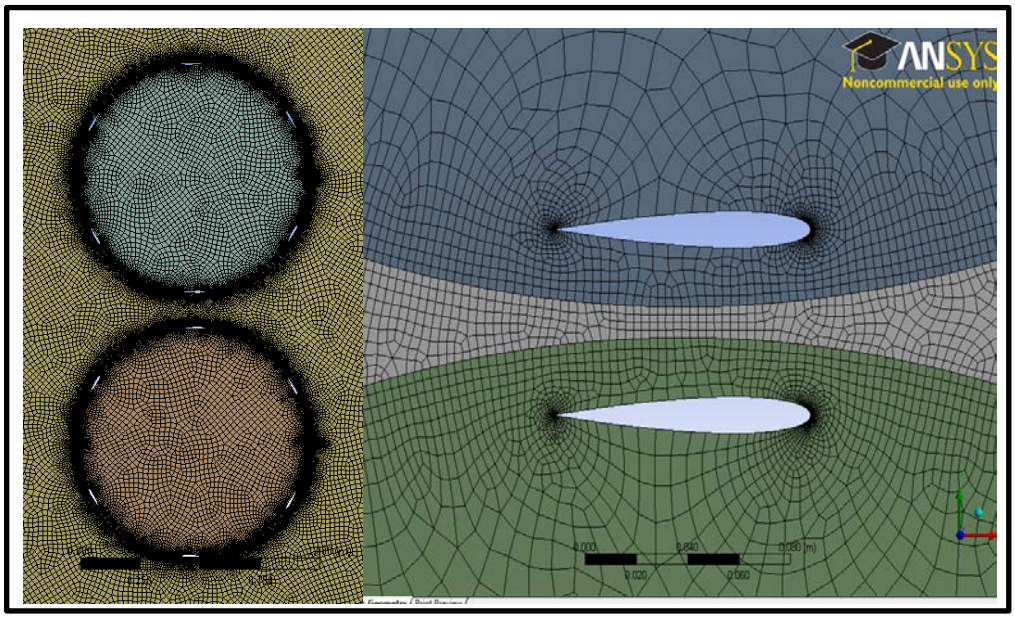

Figure 37. Mesh details of dual rotors.

Notice there are enough elements in-between the rotors. The number of mesh elements was approximately 100,000 and the number of mesh nodes was about 220,000. The number of mesh elements and mesh nodes were approximately the same for each VAWT simulation. Refer to Appendix H for the mesh details. Figure 38 displays the set-up of the dual VAWT analysis in ANSYS CFX.

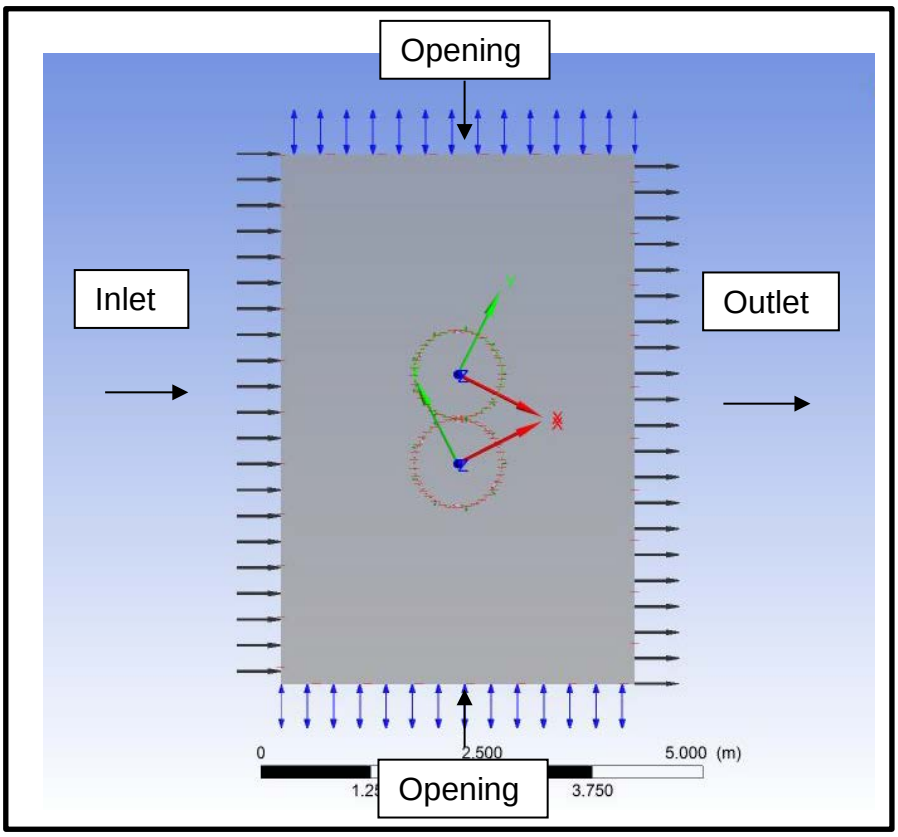

Figure 38. ANSYS CFX Set-up of dual rotor tests.

The boundary conditions were the same as that of the single rotor analysis to meet the same physical requirements. The top and bottom were “openings” to imitate open air conditions. The interfaces between the blades were “no-slip walls”. A summary of the numerical model settings is presented in Table 3. Appendix I displays the ANSYS CFX simulation specifications for the dual rotor analysis.

Numerical Model Settings	
Analysis Type	Transient, 2D
Turbulence Model	k- epsilon
Target Residual	1E -4
Transient Scheme	Second order backward Euler
Degree-Stepping	One degree of revolution per time-step
Boundary Conditions	Inlet: air ideal gas, velocity 4 m/s
	Outlet: average static pressure 0 kPa
	Sides: symmetry boundaries
	Top/ bottom: opening with entrainment
	Blades: No slip wall

Table 3. Numerical Model settings for dual VAWT analysis.

4. Results

The effects of close spacing impact the performance of the VAWTS. Figures 39 and 40 illustrate this conclusion. The simulations were performed as a TSR of approximately 0.5 and at an inlet velocity of 4 m/s. Figure 39 shows the C_p versus the rotor separation for each pair of VAWTS.

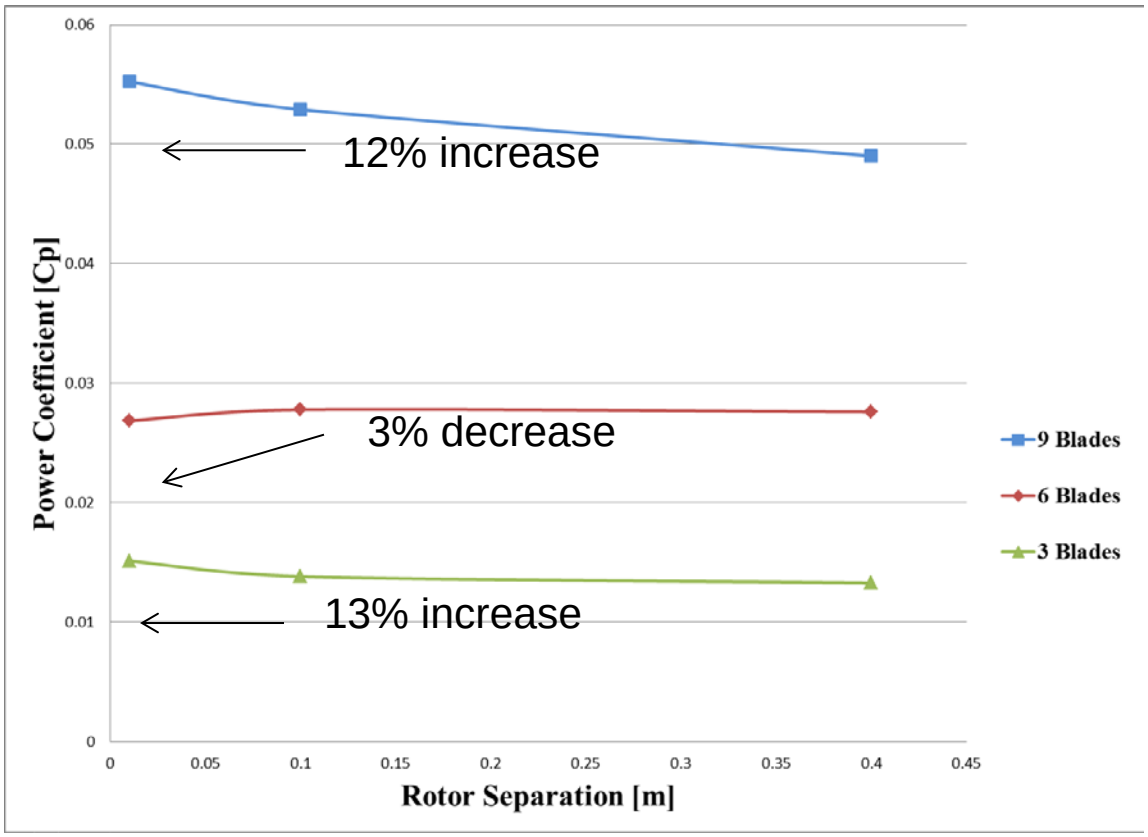

Figure 39. Rotor Separation vs C_p.

Closer spacing improved the C_p by 12% for the nine-bladed VAWTS and by 13% for the three-bladed VAWTS. The six–bladed VAWTS had a 3% detriment in C_p. Figure 39 illustrates that the C_p was greatest for the nine-bladed VAWTS, which agrees with the single rotor analysis. The single rotor analysis determined that at lower TSRs the higher-bladed VAWTS have greater C_p.

Figure 40 depicts the average torque versus rotor separation.

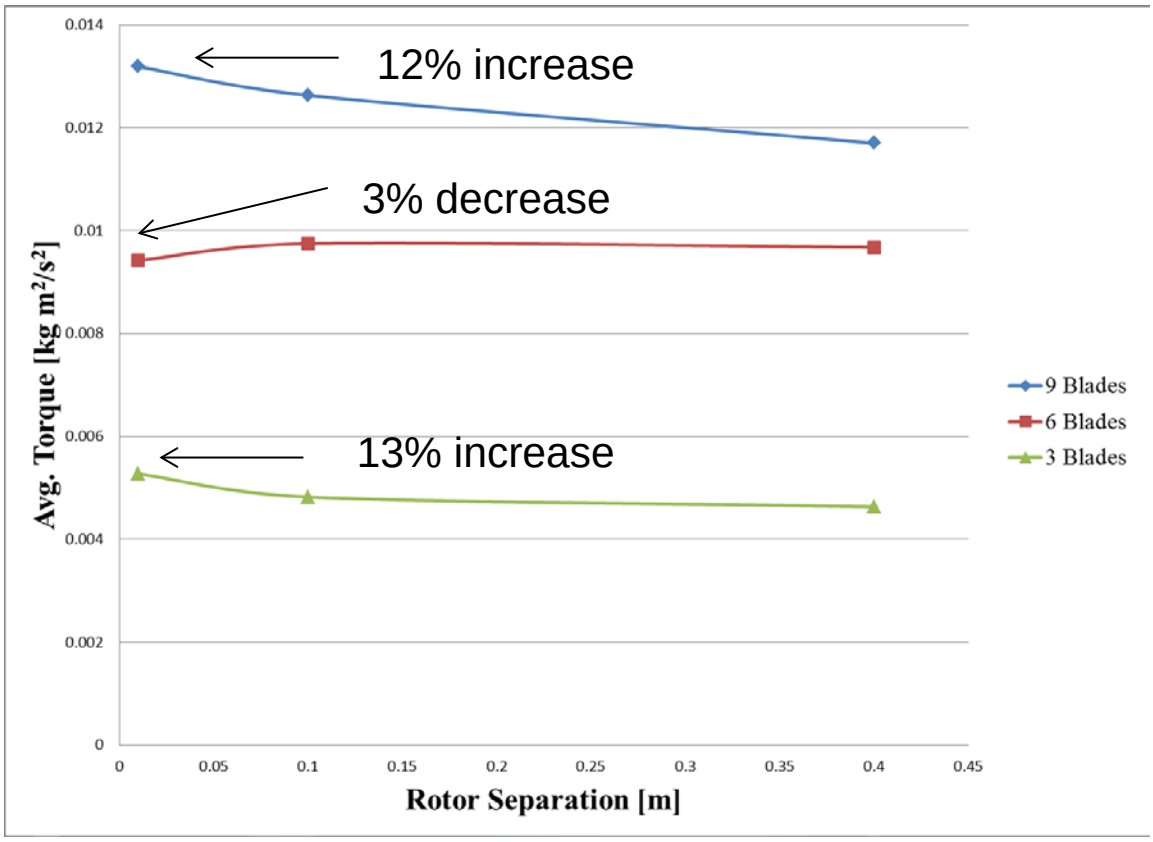

Figure 40. Average Torque vs Rotor Separation.

The torque effects are similar to that of the C_p effects. The torque is influenced by close spacing between wind turbine rotors. Detailed results of the dual rotor analysis can be found in Appendix J. The torque and C_p results display that there is a potential benefit to close spacing between VAWT's.

Although the nine-bladed VAWTS had the highest C_p and torque, it is important to realize that they did not necessarily have the best performance. The dual rotor simulations were conducted at a low TSR. Further simulations should be conducted across a range of TSRs to evaluate the performance of the VAWTS.

Velocity images of the six-bladed and nine-bladed VAWTS at a spacing of 0.01m are illustrated in Figure 41.

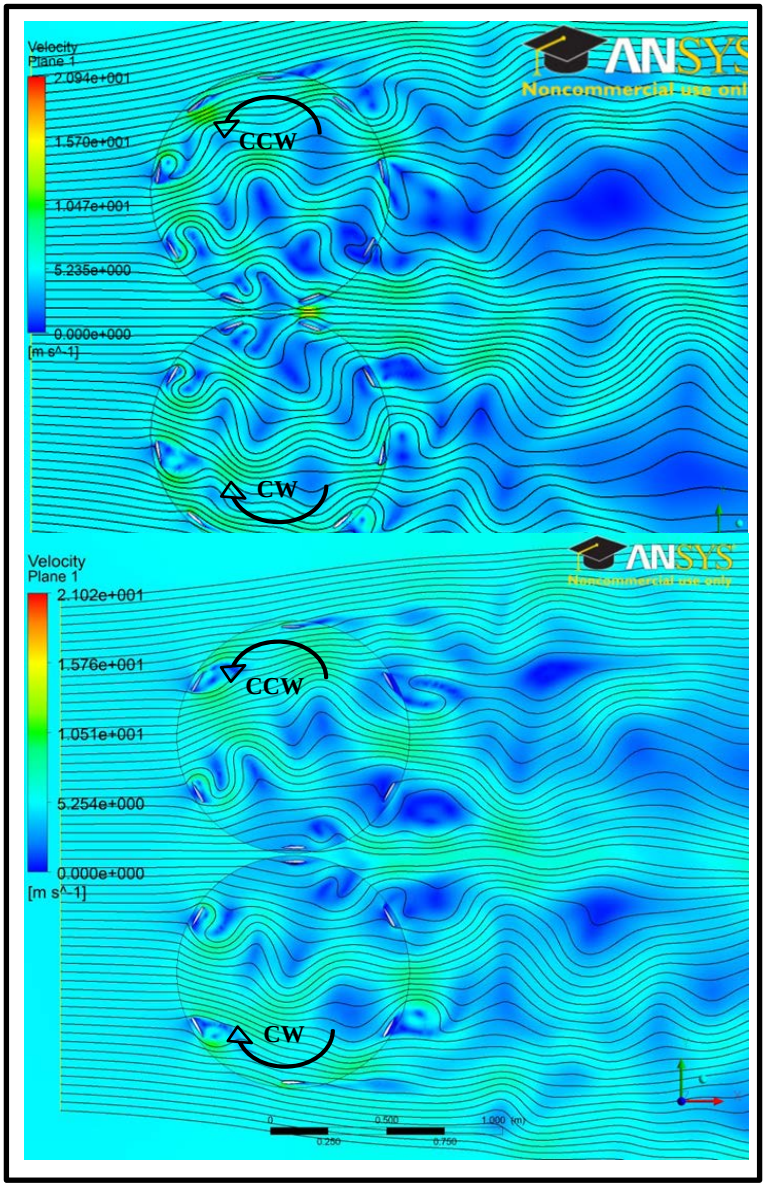

Figure 41. The 6 and 9-bladed dual VAWTS at a separation distance of 0.01m.

The top blade is moving counter clock wise and the bottom blade is moving clock wise. The results of these simulations are helpful for the placement of the VAWTS on the roof of Building 216. The VAWTS can be spaced closely with a potential gain in performance.

E. BEAM DESIGN FOR VAWTS

1. Motivation

The VAWTS must not be placed directly onto the roof of Building 216. Although the roof is likely strong enough to support the VAWTS, it was decided not to permanently fix anything to it. This provides flexibility to move the wind turbines around the roof if necessary. A beam support structure provides mobility to the VAWT array if alterations need to be made in the future. For example, the addition of more VAWTS might require rearranging of the previous configuration. Adjustments can more easily be made to the beam structures then to the roof. Additionally, adjustments to the beam structures do not impact the structural integrity of the roof.

2. Overview

A beam structure for the 4kW VAWTS was designed in Solidworks and simulated in ANSYS Static Structural. The beams support the weight of the VAWTS and resist the bending moment and torque produced by wind gusts. UGE provided the load speciation's for the 4kW VAWT. Engineering drawings were made of the final beam support structures.

3. Methodology

The load specifications of UGE's 4kW VAWT are displayed in Appendix K. These load specifications are dependent on the selected tower height, which is the height of the center pole.

Figure 42 illustrates the tower height of a wind turbine. The wind turbine in Figure 42 is a UGE 4kW VAWT.

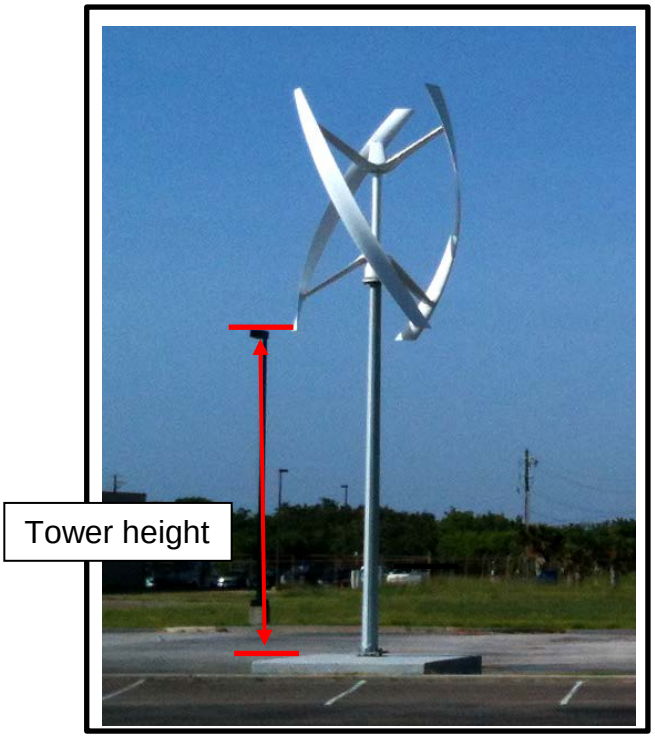

Figure 42. Tower height explanation. After [20].

A 3m tower height was selected for application of the VAWTS onto Building 216. This is the shortest tower available. It is necessary so that the VAWTS sit within the building profile and do not protrude past the roof. A summary of the VAWT load conditions for the 3m tower are described in Table 4.

UGE 4kW VAWT Specifications: Load specifications at base of tower at 50 m/s.	
N max (Axial)	13.15 kN [2.96 kips]
Q max (Shear)	7.78 kN [1.75 kips]
M max (Moment)	33.81 kN*m [24.93 k*ft]
Deflection	0.045 m

Table 4. UGE 4kW VAWT Load Specifications. After [21].

The forces are defined in Figure 43. Notice that the load specifications in Table 4 are defined at a wind speed of 50 m/s, or 112 mph. Winds of this velocity are extremely unlikely to occur.

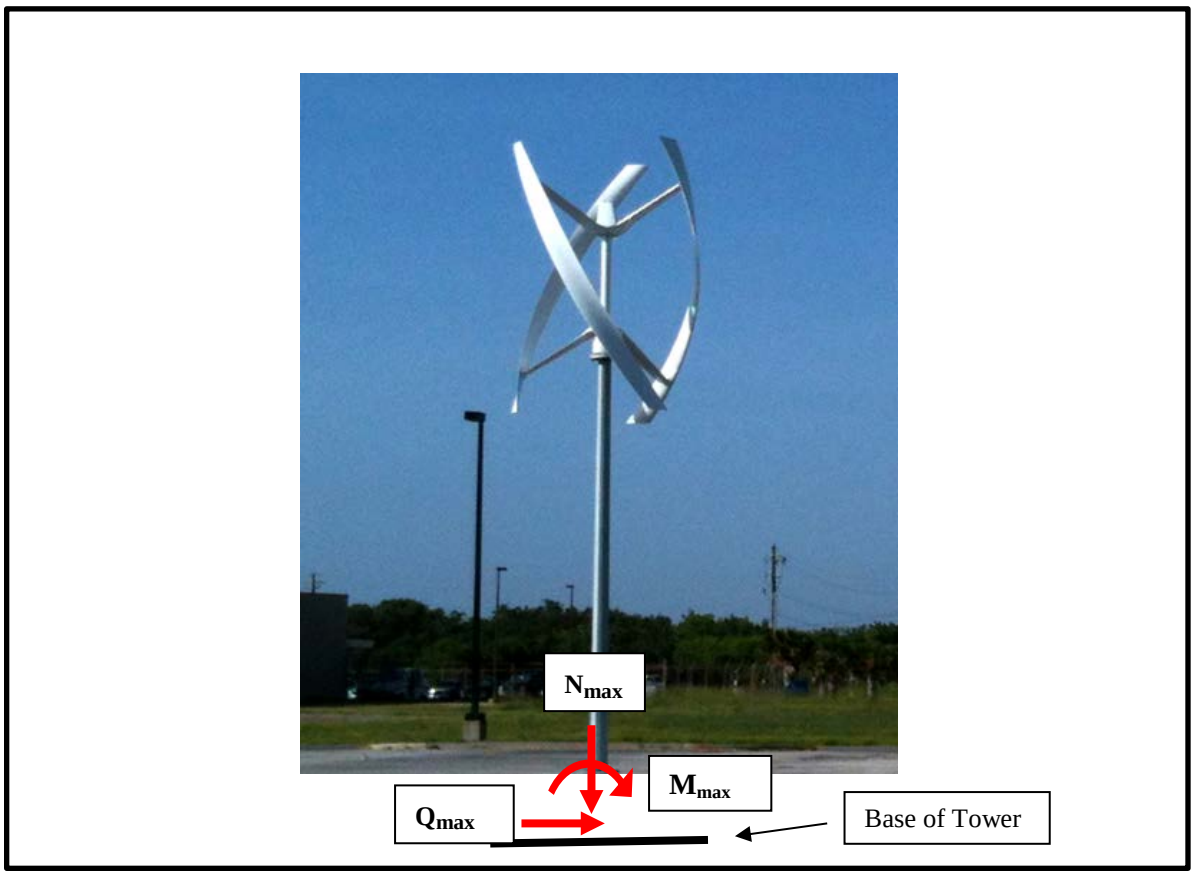

Figure 43. Load definitions. After [20].

A force representation was developed. Using the maximum axial, shear, and moment loads from Table 4, a basic statics analysis was used to calculate an equivalent distance with the same forces. The equivalent distance was used as the length of a representative wind turbine pole in Solidworks. The representative pole has the equivalent forces of the 4kW turbine and it provides a model for computational analysis.

Figure 44 illustrates the equivalent force concept.

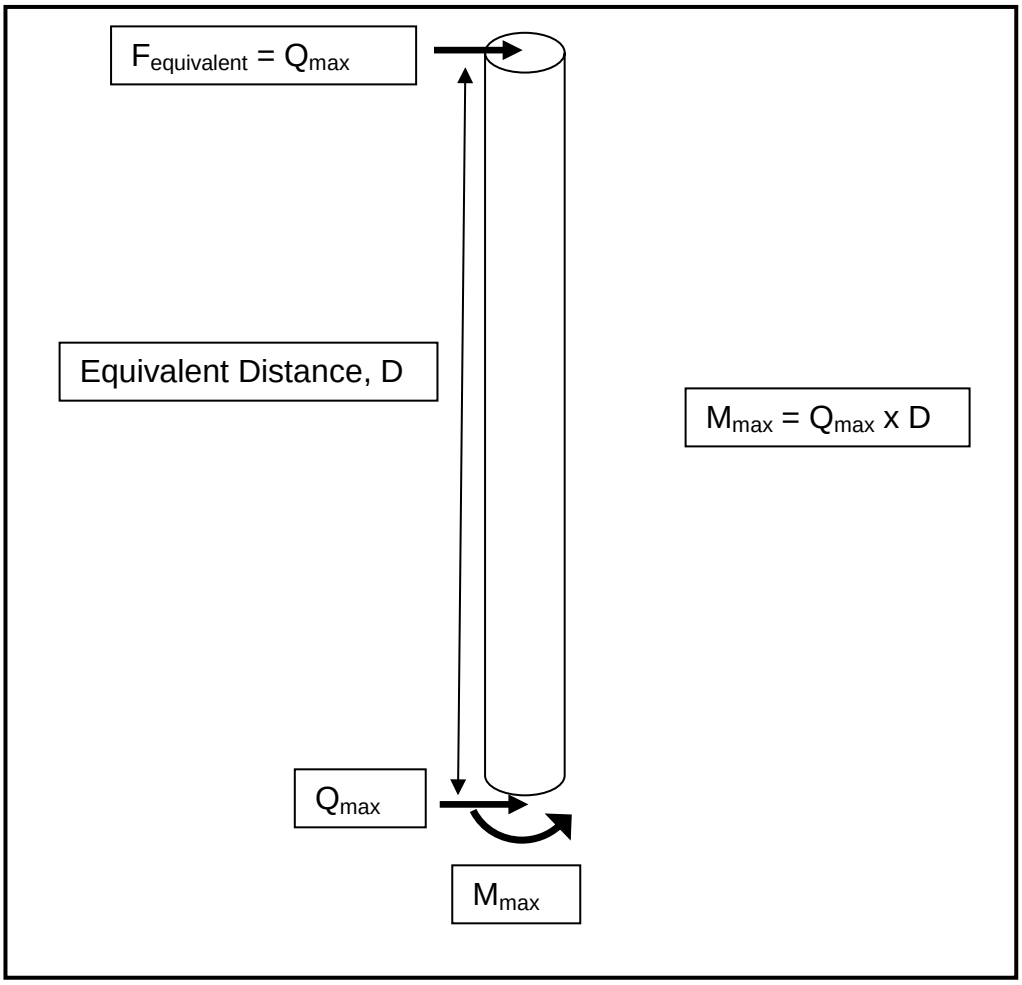

Figure 44. Equivalent force diagram.

Calculations determined that the length of the representative wind turbine pole is 4.34 m (171 inches). This pole was created in Solidworks. In the computational simulation, the shear force provide in Table 4 was applied to the top of the representative turbine pole to simulate the forces on the wind turbine.

Figure 45 is the Solidworks model of the representative turbine pole.

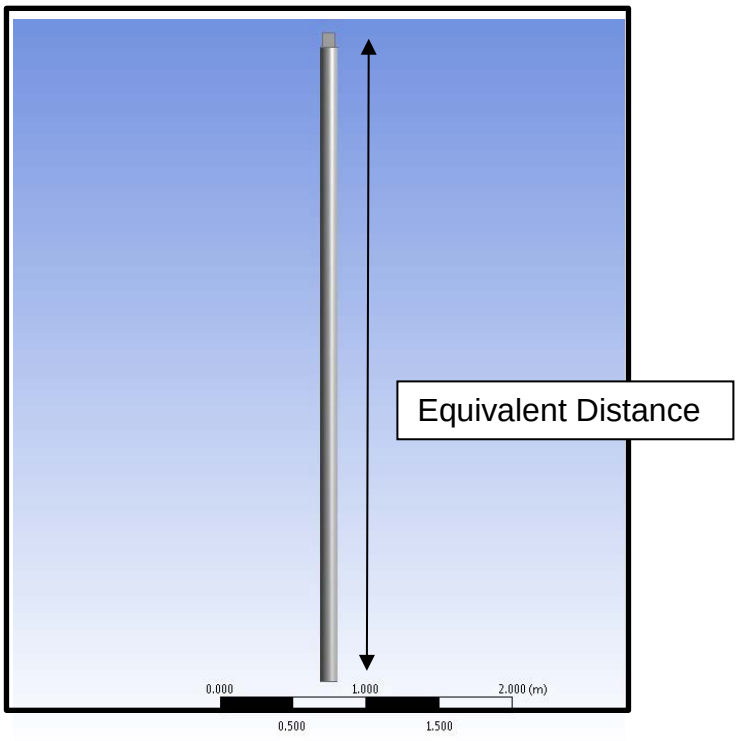

Figure 45. Representative turbine pole.

An I- beam with a designation of w12X40 was selected to support the VAWT's. A w12x40 beam has suitable strength and its weight is not excessive. The dimensions of a w12x40 beam are displayed in Figure 46.

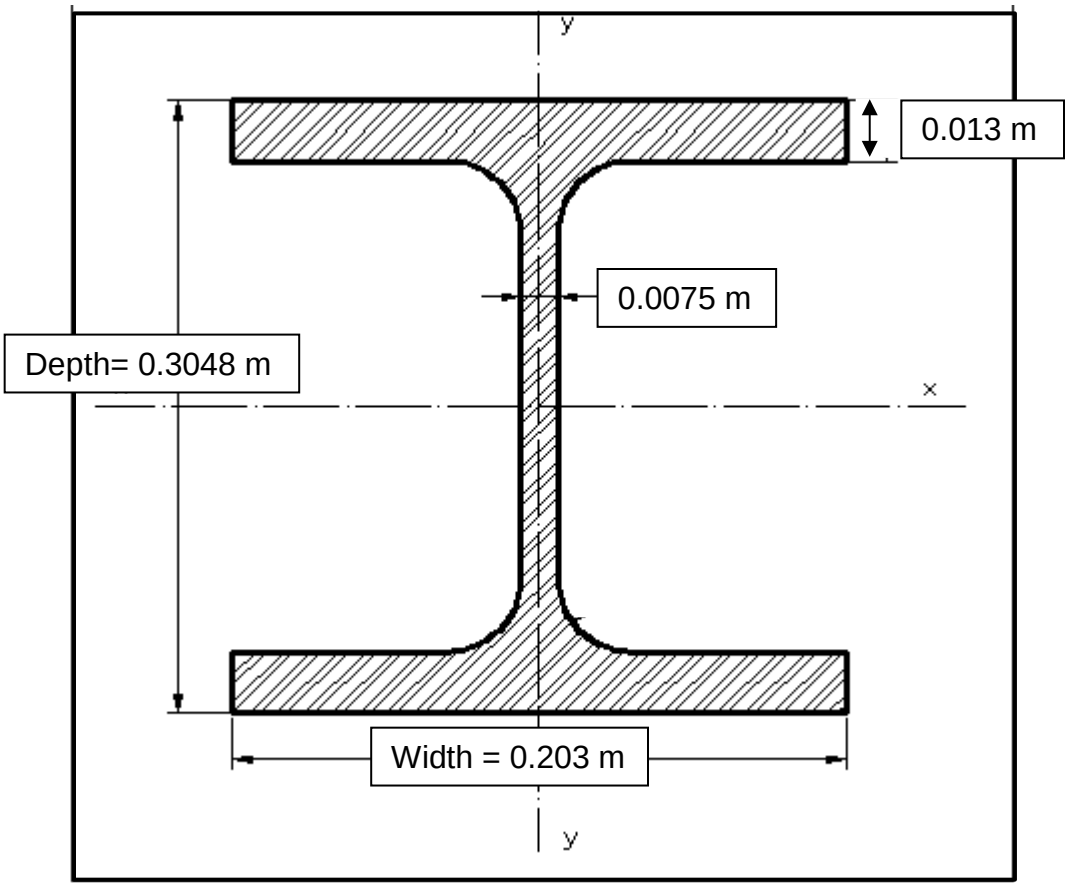

Figure 46. Dimensions of w12 x 40 I-Beam. After [22].

Successive iterations of the beam structure led to the development of a series of I-beams arranged in a quadrature. Shorter I-beams run perpendicular to the orientation of the quadrature beams to increase the strength of the design and reduce torsion. Each quadrature is designed for a single VAWT: two quadratures are planned for the two selected VAWTS. The beams are 8 m (315 inches) in length.

The initial beam design is illustrated in Figures 47, 48, and 49. Figure 49 displays the lower flange of the VAWTS. The lower flange dimensions were provided by UGE. They are listed Appendix L.

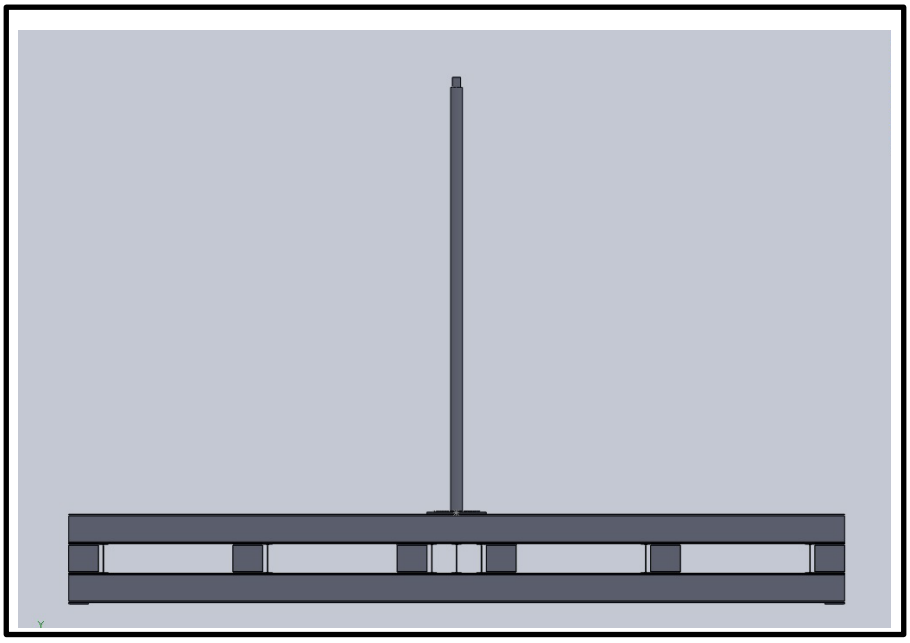

Figure 47. Front view of beam design.

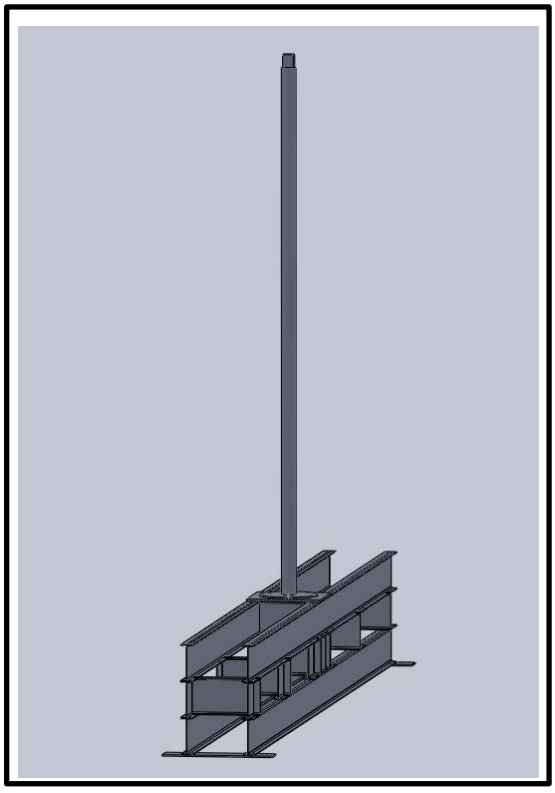

Figure 48. Corner view of beam design.

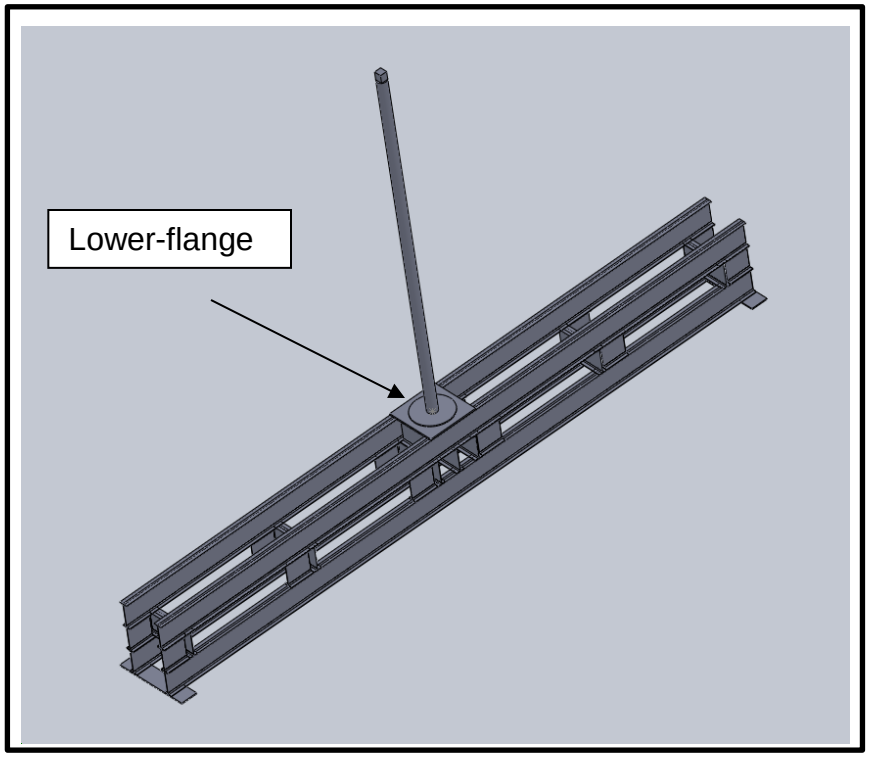

Figure 49. Isometric view of beam design.

The beam design was tested with the wind turbine representation in the center of the beam. This loading produces the greatest stress in the beams. In practice, the wind turbines will be located to the side of the beams. For design considerations it is best to check the stress in the worst case scenario, which is when the wind turbines are located in the center of the beams. Two beam designs will be necessary to support two VAWTS. They will be connected by a spine beam, which reduces torsion in the structure.

Figures 50 and 51 display the beams connected by a spine beam.

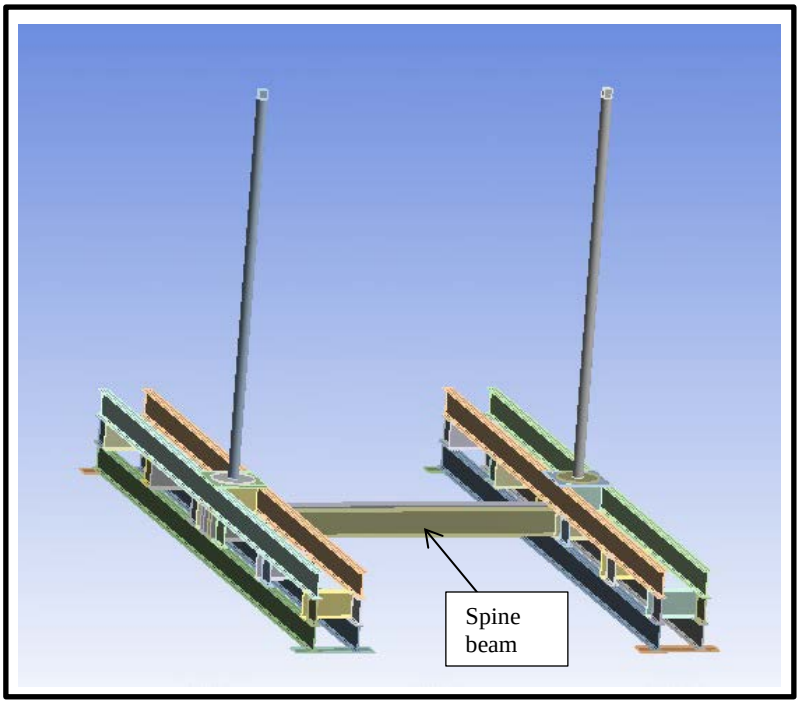

Figure 50. Beams connected by spine beam.

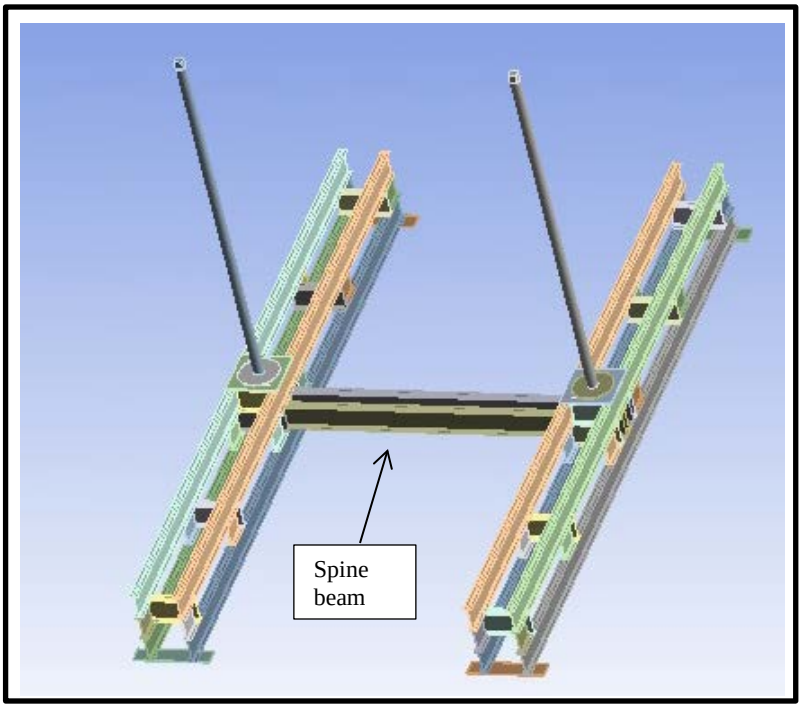

Figure 51. Beams connected by spine beam.

The model was tested using ANSYS Static Structural. A “coarse” computational mesh was used. The mesh had approximately 103,068 nodes and 16,007 elements. Mesh details are described in Appendix M. Figure 52 illustrates the mesh on the beam structure.

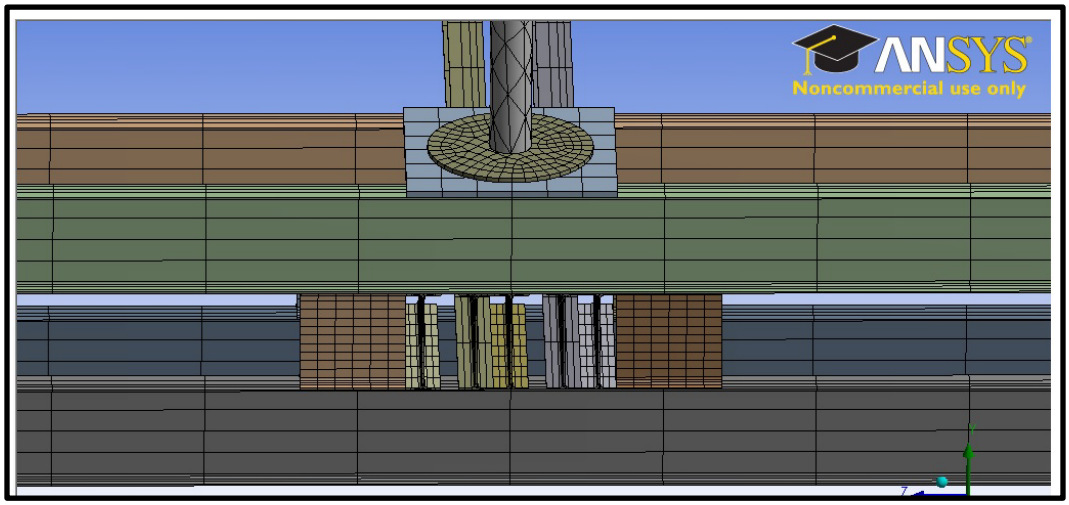

Figure 52. Mesh for beam design.

In ANSYS Static Structural, forces equal to the maximum shear stress from Table 4 were applied to the wind turbine representations. The shear forces were oriented parallel to beam. The sides of the beams were constrained as they would be in practice.

Figure 53 illustrates the problem set-up in ANSYS Static Structural.

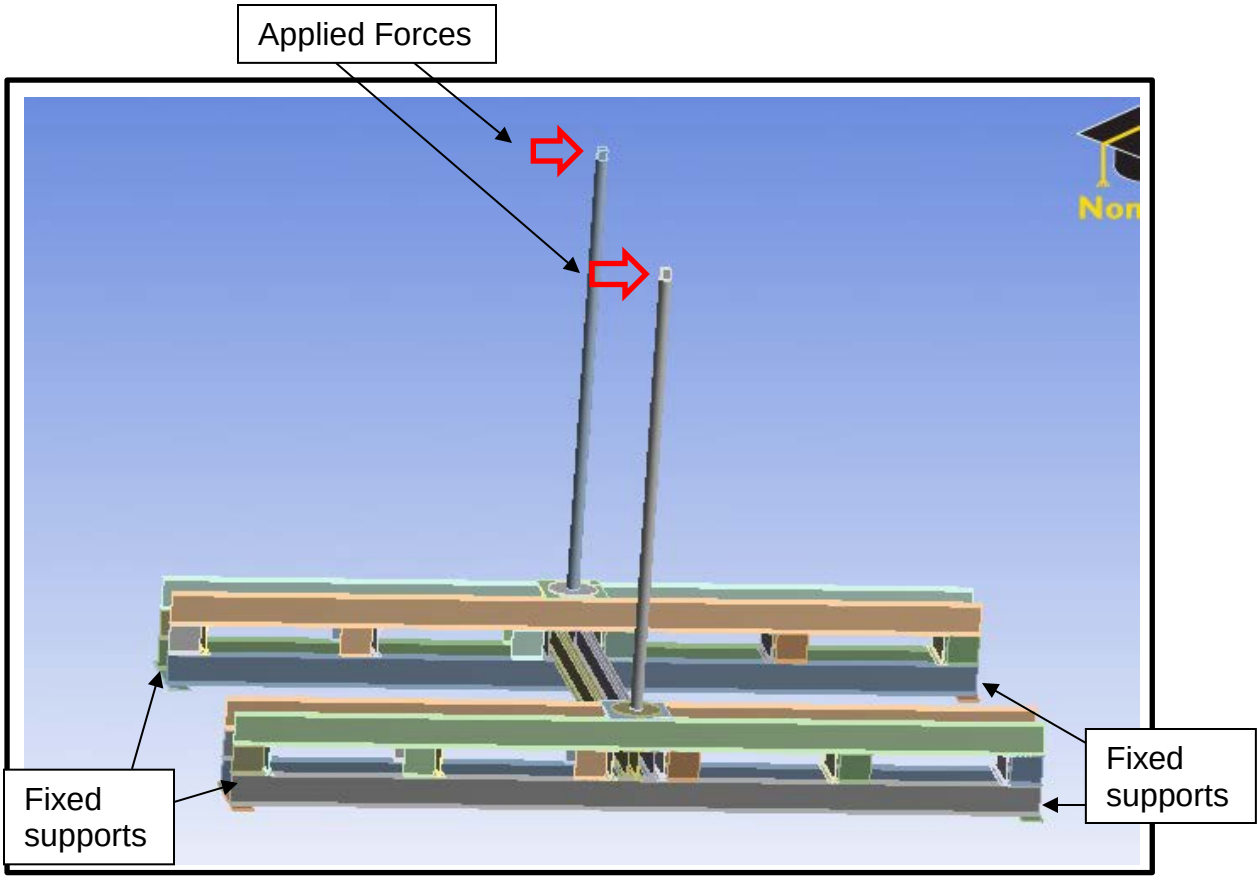

Figure 53. ANSYS Mechanical Set-up.

ANSYS Static Structural calculated the total deformation, equivalent stress, and equivalent elastic strain on the beam design. Appendix N displays the ANSYS Static Structural simulation details.

Figure 54 displays the deformation in the beams. The maximum deformation in the beams is 0.00016527 m. UGE provided that the max deformation should not be above 0.045 m: the beam design meets these standards.

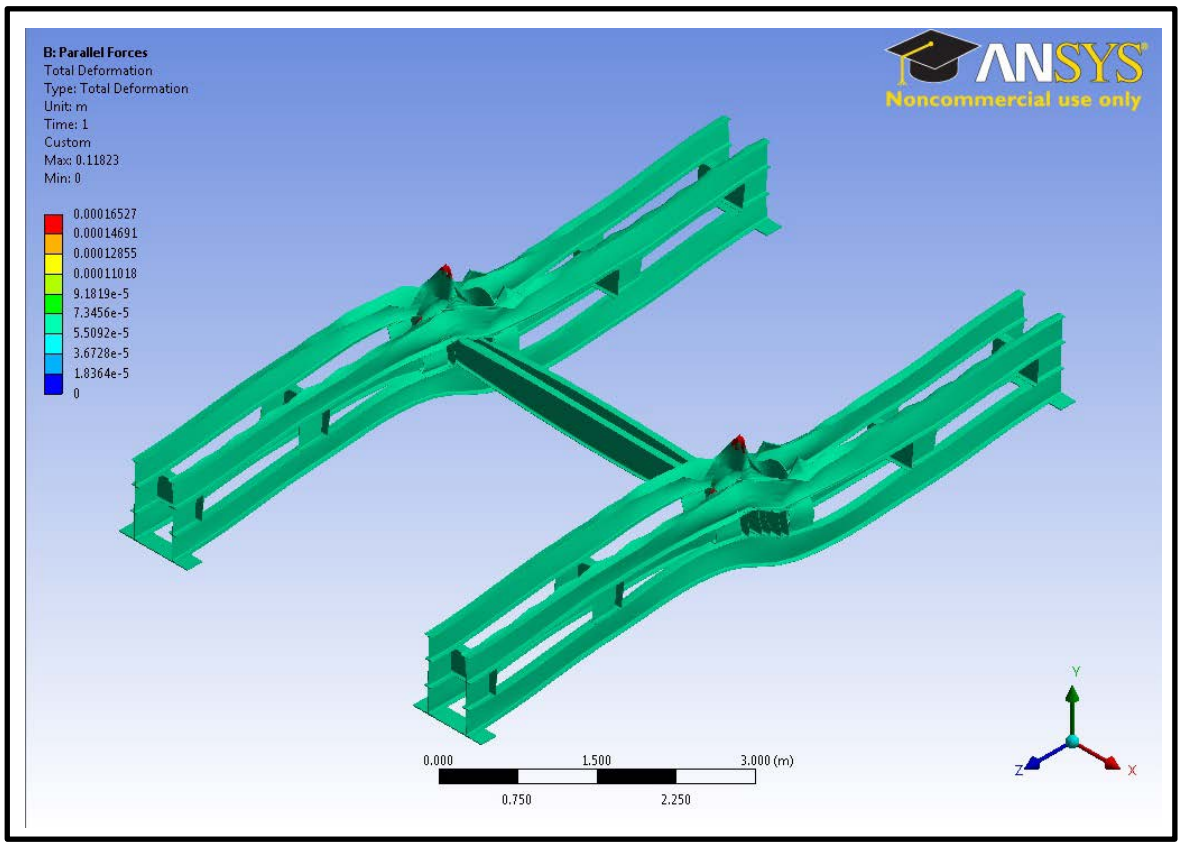

Figure 54. Total Deformation on the beams.

The stress on the beams is shown in Figure 55. The beam design experiences limited stress. The max stress in the beams is 119 MPa. This is below the yield strength of A36 structural steel, which is 250 MPa: the stiffness of the structure was the design constraint.

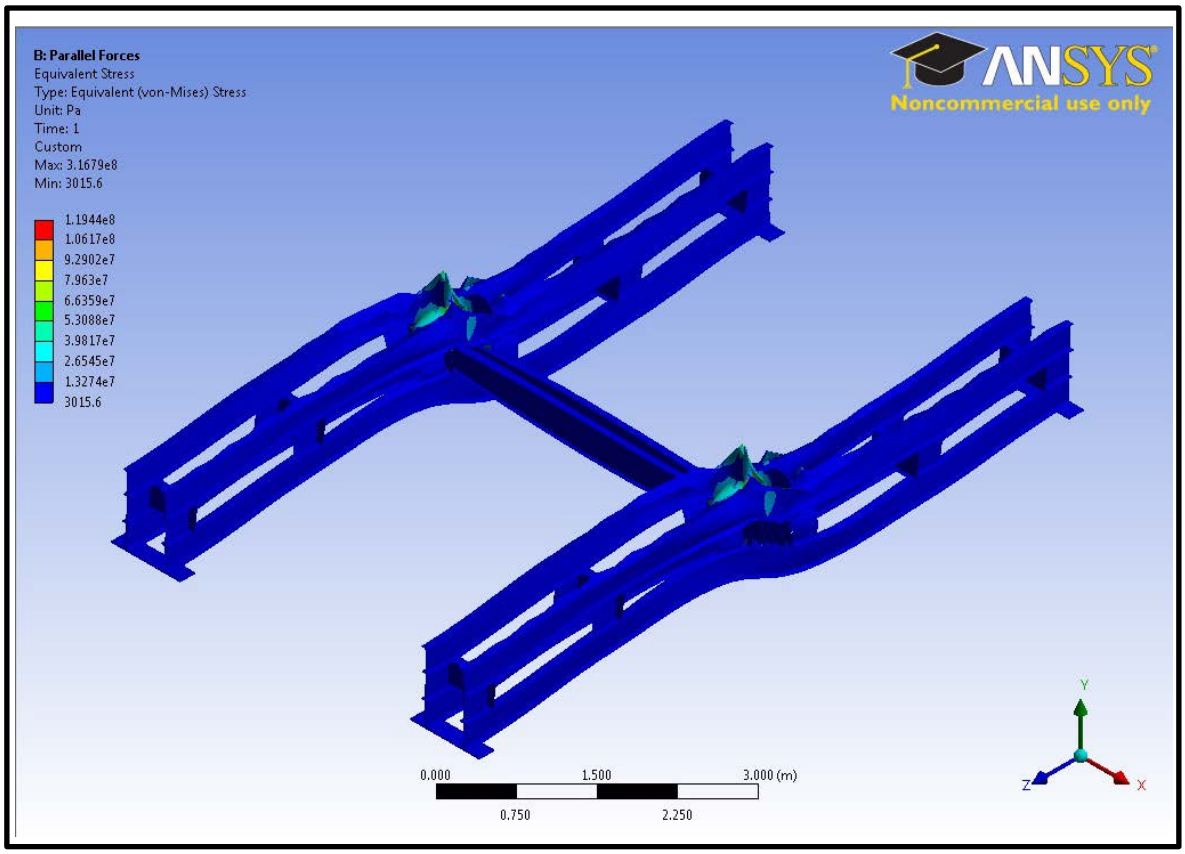

Figure 55. Equivalent stress on the beams.

Figure 56 shows the strain on the beams. The max strain on the beam design is 0.00061 m/m, which is not problematic for structural steel and ensures that the wind turbines will not deflect above their limiting rate.

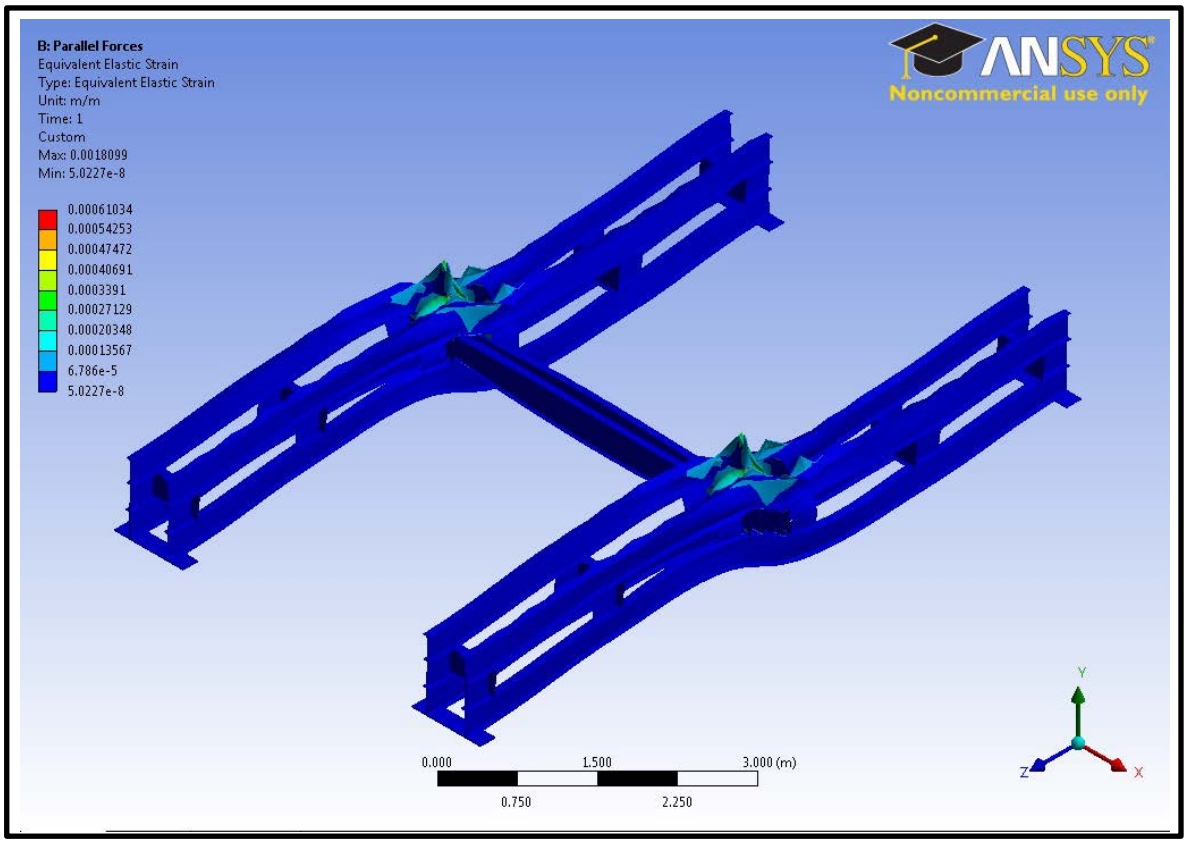

Figure 56. Equivalent strain on the beams.

The shear force was reapplied at an angle perpendicular to the quadrature beams. It is important to test the integrity of the beams at the most extreme conditions. The most extreme loading will occur when the shear forces from the wind turbines are applied parallel and perpendicular to the structure. A separate loading case was simulated with the shear force applied perpendicular to the beams orientation. The perpendicular loading produces much greater torsion on the beam.

Figure 57 displays the perpendicular loading in ANSYS Static Structural. The ANSYS Static Structural simulation details are listed in Appendix O.

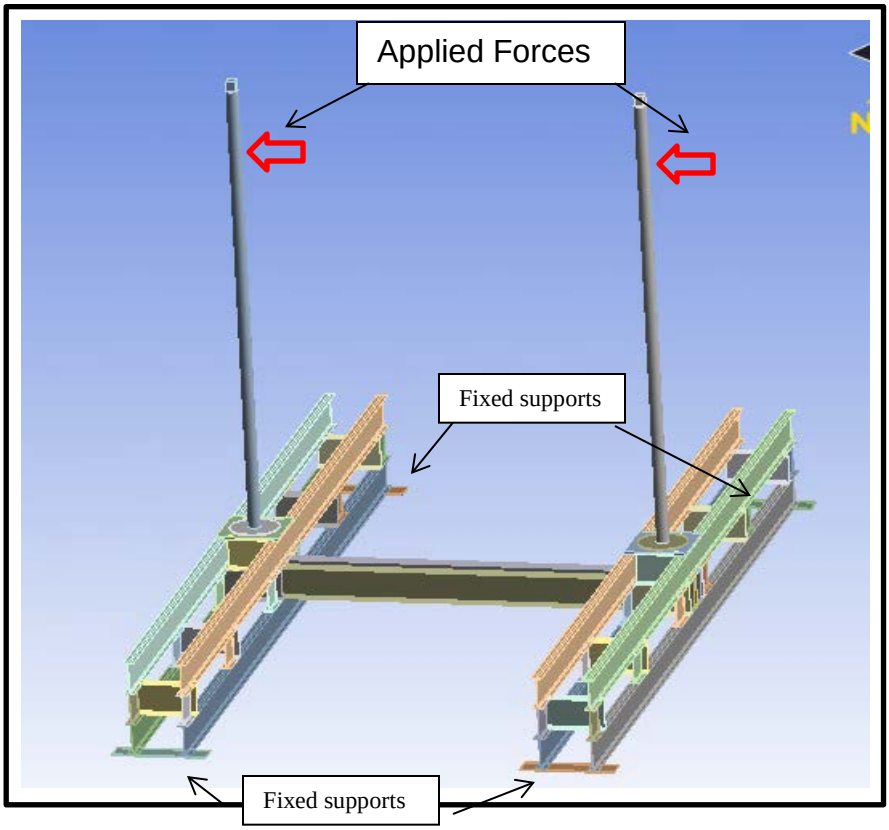

Figure 57. Perpendicular loading in ANSYS mechanical.

Figure 58 displays the results of the deformation simulation. There is very little deformation in the beam design. The max deformation is 0.0083317 m, which is below the max allowed value of 0.045 m.

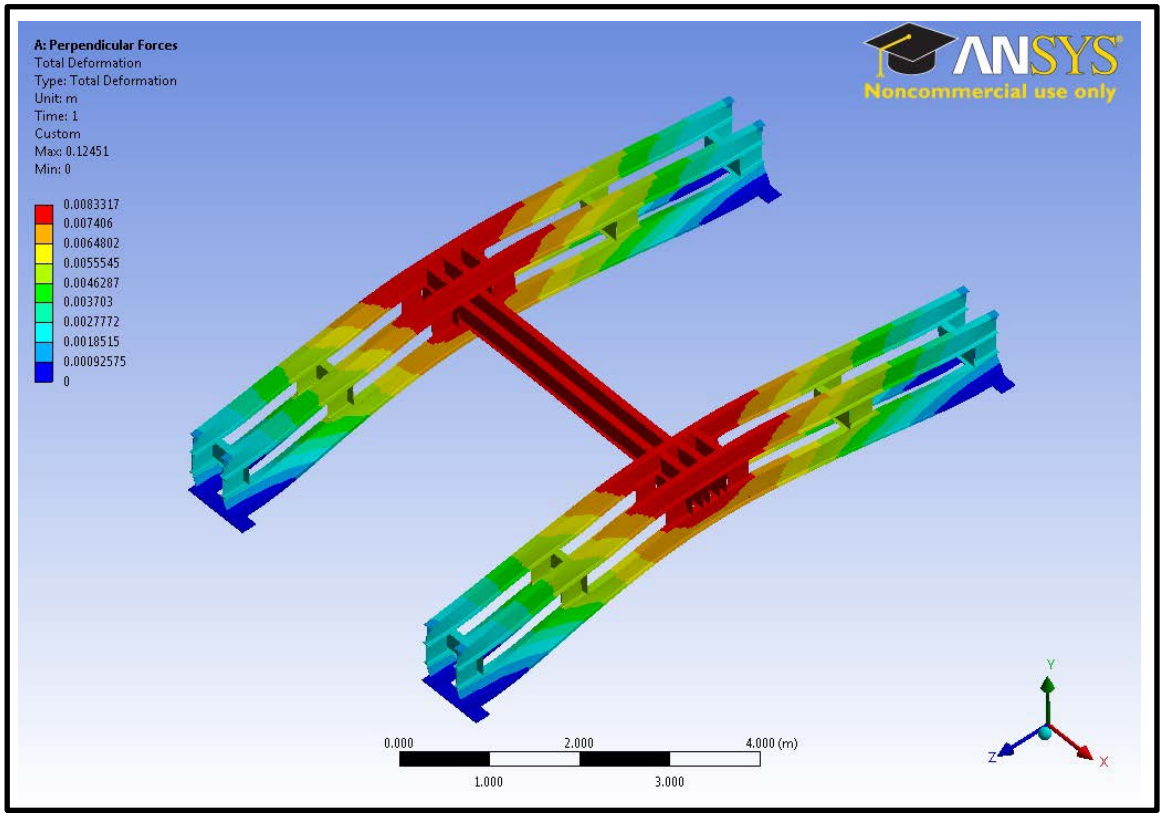

Figure 58. Deformation.

Figure 59 shows the results of the strain simulation. The equivalent strain on the beam design is limited. The max value reaches 0.001323 m/m.

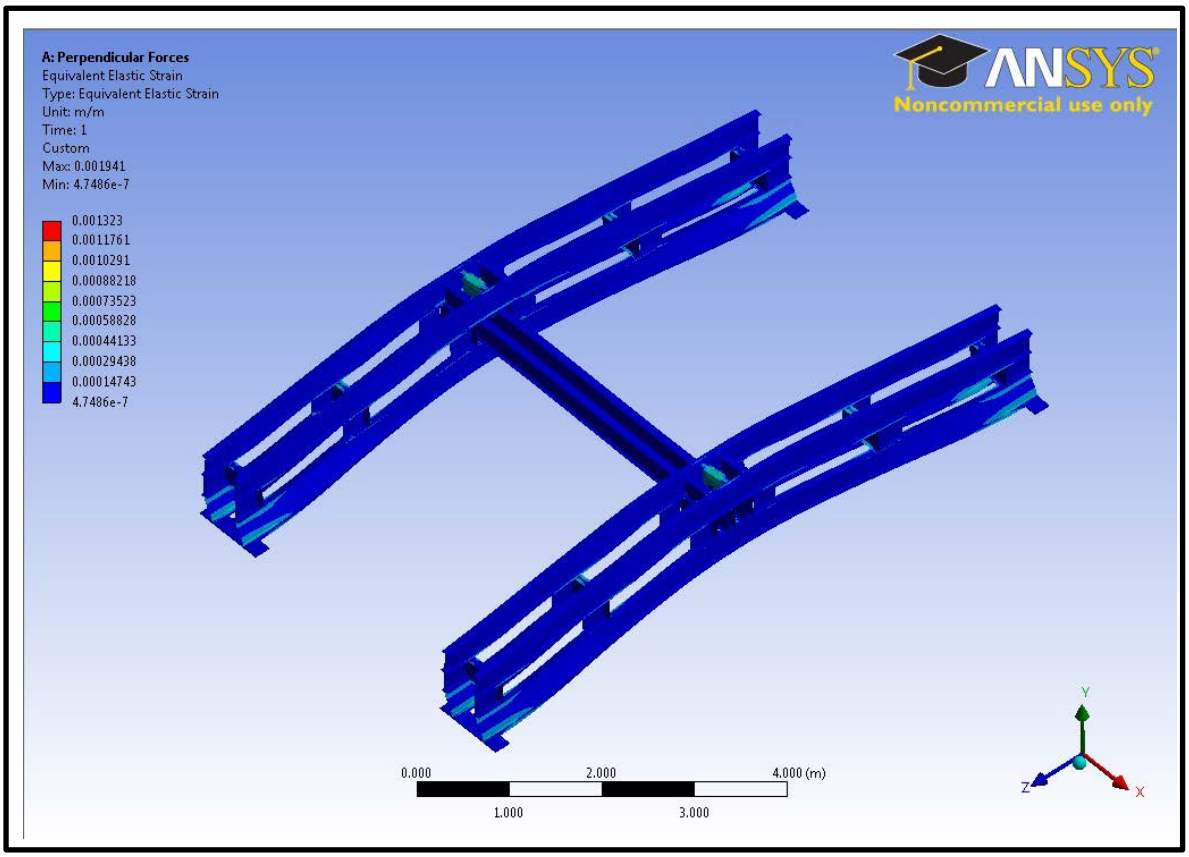

Figure 59. Equivalent strain on beam design.

Figure 60 shows the simulation stress results. The maximum stress on the beam structure is 262 MPa, which is located at the center support for the wind turbine flange.

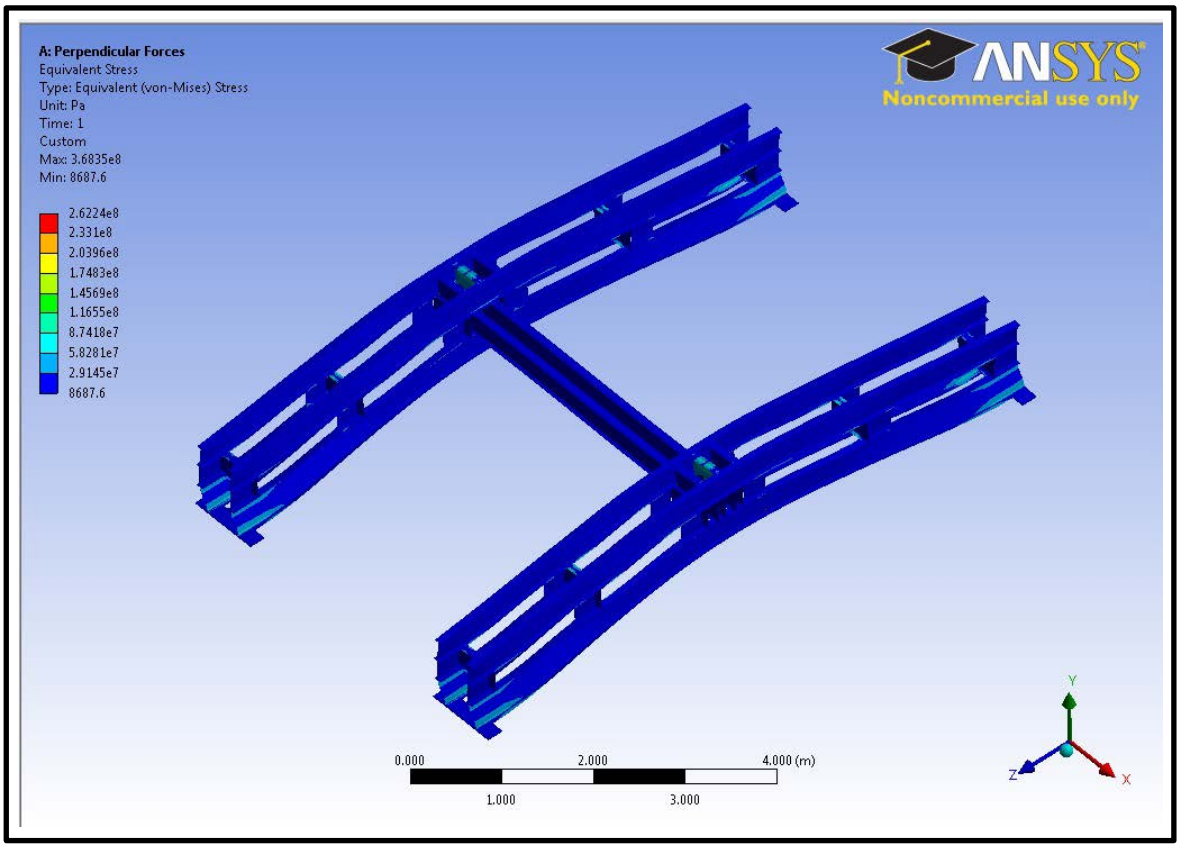

Figure 60. Equivalent Stress on beam design.

The max stress on the beams is illustrated in Figure 61.

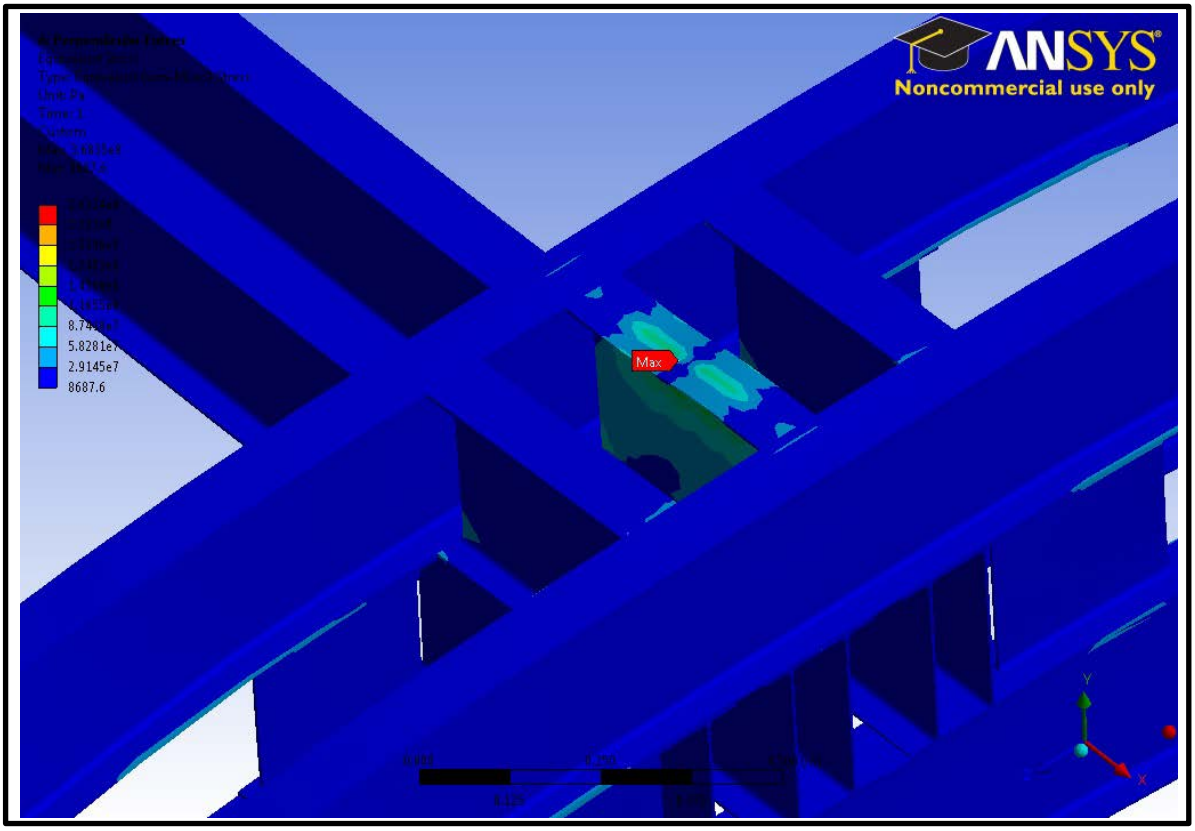

Figure 61. Max stress on beam structure.

The max stress is just above the yield strength of structural steel, which is 250 MPa. However, the loading condition used in the analysis is for the worst case scenario: the prescribed loading conditions are for winds of 50 m/s (112 mph). Winds of 50 m/s define a category III hurricane [23]. A category III hurricane would cause extensive structural damage to all structures and buildings. A category III hurricane is extremely unlikely to occur in California. It is safe to assume the beam design will withstand a wide range of operating conditions. However, it should be taken into account that if winds reach 50 m/s, there is the potential for deformation on the center flange support beams but failure will not occur.

4. Results

From the analysis in ANSYS Static Structural, the structural integrity of the beam design was proven. A few modifications were made to the final design.

The final beam design is depicted in Figures 62 and 63. A representative wind turbine is depicted on the beam. The wind turbine encompasses the same volume as the selected VAWTS. Engineering drawings of the beam structures were created in Solidworks. These were used to manufacture the beams. Refer to Appendix P for the engineering drawings.

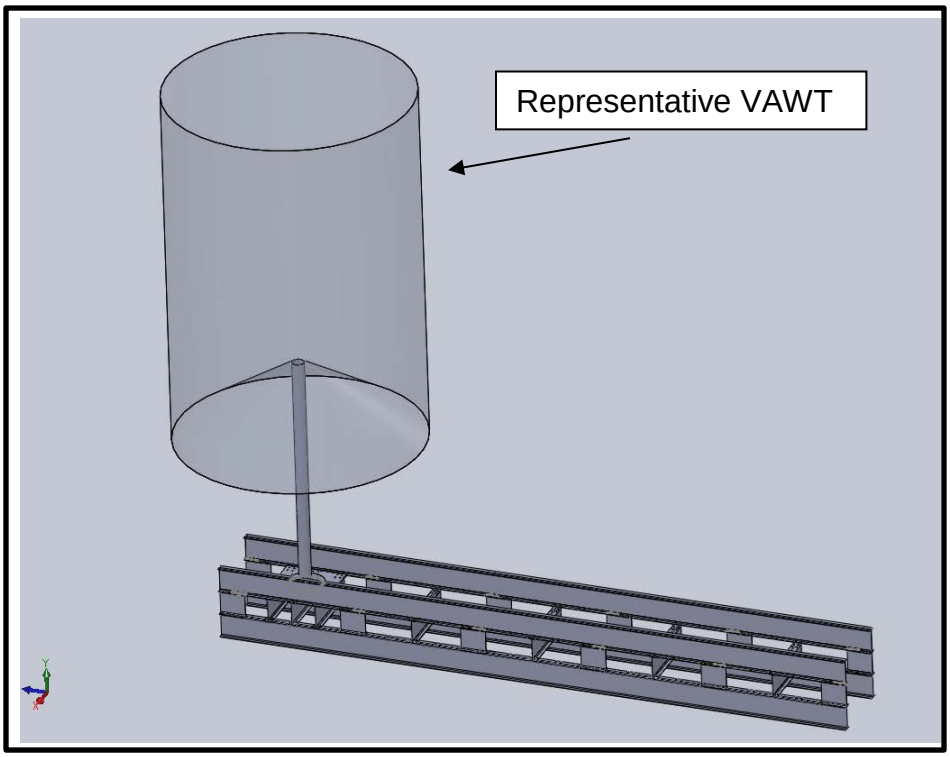

Figure 62. Final beam design front view.

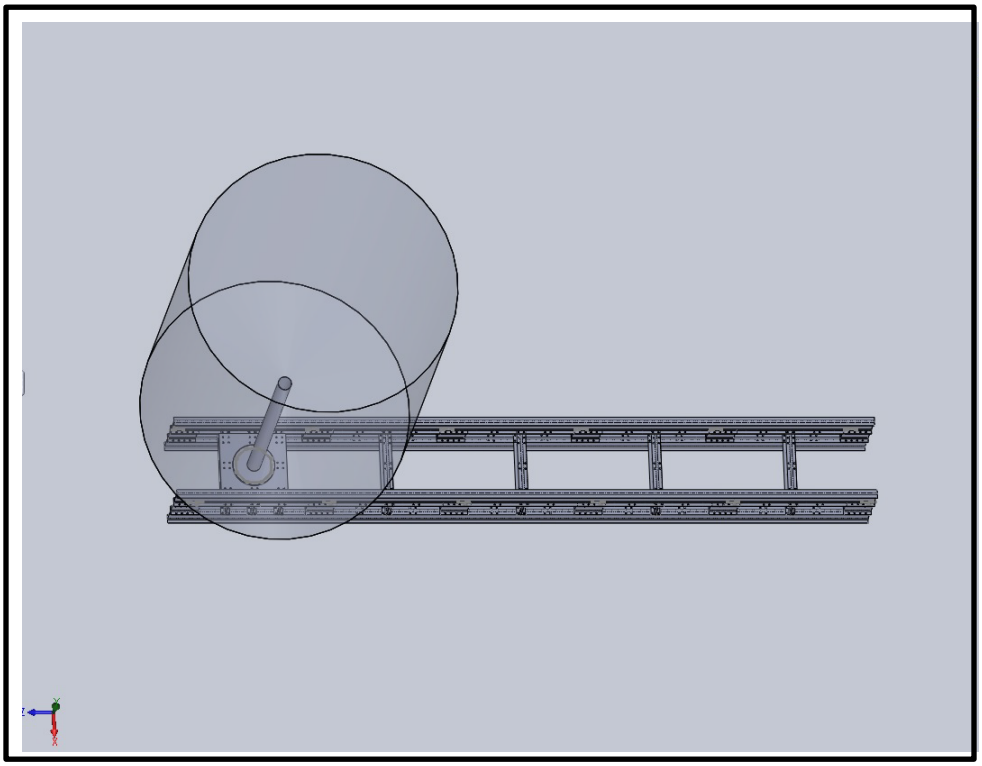

Figure 63. Final beam design front view from top.

Figures 64 and 65 display the final beam design with the connecting spine beam on the roof of Building 216.

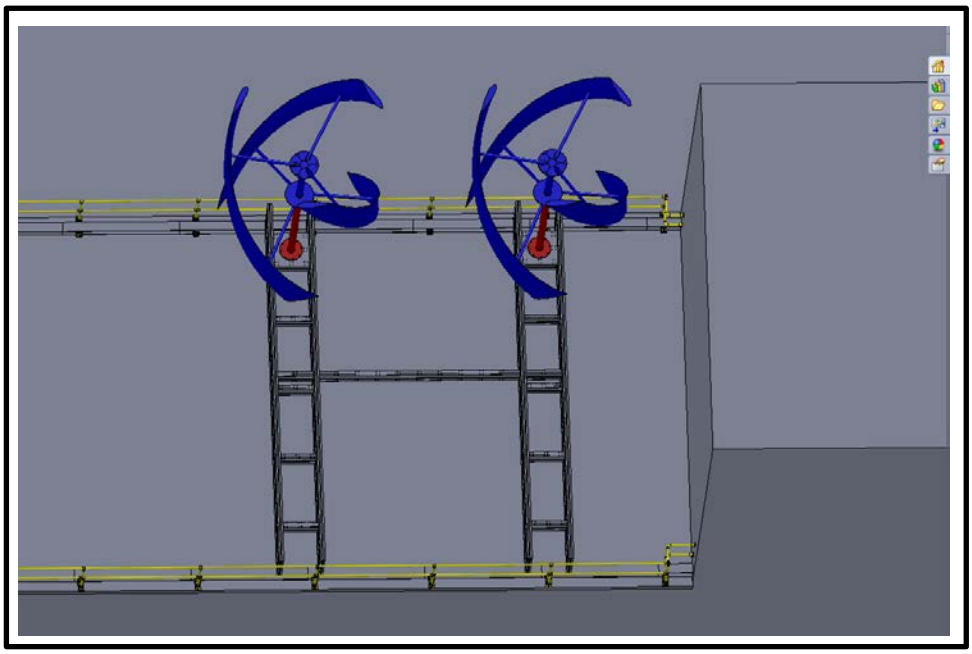

Figure 64. The final design with spine beam on Building 216. From [24].

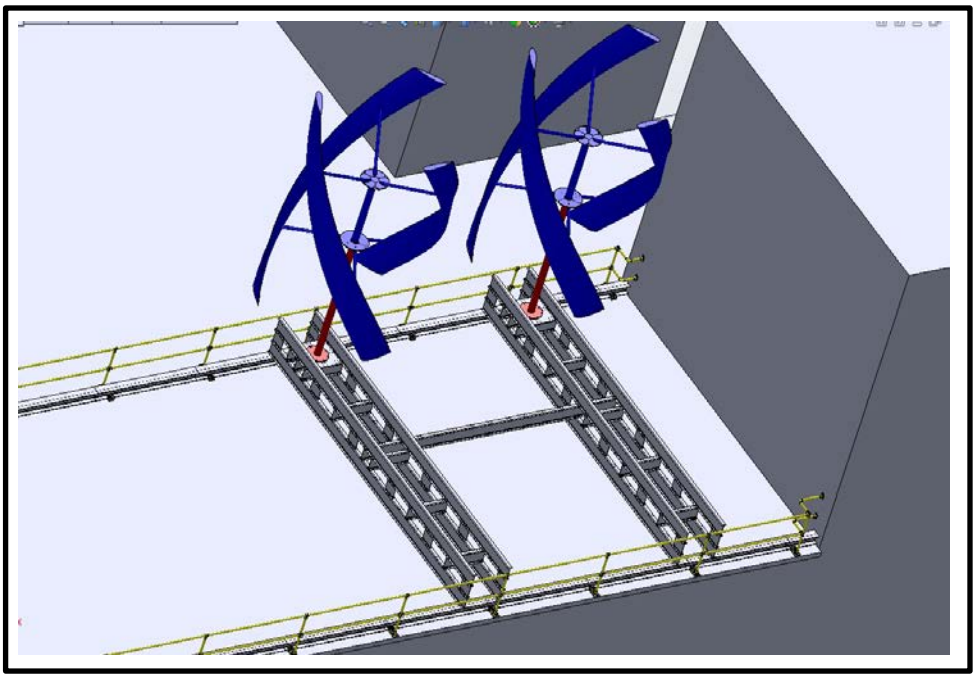

Figure 65. Closer image of final design with spine beam on Building 216. From [24].

Figure 66 is a summary of the VAWT placement on Building 216. It illustrates VAWTS with three helically shaped blades placed at the northern edge of the south roof. The wind turbines are closely spaced. The beam support structure is connected by a cross sectional beam for additional torsional support.

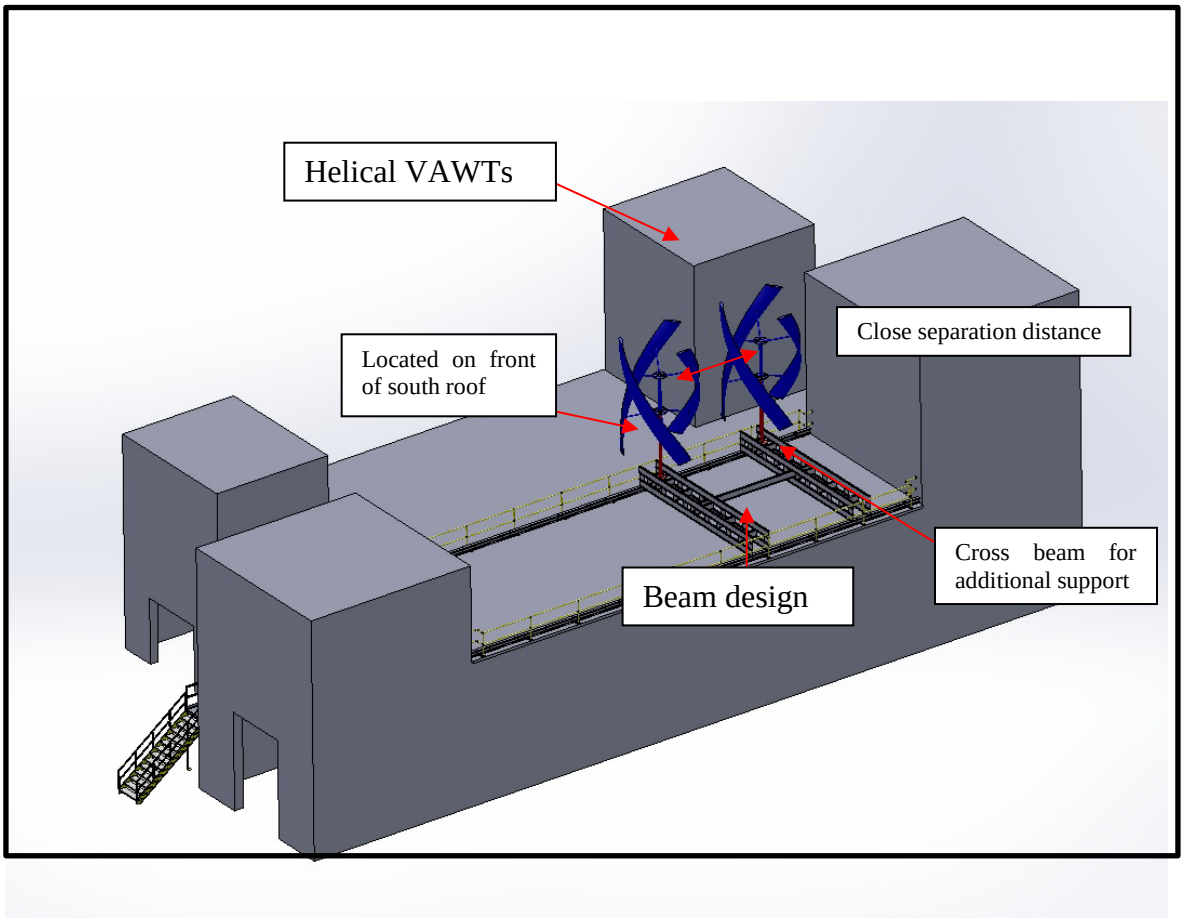

Figure 66. Summary of VAWT placement. From [24].

Figure 67 displays the construction on Building 216 at the time this thesis report was completed. The railings and stairways have been installed up to the upper south ledge.

Figure 67. Construction on Building 216 at time of report.

IV. CONCLUSIONS

The analysis presented above resulted in the following conclusions to the previously stated objectives:

1. The optimal location for the wind turbines in on the northern edge of the south roof of the TPL.

2. A two-bladed helical VAWT has the best performance.

3. For the application onto the roof of the TPL, a lack of availability led to the selection of the next best performing VAWT, a three-bladed helical design.

4. A beam structure was created to support the wind turbines on the roof.

5. Close spacing between VAWTS potentially benefits their performance. The VAWTS will be tightly spaced onto the roof of Building 216.

THIS PAGE INTENTIONALLY LEFT BLANK

V. RECOMMENDATIONS FOR FUTURE WORK

There are a few important recommendations for future research to expand on this thesis. It is worth researching how side winds affect the performance of VAWTS. This thesis was limited to analyzing winds approaching from the average wind direction. The wind turbines were placed so they would directly capture wind flow around the building: they were not positioned so that one wind turbine would receive wind flow through the other. If the wind approaches from a skewed wind direction, there could be some blockage effects on one wind turbine by the other wind turbine. These blockage effects should be further investigated to determine if there is any detriment to the performance of the wind turbines.

Additional future research is to analyze how VAWTS perform at close spacing across a full range of TSRs. This thesis conducted these simulations at a single TSR of 0.5. Another topic worthy of investigation is to analyze how modifications to the roofs of buildings can improve wind flow for wind turbines. For example, the addition of curved roof ledges could decrease early fluid separation on the building structure, resulting in a higher velocity fluid flow for the wind turbines.

THIS PAGE INTENTIONALLY LEFT BLANK

APPENDIX A: SAMPLE OF WIND DATA PROVIDED BY FNMOC

WBAN	YR--MODAHRMN	DIR	SPD MPH			
23245	198001010000	999	0			
23245	198001010100	999	0		Total number of observations:	282,494
23245	198001010200	999	0		Average overall wind speed:	6.06147
23245	198001010300	120	7			
23245	198001010400	110	6			
23245	198001010415	999	0		Variable	0.023239
23245	198001010500	999	0		Calm	0.208256
23245	198001010520	30	4		N	0.021377
23245	198001010600	40	3		NNE	0.005062
23245	198001010700	999	0		NE	0.006248
23245	198001010800	999	0		ENE	0.010659
23245	198001010900	999	0		E	0.052185
23245	198001011000	999	0		ESE	0.06398
23245	198001011100	999	0		SE	0.035983
23245	198001011200	999	0		SSE	0.018726
23245	198001011300	999	0		S	0.032358
23245	198001011400	999	0		SSW	0.034748
23245	198001011500	999	0		SW	0.050851
23245	198001011519	999	0		WSW	0.080738
23245	198001011600	999	0		W	0.144201
23245	198001011700	999	0		WNW	0.099379
23245	198001011800	100	4		NW	0.083712
23245	198001011900	100	4		NNW	0.046167
23245	198001012000	999	0			
23245	198001012100	290	9			
23245	198001012102	270	8			
23245	198001012200	270	9			
23245	198001012220	270	7			
23245	198001012300	270	7			
23245	198001020000	290	6			
23245	198001020100	999	0			
23245	198001020200	140	4			
23245	198001020300	999	0			
23245	198001020400	999	0			
23245	198001020500	90	6			
23245	198001020600	80	6			
23245	198001020700	110	6			
23245	198001020800	100	6			
23245	198001020900	100	6			

THIS PAGE INTENTIONALLY LEFT BLANK

APPENDIX B: MESH DETAILS FOR WIND FLOW ANALYSIS

Meshing Highlights	
Mesh Methods	Inflation and Face Sizing
Use Advanced Sizing Method	On: Proximity and Curvature
Relevance Center	Fine
Span Angle Center	Fine
Number of Nodes	172,957
Number of Elements	582,531

THIS PAGE INTENTIONALLY LEFT BLANK

APPENDIX C: ANSYS CFX SPECIFICAITONS FOR WIND FLOW ANALYSIS

Physics Report

Domain Physics for Vel_4m s_30deg
Domain - Default Domain
Type Fluid
Location B72
Materials
Air Ideal Gas
Fluid Definition Material Library
Morphology Continuous Fluid
Settings
Buoyancy Model Non Buoyant
Domain Motion Stationary
Reference Pressure 1.0000e+00 [atm]
Heat Transfer Model Total Energy
Include Viscous Work Term On
Turbulence Model k epsilon
Turbulent Wall Functions Scalable
High Speed Model Off

Boundary Physics for Vel_4m s_30deg
Domain Boundaries
Default Domain Boundary - Inlet
Type INLET
Location Inlet
Settings
Flow Regime Subsonic
Heat Transfer Total Temperature
Total Temperature 2.8815e+02 [K]
Mass And Momentum Normal Speed
Normal Speed 4.0000e+00 [m s^-1]
Turbulence Medium Intensity and Eddy Viscosity Ratio
Boundary - Openings
Type OPENING
Location Openings
Settings
Flow Regime Subsonic
Heat Transfer Opening Temperature
Opening Temperature 2.8815e+02 [K]
Mass And Momentum Entrainment

Relative Pressure 0.0000e+00 [Pa]
Turbulence Zero Gradient
Boundary - Outlet
Type OUTLET
Location Outlet
Settings
Flow Regime Subsonic
Mass And Momentum Average Static Pressure
Pressure Profile Blend 5.0000e-02
Relative Pressure 0.0000e+00 [Pa]
Pressure Averaging Average Over Whole Outlet
Boundary - Default Domain Default
Type WALL
Location "F163.72, F164.72, F165.72, F166.72, F167.72, F168.72, F169.72, F170.72, F171.72, F172.72, F173.72, F174.72, F175.72, F74.72, F79.72, F80.72, F81.72, F82.72, F83.72, F84.72, F85.72, F86.72, F87.72, F88.72, F89.72, F90.72, F91.72, F92.72, F93.72, F94.72, F95.72, F96.72, F97.72"
Settings
Heat Transfer Adiabatic
Mass And Momentum No Slip Wall
Wall Roughness Smooth Wall

APPENDIX D: SINGLE ROTOR ANALYSIS ANSYS CFX MESH DETAILS

Details of "Mesh"	
Defaults	
Sizing	
Use Advanced Size Fun...	On: Curvature
Relevance Center	Fine
Initial Size Seed	Active Assembly
Smoothing	Medium
Transition	Slow
Span Angle Center	Fine
Curvature Normal A...	1.0 °
Min Size	1.e-004 m
Max Face Size	2.e-002 m
Max Size	2.e-002 m
Growth Rate	1.20
Minimum Edge Length	3.6435e-004 m
Inflation	
Use Automatic Inflation	None
Inflation Option	Smooth Transition
Transition Ratio	0.77
Maximum Layers	5
Growth Rate	1.2
Inflation Algorithm	Pre
View Advanced Options	No
Patch Conforming Options	
Advanced	
Shape Checking	CFD
Element Midside Nodes	Dropped
Straight Sided Elements	
Number of Retries	0
Extra Retries For Assem...	Yes
Rigid Body Behavior	Dimensionally Reduced
Mesh Morphing	Disabled
Defeaturing	
Statistics	
Nodes	186898
Elements	91047
Mesh Metric	None

Details of "Sweep Method" - Method	
Scope	
Scoping Method	Geometry Selection
Geometry	1 Body
Definition	
Suppressed	No
Method	Sweep
Element Midside Nodes	Use Global Setting
Src/Trg Selection	Automatic
Source	Program Controlled
Target	Program Controlled
Free Face Mesh Type	All Quad
Type	Number of Divisions
Sweep Num Divs	1
Sweep Bias Type	No Bias
Element Option	Solid

THIS PAGE INTENTIONALLY LEFT BLANK

APPENDIX E: SINGLE ROTOR ANALYSIS, ANSYS CFX SPECIFICS

Physics Report

Table 3. Domain Physics for CFX

Domain - Rotor	
Type	Fluid
Location	B122
Materials	
Air Ideal Gas	
Fluid Definition	Material Library
Morphology	Continuous Fluid
Settings	
Buoyancy Model	Non Buoyant
Domain Motion	Rotating
Angular Velocity	Rotor Omega
Axis Definition	Coordinate Axis
Rotation Axis	Coord 0.3
Reference Pressure	1.0000e+00 [atm]
Heat Transfer Model	Total Energy
Turbulence Model	k epsilon
Turbulent Wall Functions	Scalable
High Speed Model	Off
Domain - Stator	
Type	Fluid
Location	B242
Materials	
Air Ideal Gas	
Fluid Definition	Material Library
Morphology	Continuous Fluid
Settings	
Buoyancy Model	Non Buoyant
Domain Motion	Stationary
Reference Pressure	1.0000e+00 [atm]
Heat Transfer Model	Total Energy
Turbulence Model	k epsilon
Turbulent Wall Functions	Scalable
High Speed Model	Off
Domain Interface - Domain Interface 1	
Boundary List1	Domain Interface 1 Side 1
Boundary List2	Domain Interface 1 Side 2
Interface Type	Fluid Fluid
Settings	

Interface Models General Connection
Frame Change Transient Rotor Stator
Mass And Momentum Conservative Interface Flux
Mesh Connection GGI

Table 4. Boundary Physics for CFX
Domain Boundaries
Rotor Boundary - Domain Interface 1 Side 1
Type INTERFACE
Location R1_int
Settings
Heat Transfer Conservative Interface Flux
Mass And Momentum Conservative Interface Flux
Turbulence Conservative Interface Flux
Boundary - Sym1a
Type SYMMETRY
Location Sym1a
Settings
Boundary - Sym1b
Type SYMMETRY
Location Sym1b
Settings
Boundary - Rotor Default
Type WALL
Location "F116.122, F117.122, F118.122, F119.122, F120.122, F124.122, F125.122, F127.122, F128.122, F129.122, F130.122, F131.122, F132.122, F133.122, F134.122, F135.122, F136.122, F137.122, F138.122, F139.122, F140.122, F141.122, F142.122, F143.122, F144.122, F145.122, F146.122, F147.122, F148.122, F149.122, F150.122, F151.122, F152.122, F153.122, F154.122, F155.122"
Settings
Heat Transfer Adiabatic
Mass And Momentum No Slip Wall
Wall Roughness Smooth Wall
Stator Boundary - Inlet
Type INLET
Location Inlet
Settings
Flow Regime Subsonic
Heat Transfer Static Temperature
Static Temperature 2.8815e+02 [K]
Mass And Momentum Cartesian Velocity Components
U Inlet U
V 0.0000e+00 [m s^-1]
W 0.0000e+00 [m s^-1]

Turbulence Medium Intensity and Eddy Viscosity Ratio
Boundary - Domain Interface 1 Side 2
Type INTERFACE
Location S1_int
Settings
Heat Transfer Conservative Interface Flux
Mass And Momentum Conservative Interface Flux
Turbulence Conservative Interface Flux
Boundary - Bottom
Type OPENING
Location Bottom
Settings
Flow Regime Subsonic
Heat Transfer Static Temperature
Static Temperature 2.8815e+02 [K]
Mass And Momentum Entrainment
Relative Pressure 0.0000e+00 [Pa]
Turbulence Zero Gradient
Boundary - Top
Type OPENING
Location Top
Settings
Flow Regime Subsonic
Heat Transfer Opening Temperature
Opening Temperature 2.8815e+02 [K]
Mass And Momentum Entrainment
Relative Pressure 0.0000e+00 [Pa]
Turbulence Zero Gradient
Boundary - Outlet
Type OUTLET
Location Outlet
Settings
Flow Regime Subsonic
Mass And Momentum Average Static Pressure
Pressure Profile Blend 5.0000e-02
Relative Pressure 0.0000e+00 [Pa]
Pressure Averaging Average Over Whole Outlet
Boundary - Sym1
Type SYMMETRY
Location Sym1
Settings
Boundary - Sym2
Type SYMMETRY
Location Sym2

THIS PAGE INTENTIONALLY LEFT BLANK

APPENDIX F: DETAILED RESULTS OF SINGLE ROTOR SIMULATIONS

	Wind Speed	Rotor Omega (rad/s)	RPM	TSR	Torque (N m)	ρ_{air} Inlet (kg/m^3)	Power (W)	Cp
3 Blades	4	2	19.099	0.25	0.00138087	1.17	0.00276174	0.007376
	4	4	38.197	0.5	0.00117457	1.17	0.00469827	0.012549
	4	8	76.394	1	0.00106728	1.17	0.00853826	0.022805
	4	10	95.493	1.25	0.00175109	1.17	0.01751087	0.04677
	4	12	114.59	1.5	0.00283	1.17	0.03396	0.090705
	4	16	152.79	2	0.00437294	1.17	0.06996701	0.186878
	4	24	229.18	3	0.00700504	1.17	0.16812099	0.449041
	4	32	305.58	4	0.00401367	1.17	0.12843729	0.343048
	4	36	343.77	4.5	0.00176409	1.17	0.06350708	0.169624
	4	48	458.37	6	-0.003217	1.17	-0.1544163	-0.41244
18 blades	4	2	19.099	0.25	0.00349041	1.17	0.00698081	0.018645
	4	4	38.197	0.5	0.00302002	1.17	0.01208009	0.032265
	4	8	76.394	1	0.00384841	1.17	0.03078726	0.082231
	4	16	152.79	2	0.00028854	1.17	0.00461658	0.012331
6 Blades	4	2	19.099	0.25	0.00237173	1.17	0.00474345	0.012669
	4	4	38.197	0.5	0.00236026	1.17	0.00944104	0.025216
	4	8	76.394	1	0.00292137	1.17	0.02337098	0.062422
	4	12	114.59	1.5	0.00433789	1.17	0.05205469	0.139035
	4	24	152.79	3	0.00150096	1.17	0.02401533	0.064144
2 Blades	4	2	19.099	0.25	0.00091042	1.17	0.00182085	0.004863
	4	4	38.197	0.5	0.00081414	1.17	0.00325657	0.008698
	4	8	76.394	1	0.00064376	1.17	0.00515011	0.013756
	4	12	114.59	1.5	0.00172908	1.17	0.02074902	0.055419
	4	16	152.79	2	0.0028818	1.17	0.04610879	0.123154
	4	24	229.18	3	0.0072795	1.17	0.17470798	0.466635
	4	28	267.38	3.5	0.00627624	1.17	0.17573485	0.469377
	4	32	305.58	4	0.00542155	1.17	0.17348956	0.46338
	4	48	458.37	6	-0.0001348	1.17	-0.0064707	-0.01728

THIS PAGE INTENTIONALLY LEFT BLANK

APPENDIX G: UGE 4KW VAWT DIMENSIONAL DRAWINGS

Technical Documentation

UGE-4K Dimensional Drawing

Document Number (s): UGE-4K-DIM-001

Original Date: April 6, 2011

Revised On: July 20, 2011

Version: 1.12

Completed by: ST

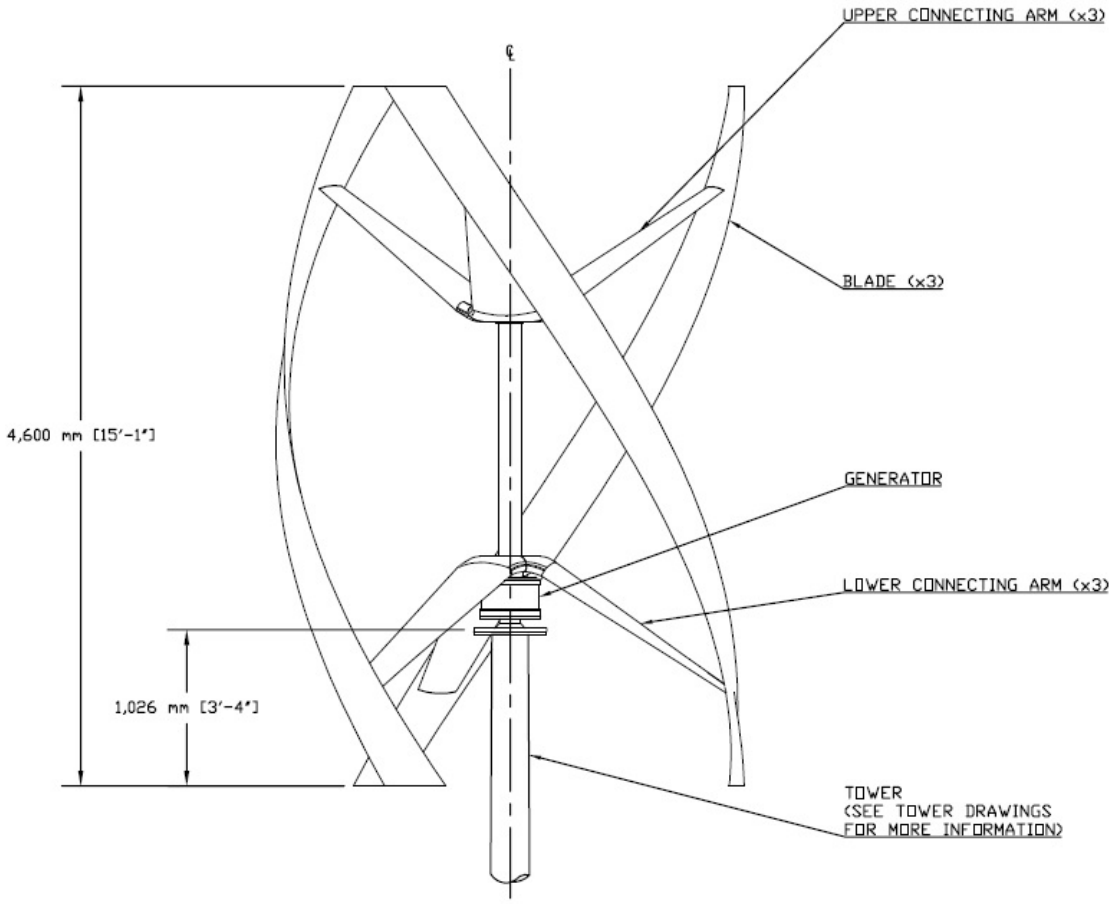

TURBINE - SIDE VIEW

DRAWING NOTES:

1. THIS DRAWING IS BEING ISSUED FOR INFORMATION ONLY.
2. ALL VALUES ARE SHOWN "METRIC [ENGLISH]"
3. DRAWING NOT TO SCALE. DO NOT SCALE DIMENSIONS FROM DRAWING.

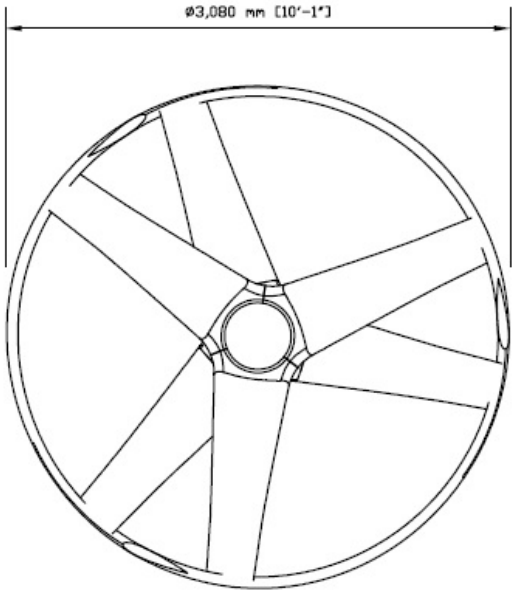

TURBINE – TOP VIEW

THIS PAGE INTENTIONALLY LEFT BLANK

APPENDIX H: DUAL ROTOR MESH DETAILS

Details of "Mesh"	
Defaults	
Physics Preference	CFD
Solver Preference	CFX
Relevance	0
Sizing	
Use Advanced Size Function	On: Curvature
Relevance Center	Fine
Initial Size Seed	Active Assembly
Smoothing	Medium
Transition	Slow
Span Angle Center	Fine
Curvature Normal Angle	1.0 °
Min Size	1.e-004 m
Max Face Size	2.e-002 m
Max Size	2.e-002 m
Growth Rate	1.20
Minimum Edge Length	3.6435e-004 m
Inflation	
Patch Conforming Options	
Triangle Surface Mesher	Program Controlled
Advanced	
Shape Checking	CFD
Element Midside Nodes	Dropped
Straight Sided Elements	
Number of Retries	0
Extra Retries For Assembly	Yes
Rigid Body Behavior	Dimensionally Reduced
Mesh Morphing	Disabled
Defeaturing	
Statistics	
Nodes	216380
Elements	104776
Mesh Metric	None

Details of "Edge Sizing 3" - Sizing	
Scope	
Scoping Method	Geometry Selection
Geometry	1 Edge
Definition	
Suppressed	No
Type	Number of Divisions
Number of Divisions	1000
Behavior	Soft
Curvature Normal Angle	1.0 °
Growth Rate	1.20
Bias Type	No Bias

Details of "Sweep Method" - Method	
Scope	
Scoping Method	Geometry Selection
Geometry	1 Body
Definition	
Suppressed	No
Method	Sweep
Element Midside Nodes	Use Global Setting
Src/Trg Selection	Automatic
Source	Program Controlled
Target	Program Controlled
Free Face Mesh Type	All Quad
Type	Number of Divisions
Sweep Num Divs	1
Sweep Bias Type	No Bias
Element Option	Solid

APPENDIX I: DUAL ROTOR ANALYSIS- ANSYS CFX SPECIFICATIONS (6 BLADED VAWTS)

Physics Report

Table 3. Domain Physics for Fluid Flow CFX_010

Domain - Rotor 1
Type Fluid
Location B242
Materials
Air Ideal Gas
Fluid Definition Material Library
Morphology Continuous Fluid
Settings
Buoyancy Model Non Buoyant
Domain Motion Rotating
Angular Velocity 4.0000e+01 [rev min^-1]
Axis Definition Two Points
Rotation Axis From "0 [m], 0.505 [m], 0 [m]"
Rotation Axis To "0 [m], 0.505 [m], 0.01 [m]"
Reference Pressure 1.0000e+00 [atm]
Heat Transfer Model Total Energy
Turbulence Model k epsilon
Turbulent Wall Functions Scalable
High Speed Model Off

Domain - Rotor 2
Type Fluid
Location B320
Materials
Air Ideal Gas
Fluid Definition Material Library
Morphology Continuous Fluid
Settings
Buoyancy Model Non Buoyant
Domain Motion Rotating
Angular Velocity -4.0000e+01 [rev min^-1]
Axis Definition Two Points
Rotation Axis From "0 [m], -0.505 [m], 0 [m]"
Rotation Axis To "0 [m], -0.505 [m], 0.01 [m]"
Reference Pressure 1.0000e+00 [atm]
Heat Transfer Model Total Energy
Turbulence Model k epsilon
Turbulent Wall Functions Scalable
High Speed Model Off

Domain - Stator
Type Fluid
Location B24
Materials
Air Ideal Gas
Fluid Definition Material Library
Morphology Continuous Fluid
Settings
Buoyancy Model Non Buoyant
Domain Motion Stationary
Reference Pressure 1.0000e+00 [atm]
Heat Transfer Model Total Energy
Turbulence Model k epsilon
Turbulent Wall Functions Scalable
High Speed Model Off
Domain Interface - Domain Interface 1
Boundary List1 Domain Interface 1 Side 1
Boundary List2 Domain Interface 1 Side 2
Interface Type Fluid Fluid
Settings
Interface Models General Connection
Frame Change Transient Rotor Stator
Mass And Momentum Conservative Interface Flux
Mesh Connection GGI
Domain Interface - Domain Interface 2
Boundary List1 Domain Interface 2 Side 1
Boundary List2 Domain Interface 2 Side 2
Interface Type Fluid Fluid
Settings
Interface Models General Connection
Frame Change Transient Rotor Stator
Mass And Momentum Conservative Interface Flux
Mesh Connection GGI

Boundary Physics for Fluid Flow CFX_010
Domain Boundaries
Rotor 1 Boundary - Domain Interface 2 Side 1
Type INTERFACE
Location R2_int
Settings
Heat Transfer Conservative Interface Flux
Mass And Momentum Conservative Interface Flux
Turbulence Conservative Interface Flux
Boundary - Sym 1a

Type SYMMETRY
Location Sym 1a
Settings
Boundary - Sym 2a
Type SYMMETRY
Location Sym 2a
Settings
Boundary - Rotor 1 Default
Type WALL
Location "F245.242, F246.242, F247.242, F248.242, F249.242, F250.242, F251.242, F252.242, F253.242, F254.242, F255.242, F256.242"
Settings
Heat Transfer Adiabatic
Mass And Momentum No Slip Wall
Wall Roughness Smooth Wall
Rotor 2 Boundary - Domain Interface 1 Side 1
Type INTERFACE
Location R1_int
Settings
Heat Transfer Conservative Interface Flux
Mass And Momentum Conservative Interface Flux
Turbulence Conservative Interface Flux
Boundary - Sym 1b
Type SYMMETRY
Location Sym 1b
Settings
Boundary - Sym 2b
Type SYMMETRY
Location Sym 2b
Settings
Boundary - Rotor 2 Default
Type WALL
Location "F323.320, F324.320, F325.320, F326.320, F327.320, F328.320, F329.320, F330.320, F331.320, F332.320, F333.320, F334.320"
Settings
Heat Transfer Adiabatic
Mass And Momentum No Slip Wall
Wall Roughness Smooth Wall
Stator Boundary - Inlet
Type INLET
Location Inlet
Settings
Flow Regime Subsonic
Heat Transfer Static Temperature
Static Temperature 3.0000e+02 [K]

Mass And Momentum Cartesian Velocity Components
U 5.0000e+00 [m s^-1]
V 0.0000e+00 [m s^-1]
W 0.0000e+00 [m s^-1]
Turbulence Medium Intensity and Eddy Viscosity Ratio
Boundary - Domain Interface 1 Side 2
Type INTERFACE
Location S1_int
Settings
Heat Transfer Conservative Interface Flux
Mass And Momentum Conservative Interface Flux
Turbulence Conservative Interface Flux
Boundary - Domain Interface 2 Side 2
Type INTERFACE
Location S2_int
Settings
Heat Transfer Conservative Interface Flux
Mass And Momentum Conservative Interface Flux
Turbulence Conservative Interface Flux
Boundary - Bottom
Type OPENING
Location Bottom
Settings
Flow Regime Subsonic
Heat Transfer Opening Temperature
Opening Temperature 3.0000e+02 [K]
Mass And Momentum Cartesian Velocity Components
U 5.0000e+00 [m s^-1]
V 0.0000e+00 [m s^-1]
W 0.0000e+00 [m s^-1]
Turbulence Medium Intensity and Eddy Viscosity Ratio
Boundary - Top
Type OPENING
Location Top
Settings
Flow Regime Subsonic
Heat Transfer Opening Temperature
Opening Temperature 3.0000e+02 [K]
Mass And Momentum Cartesian Velocity Components
U 5.0000e+00 [m s^-1]
V 0.0000e+00 [m s^-1]
W 0.0000e+00 [m s^-1]
Turbulence Medium Intensity and Eddy Viscosity Ratio
Boundary - Outlet
Type OUTLET

Location Outlet
Settings
Flow Regime Subsonic
Mass And Momentum Average Static Pressure
Pressure Profile Blend 5.0000e-02
Relative Pressure 0.0000e+00 [Pa]
Pressure Averaging Average Over Whole Outlet
Boundary - Sym 1
Type SYMMETRY
Location Sym 1
Settings
Boundary - Sym 2
Type SYMMETRY
Location Sym 2
Settings

THIS PAGE INTENTIONALLY LEFT BLANK

APPENDIX J: DUAL ROTOR ANALYSIS- DETAILED RESULTS

# of Blades	Spacing (m)	RPM	Wind-speed (m/s)	In/ Outwards	Total Time (s)	Time-Step (s/deg)	Upper Torque (N m)	Lower Torque (N m)
6	0.01	40	4	In	9	0.0042	0.00462	0.00480109
6	0.1	40	4	In	9	0.0042	0.004604	0.0051441
6	0.4	40	4	In	9	0.0042	0.004967	0.00471179
9	0.01	40	4	In	9	0.0042	0.006252	0.00693616
9	0.1	40	4	In	9	0.0042	0.005818	0.006813
9	0.4	40	4	In	9	0.0042	0.006038	0.00566301
3	0.01	40	4	In	9	0.0042	0.002662	0.00261224
3	0.1	40	4	In	9	0.0042	0.002441	0.00238132
3	0.4	40	4	In	9	0.0042	0.002377	0.00225533
18	0.1	40	4	In	9	0.0042	0.009404	0.0094158

# of Blades	Spacing (m)	Total Torque (N m)	Velocity Inlet (m/s)	ρ_{air} Inlet (kg/m^3)	Power (W)	Cp	TSR
6	0.01	0.0094	4.999	1.1764	0.03946474	0.026853	0.52359878
6	0.1	0.0097	4.999	1.1765	0.04083104	0.027782	0.52359878
6	0.4	0.0097	4.999	1.176	0.04054179	0.027596	0.52359878
9	0.01	0.0132	5	1.1765	0.05524166	0.037563	0.52359878
9	0.1	0.0126	5	1.1765	0.0529104	0.035977	0.52359878
9	0.4	0.0117	5	1.1765	0.0490136	0.033328	0.52359878
3	0.01	0.0053	5	1.17	0.02209282	0.015106	0.52359878
3	0.1	0.0048	5	1.17	0.02020166	0.013813	0.52359878
3	0.4	0.0046	5	1.17	0.01940208	0.013266	0.52359878
18	0.1	0.0188	5	1.1767	0.07883141	0.053597	0.52359878

THIS PAGE INTENTIONALLY LEFT BLANK

APPENDIX K: UGE 4KW VAWT LOAD SPECIFICATIONS

Technical Documentation

Loads Specifications for UGE-4K
112 mph (50 m/s)

Document Number (s): UGE-4K-LDS-001

Original Date: March 16, 2012

Revised On: April 12, 2012

Version: 1.1

Completed by: JATG

Checked by: SVP

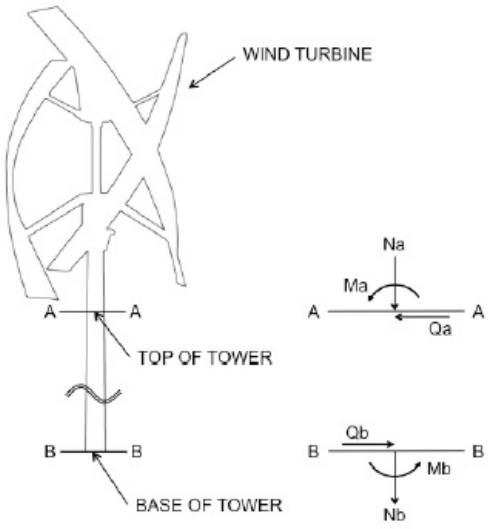

UGE-4K
Vertical Axis Wind Turbine Specifications

Load Specifications
50 m/s (112 mph)

Maximum Loads at the A-A plane (For all of towers)	
Nmax	4.52 KN [1.02 k]
Qmax	5.28 KN [1.19 k]
Mmax	8.34 KN*m [6.15 k*ft]

Maximum Loads at the B-B plane	
3M Tower	
Nmax	13.15 KN [2.96 k]
Qmax	7.78 KN [1.75 k]
Mmax	33.81 KN*m [24.93 k*ft]
7M Tower	
Nmax	15.29 KN [3.44 k]
Qmax	8.86 KN [1.99 k]
Mmax	69.18 KN*m [51.0 k*ft]
13M Tower	
Nmax	21.19 KN [4.76 k]
Qmax	14.93 KN [3.36 k]
Mmax	158.96 KN*m [117.21 k*ft]
20M Tower	
Nmax	30.93 KN [6.95 k]
Qmax	23.97 KN [5.39 k]
Mmax	321.86 KN*m [237.33 k*ft]

Tower Notes:

- Maximum wind speed: 50 m/s
- When the applicable load per the table above is applied to the turbine and tower, the maximum deflection of the structure supporting the turbine and tower should meet the standard deflection tolerances of the local building code. For steel and concrete structures in the USA, deflections should meet the requirements of the AISC or ACI codes respectively. The lateral deflection of the top of the tower should under no circumstances be above 1.5% of the tower height.
- The turbine operating frequency ranges between 0 and 2.1Hz. Care should be taken to prevent resonance between the turbine and the supporting structure.
- Tower should include a J-hook or other means of strain relief for the leads leaving the generator, upper and lower hand holes at either end of the tower, and be properly grounded and connected to a lightning protection system (if present) per the NEC or the local electrical code.
- Please see the UGE Warranty Agreement for information about the implications of designing your own tower on the turbine's warranty.

THIS PAGE INTENTIONALLY LEFT BLANK

APPENDIX L: LOWER FLANGE DRAWING UGE 4KW VAWT

Technical Documentation

Lower Flange Drawing for UGE-4K

Drawing Number (s): UGE-4K-FNG-001

Original Date: March 7, 2011

Revised On: June 15, 2012

Version: 1.1

Completed by: MCO

Checked by: SVP

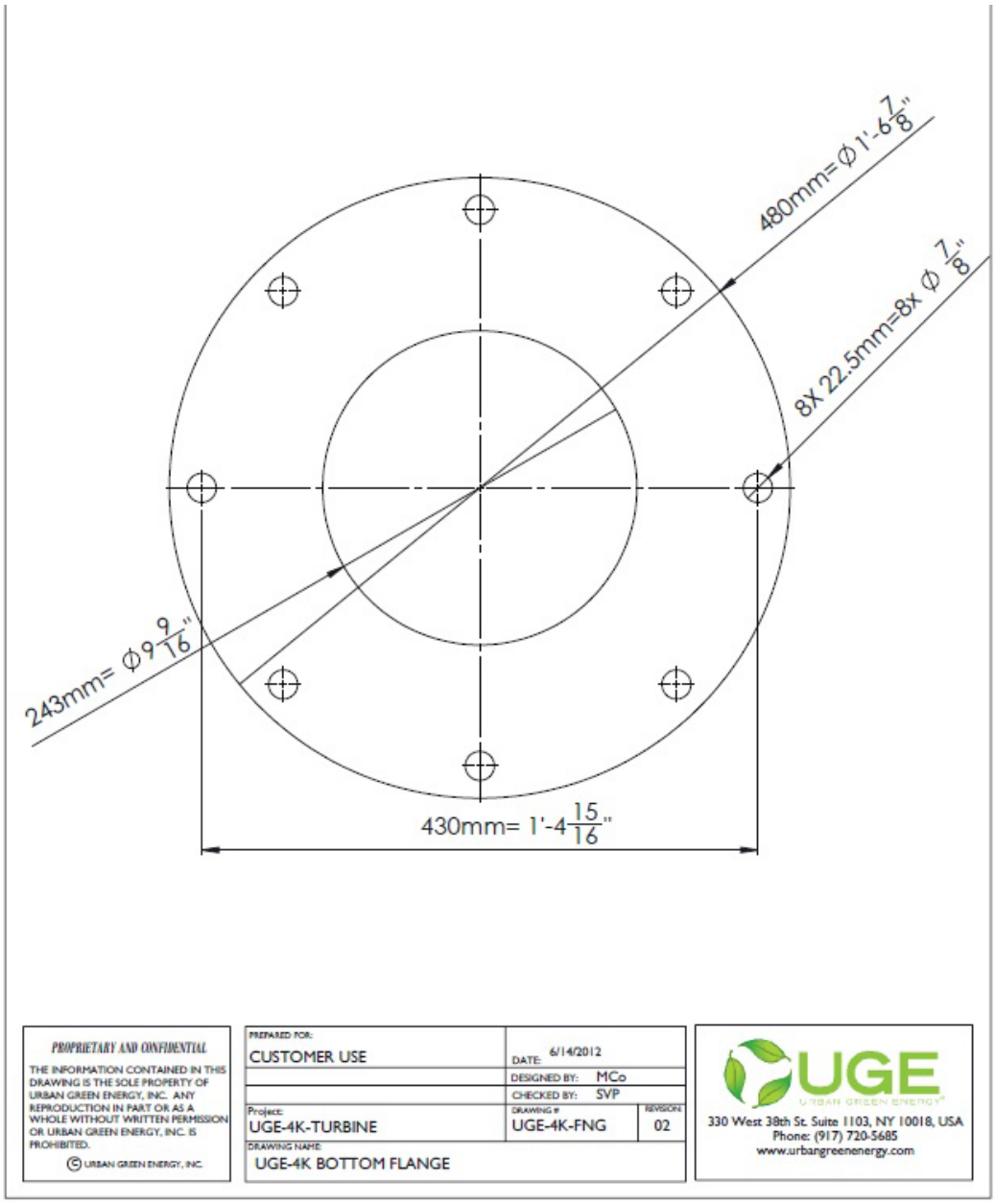

PROPRIETARY AND CONFIDENTIAL

THE INFORMATION CONTAINED IN THIS DRAWING IS THE SOLE PROPERTY OF URBAN GREEN ENERGY, INC. ANY REPRODUCTION IN PART OR AS A WHOLE WITHOUT WRITTEN PERMISSION OR URBAN GREEN ENERGY, INC. IS PROHIBITED.

© URBAN GREEN ENERGY, INC.

PREPARED FOR: CUSTOMER USE	DATE: 6/14/2012	
	DESIGNED BY: MCo	
	CHECKED BY: SVP	
Project: UGE-4K-TURBINE	DRAWING #: UGE-4K-FNG	REVISION: 02
DRAWING NAME: UGE-4K BOTTOM FLANGE		

UGE
URBAN GREEN ENERGY
330 West 38th St. Suite 1103, NY 10018, USA
Phone: (917) 720-5685
www.urbangreenenergy.com

APPENDIX M: MESH DETAILS BEAM DESIGN ANALYSIS

Object Name	*Mesh*
State	Solved
Defaults	
Physics Preference	Mechanical
Relevance	0
Sizing	
Use Advanced Size Function	Off
Relevance Center	Coarse
Element Size	Default
Initial Size Seed	Active Assembly
Smoothing	Medium
Transition	Fast
Span Angle Center	Coarse
Minimum Edge Length	5.715e-003 m
Inflation	
Use Automatic Inflation	None
Inflation Option	Smooth Transition
Transition Ratio	0.272
Maximum Layers	5
Growth Rate	1.2
Inflation Algorithm	Pre
View Advanced Options	No
Patch Conforming Options	
Triangle Surface Mesher	Program Controlled
Advanced	
Shape Checking	Standard Mechanical
Element Midside Nodes	Program Controlled
Straight Sided Elements	No
Number of Retries	Default (4)
Extra Retries For Assembly	Yes
Rigid Body Behavior	Dimensionally Reduced
Mesh Morphing	Disabled
Defeaturing	
Pinch Tolerance	Please Define
Generate Pinch on Refresh	No
Automatic Mesh Based Defeaturing	On
Defeaturing Tolerance	Default
Statistics	
Nodes	103068
Elements	16007
Mesh Metric	None

THIS PAGE INTENTIONALLY LEFT BLANK

APPENDIX N: ANSYS STATIC STRUCTURAL BEAM DESIGN SPECIFICS FOR APPLIED PARALLEL FORCES

STATIC STRUCTURAL (A5)

TABLE 60
Model (A4) > Analysis

Object Name	*Static Structural (A5)*
State	Solved
Definition	
Physics Type	Structural
Analysis Type	Static Structural
Solver Target	Mechanical APDL
Options	
Environment Temperature	22. °C
Generate Input Only	No

TABLE 61
Model (A4) > Static Structural (A5) > Analysis Settings

Object Name	*Analysis Settings*
State	Fully Defined
Step Controls	
Number Of Steps	1.
Current Step Number	1.
Step End Time	1. s
Auto Time-Stepping	Program Controlled
Solver Controls	
Solver Type	Program Controlled
Weak Springs	Program Controlled
Large Deflection	Off
Inertia Relief	Off
Restart Controls	
Generate Restart Points	Program Controlled
Retain Files After Full Solve	No
Nonlinear Controls	
Force Convergence	Program Controlled
Moment Convergence	Program Controlled
Displacement Convergence	Program Controlled
Rotation Convergence	Program Controlled
Line Search	Program Controlled
Stabilization	Off
Output Controls	
Stress	Yes
Strain	Yes
Nodal Forces	No
Contact Miscellaneous	No

General Miscellaneous	No
Calculate Results At	All Time Points
Max Number of Result Sets	Program Controlled
Analysis Data Management	
Solver Files Directory	J:\Taylor\beamanalysis_files\dp0\SYS\MECH\
Future Analysis	None
Scratch Solver Files Directory	
Save MAPDL db	No
Delete Unneeded Files	Yes
Nonlinear Solution	No
Solver Units	Active System
Solver Unit System	mks

TABLE 62
Model (A4) > Static Structural (A5) > Loads

Object Name	*Force*	*Force 2*	*Fixed Support*	*Fixed Support 2*	*Fixed Support 3*
State	Fully Defined				
Scope					
Scoping Method	Geometry Selection				
Geometry	1 Face				
Definition					
Type	Force		Fixed Support		
Define By	Vector				
Magnitude	7800. N (ramped)				
Direction	Defined				
Suppressed	No				

FIGURE 1
Model (A4) > Static Structural (A5) > Force

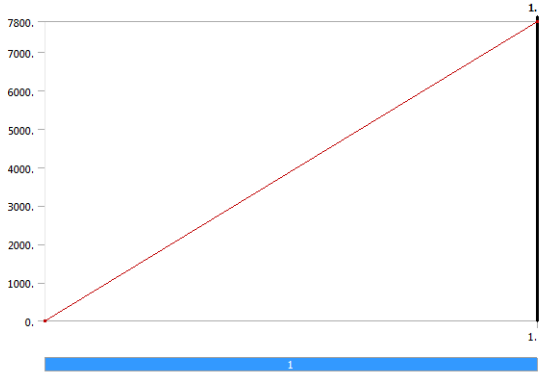

FIGURE 2
Model (A4) > Static Structural (A5) > Force 2

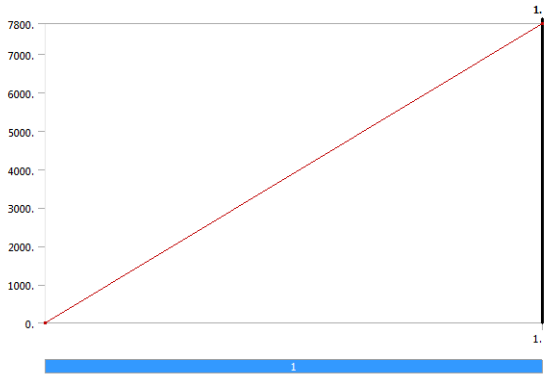

TABLE 63
Model (A4) > Static Structural (A5) > Loads

Object Name	*Fixed Support 4*
State	Fully Defined
Scope	
Scoping Method	Geometry Selection
Geometry	1 Face
Definition	
Type	Fixed Support
Suppressed	No

Solution (A6)

TABLE 64
Model (A4) > Static Structural (A5) > Solution

Object Name	*Solution (A6)*
State	Solved
Adaptive Mesh Refinement	
Max Refinement Loops	1.
Refinement Depth	2.
Information	
Status	Done

TABLE 65
Model (A4) > Static Structural (A5) > Solution (A6) > Solution Information

Object Name	*Solution Information*
State	Solved
Solution Information	
Solution Output	Solver Output
Newton-Raphson Residuals	0
Update Interval	2.5 s
Display Points	All
FE Connection Visibility	
Activate Visibility	Yes

Display	All FE Connectors
Draw Connections Attached To	All Nodes
Line Color	Connection Type
Visible on Results	No
Line Thickness	Single
Display Type	Lines

TABLE 66
Model (A4) > Static Structural (A5) > Solution (A6) > Results

Object Name	*Equivalent Stress*	*Total Deformation*	*Equivalent Elastic Strain*
State	Solved		
Scope			
Scoping Method	Geometry Selection		
Geometry	All Bodies		
Definition			
Type	Equivalent (von-Mises) Stress	Total Deformation	Equivalent Elastic Strain
By	Time		
Display Time	Last		
Calculate Time History	Yes		
Identifier			
Suppressed	No		
Integration Point Results			
Display Option	Averaged		Averaged
Results			
Minimum	8687.6 Pa	0. m	4.7486e-007 m/m
Maximum	3.6835e+008 Pa	0.12451 m	1.941e-003 m/m
Minimum Occurs On	W12x14_divider	basesupportrevised	W12x14_divider
Maximum Occurs On	lower flangenoholes	pole	lower flangenoholes
Information			
Time	1. s		
Load Step	1		
Substep	1		
Iteration Number	1		

TABLE 67
Model (A4) > Static Structural (A5) > Solution (A6) > Stress Safety Tools

Object Name	*Stress Tool*
State	Solved
Definition	
Theory	Max Equivalent Stress
Stress Limit Type	Tensile Yield Per Material

TABLE 68
Model (A4) > Static Structural (A5) > Solution (A6) > Stress Tool > Results

Object Name	*Safety Factor*
State	Solved
Scope	
Scoping Method	Geometry Selection

Geometry	All Bodies
Definition	
Type	Safety Factor
By	Time
Display Time	Last
Calculate Time History	Yes
Identifier	
Suppressed	No
Integration Point Results	
Display Option	Averaged
Results	
Minimum	0.6787
Minimum Occurs On	lower flangenoholes
Information	
Time	1. s
Load Step	1
Substep	1
Iteration Number	1

THIS PAGE INTENTIONALLY LEFT BLANK

APPENDIX O: ANSYS STATIC STRUCTURAL BEAM DESIGN SPECIFICS FOR APPLIED PERPENDICULAR FORCES

STATIC STRUCTURAL (A5)

TABLE 60
Model (A4) > Analysis

Object Name	*Static Structural (A5)*
State	Solved
Definition	
Physics Type	Structural
Analysis Type	Static Structural
Solver Target	Mechanical APDL
Options	
Environment Temperature	22. °C
Generate Input Only	No

TABLE 61
Model (A4) > Static Structural (A5) > Analysis Settings

Object Name	*Analysis Settings*
State	Fully Defined
Step Controls	
Number Of Steps	1.
Current Step Number	1.
Step End Time	1. s
Auto Time-Stepping	Program Controlled
Solver Controls	
Solver Type	Program Controlled
Weak Springs	Program Controlled
Large Deflection	Off
Inertia Relief	Off
Restart Controls	
Generate Restart Points	Program Controlled
Retain Files After Full Solve	No
Nonlinear Controls	
Force Convergence	Program Controlled
Moment Convergence	Program Controlled
Displacement Convergence	Program Controlled
Rotation Convergence	Program Controlled
Line Search	Program Controlled
Stabilization	Off
Output Controls	
Stress	Yes
Strain	Yes
Nodal Forces	No
Contact Miscellaneous	No

General Miscellaneous	No
Calculate Results At	All Time Points
Max Number of Result Sets	Program Controlled
Analysis Data Management	
Solver Files Directory	J:\Taylor\beamanalysis_files\dp0\SYS\MECH\
Future Analysis	None
Scratch Solver Files Directory	
Save MAPDL db	No
Delete Unneeded Files	Yes
Nonlinear Solution	No
Solver Units	Active System
Solver Unit System	mks

TABLE 62
Model (A4) > Static Structural (A5) > Loads

Object Name	*Force*	*Force 2*	*Fixed Support*	*Fixed Support 2*	*Fixed Support 3*
State	Fully Defined				
Scope					
Scoping Method	Geometry Selection				
Geometry	1 Face				
Definition					
Type	Force		Fixed Support		
Define By	Vector				
Magnitude	7800. N (ramped)				
Direction	Defined				
Suppressed	No				

FIGURE 1
Model (A4) > Static Structural (A5) > Force

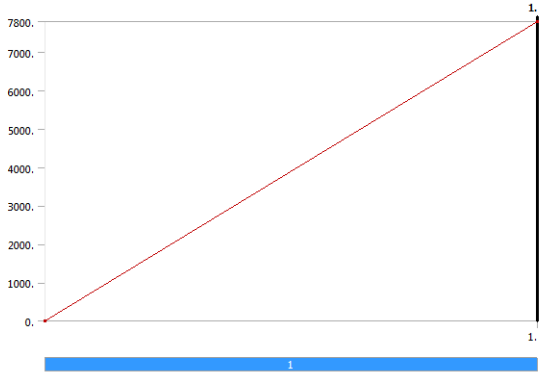

FIGURE 2
Model (A4) > Static Structural (A5) > Force 2

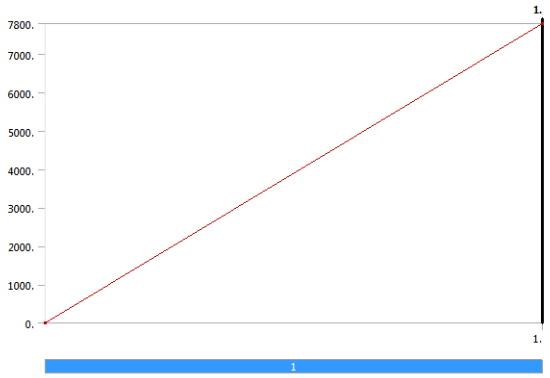

TABLE 63
Model (A4) > Static Structural (A5) > Loads

Object Name	*Fixed Support 4*
State	Fully Defined
Scope	
Scoping Method	Geometry Selection
Geometry	1 Face
Definition	
Type	Fixed Support
Suppressed	No

Solution (A6)

TABLE 64
Model (A4) > Static Structural (A5) > Solution

Object Name	*Solution (A6)*
State	Solved
Adaptive Mesh Refinement	
Max Refinement Loops	1.
Refinement Depth	2.
Information	
Status	Done

TABLE 65
Model (A4) > Static Structural (A5) > Solution (A6) > Solution Information

Object Name	*Solution Information*
State	Solved
Solution Information	
Solution Output	Solver Output
Newton-Raphson Residuals	0
Update Interval	2.5 s
Display Points	All
FE Connection Visibility	
Activate Visibility	Yes

Display	All FE Connectors
Draw Connections Attached To	All Nodes
Line Color	Connection Type
Visible on Results	No
Line Thickness	Single
Display Type	Lines

TABLE 66
Model (A4) > Static Structural (A5) > Solution (A6) > Results

Object Name	*Equivalent Stress*	*Total Deformation*	*Equivalent Elastic Strain*
State	Solved		
Scope			
Scoping Method	Geometry Selection		
Geometry	All Bodies		
Definition			
Type	Equivalent (von-Mises) Stress	Total Deformation	Equivalent Elastic Strain
By	Time		
Display Time	Last		
Calculate Time History	Yes		
Identifier			
Suppressed	No		
Integration Point Results			
Display Option	Averaged		Averaged
Results			
Minimum	8687.6 Pa	0. m	4.7486e-007 m/m
Maximum	3.6835e+008 Pa	0.12451 m	1.941e-003 m/m
Minimum Occurs On	W12x14_divider	basesupportrevised	W12x14_divider
Maximum Occurs On	lower flangenoholes	pole	lower flangenoholes
Information			
Time	1. s		
Load Step	1		
Substep	1		
Iteration Number	1		

TABLE 67
Model (A4) > Static Structural (A5) > Solution (A6) > Stress Safety Tools

Object Name	*Stress Tool*
State	Solved
Definition	
Theory	Max Equivalent Stress
Stress Limit Type	Tensile Yield Per Material

TABLE 68
Model (A4) > Static Structural (A5) > Solution (A6) > Stress Tool > Results

Object Name	*Safety Factor*
State	Solved
Scope	
Scoping Method	Geometry Selection

Geometry	All Bodies
Definition	
Type	Safety Factor
By	Time
Display Time	Last
Calculate Time History	Yes
Identifier	
Suppressed	No
Integration Point Results	
Display Option	Averaged
Results	
Minimum	0.6787
Minimum Occurs On	lower flangenoholes
Information	
Time	1. s
Load Step	1
Substep	1
Iteration Number	1

THIS PAGE INTENTIONALLY LEFT BLANK

APPENDIX P: ENGINEERING DRAWINGS

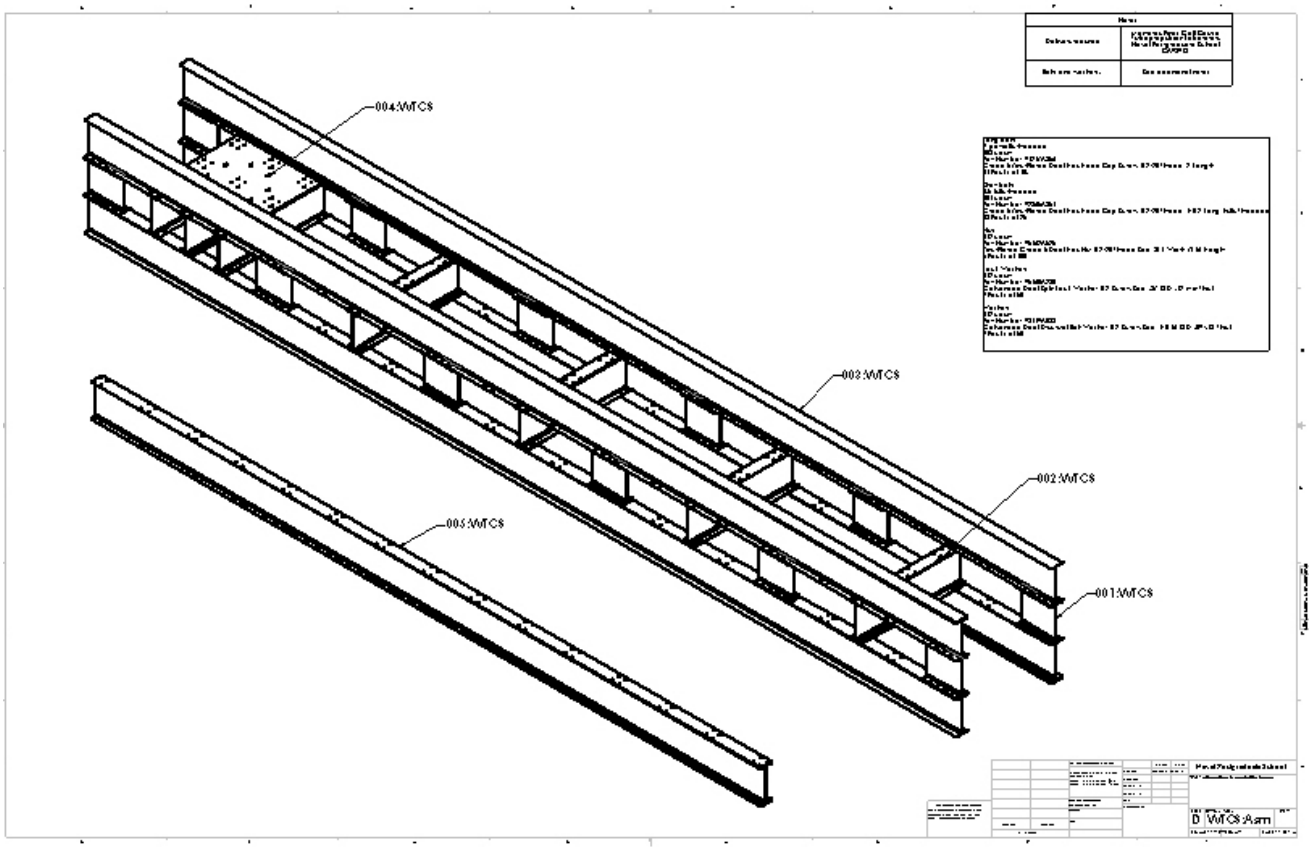

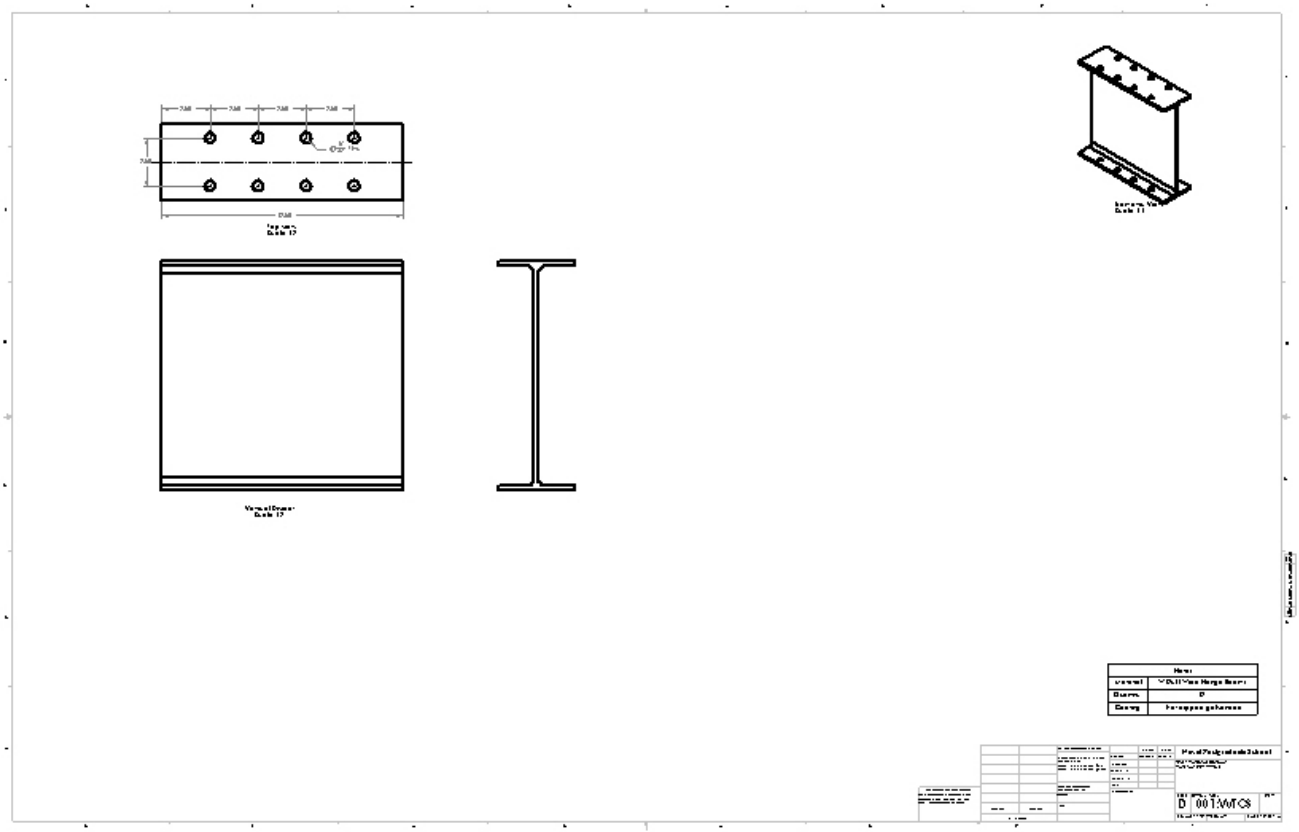

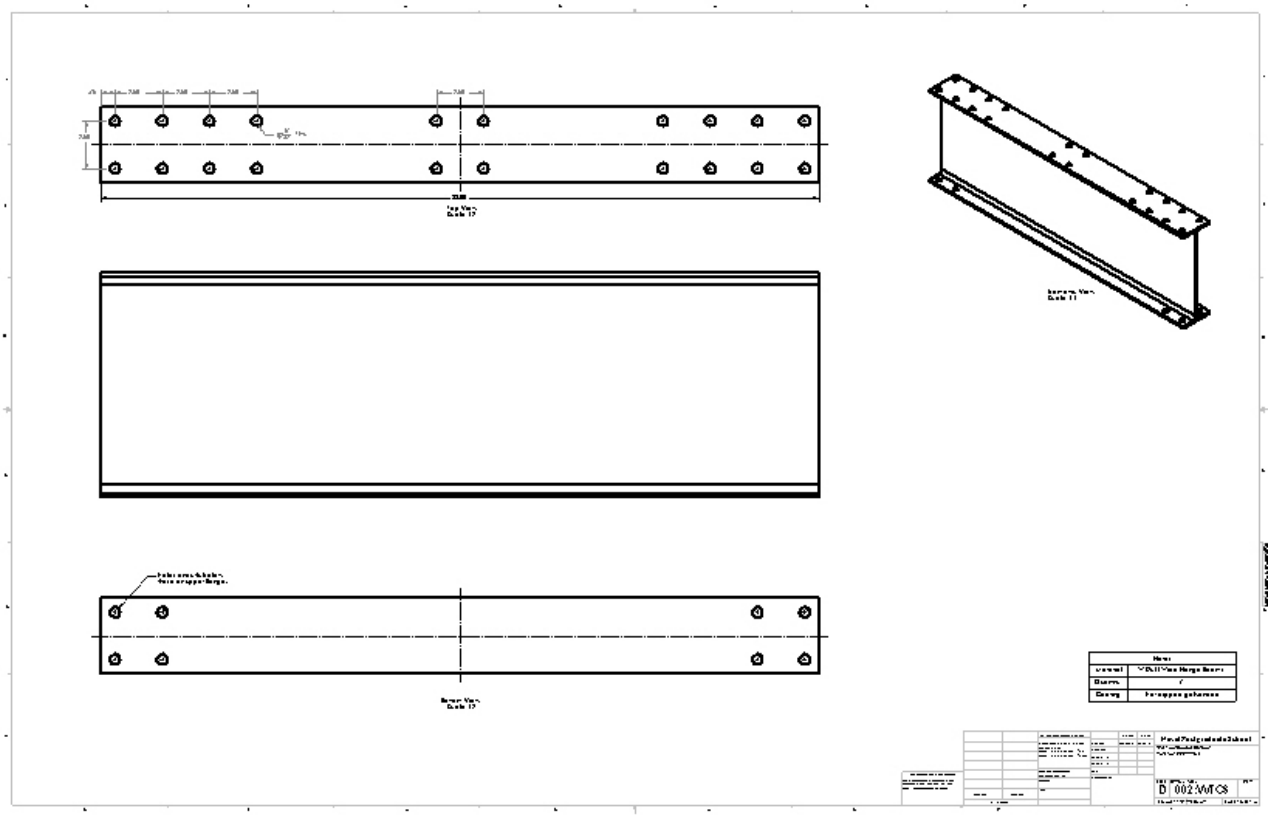

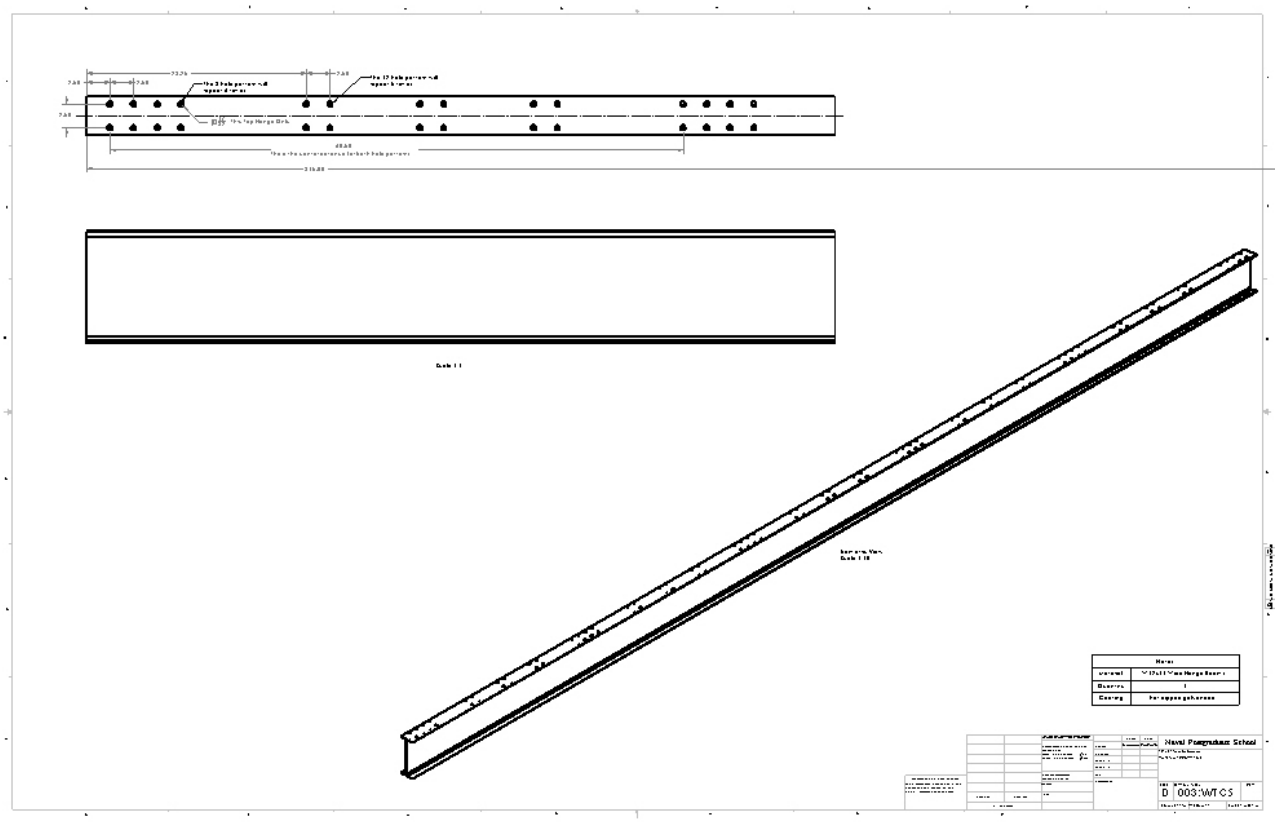

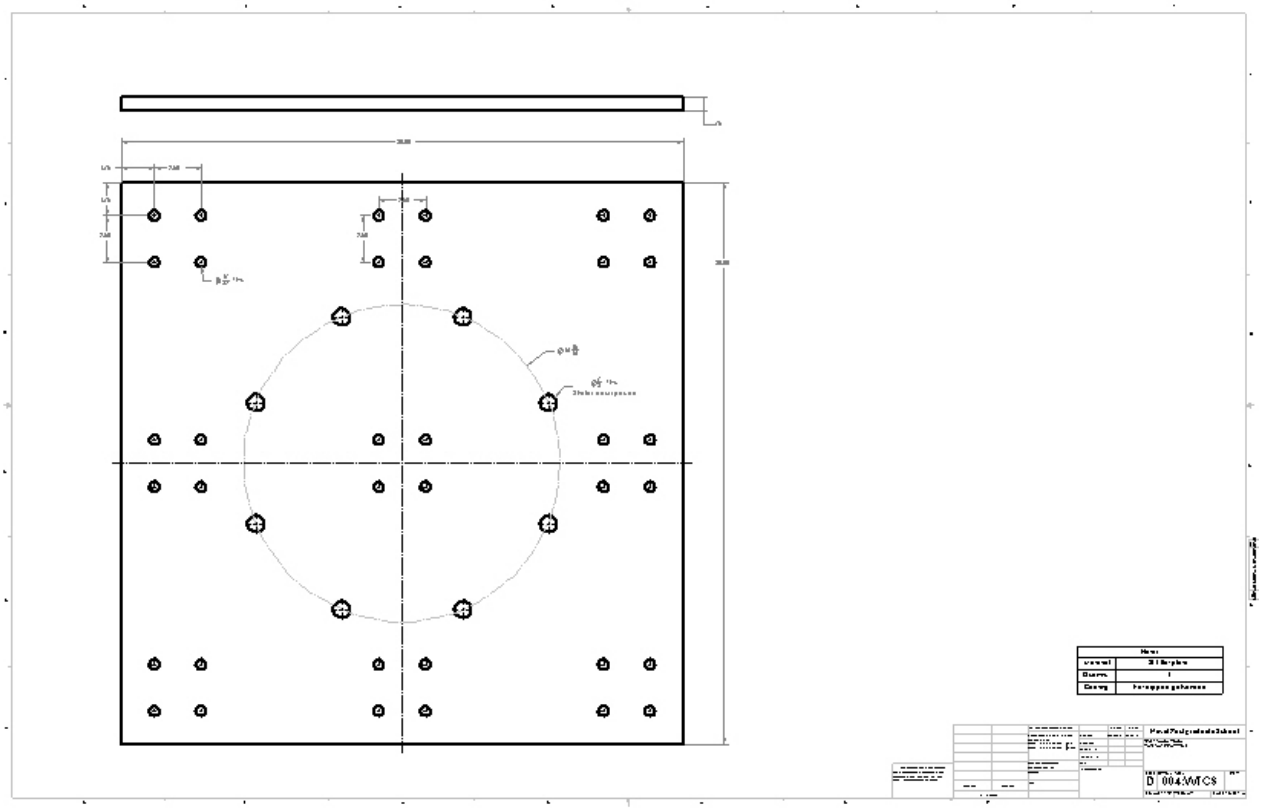

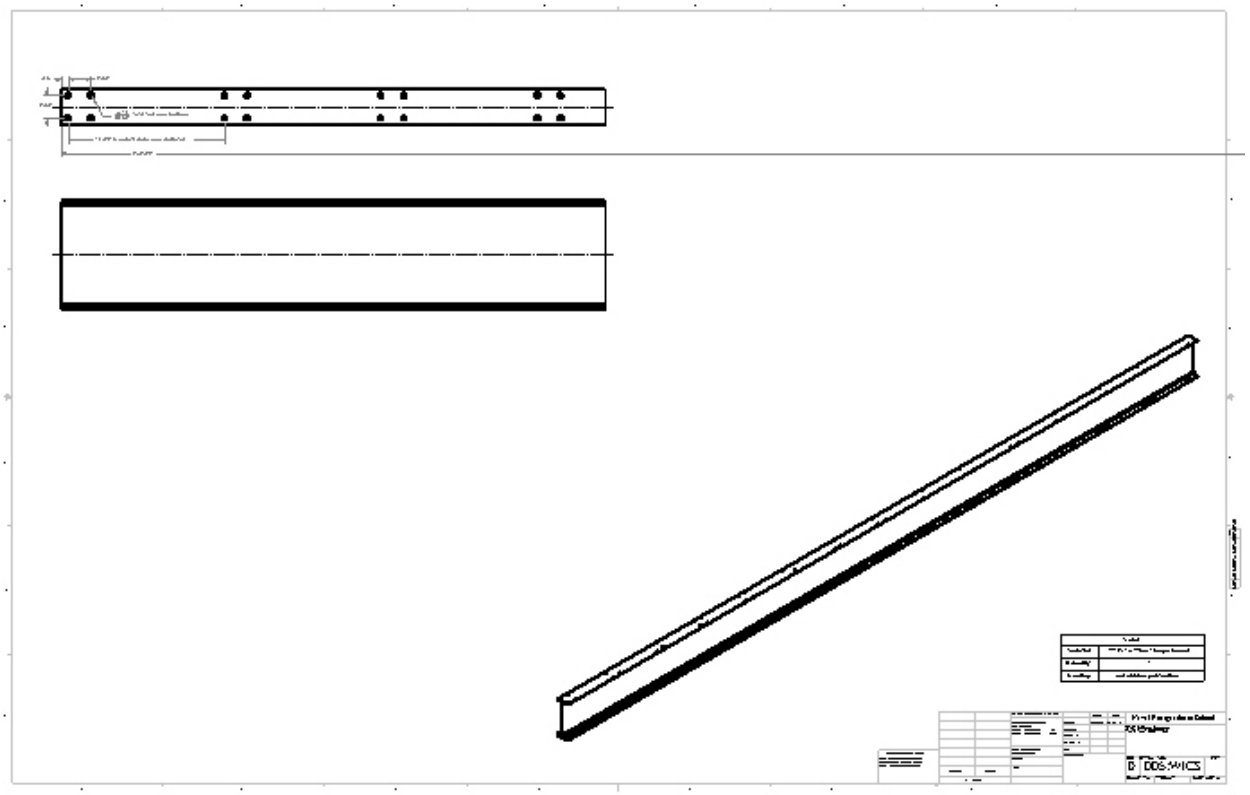

LIST OF REFERENCES

[1] America's Navy. (2010, Jan. 21) "USDA, Navy Sign Agreement to Encourage the Development, Use of Renewable Energy." [Online] Available: http://www.navy.mil/submit/display.asp?story_id=50710

[2] L.E. Chaar, "Wind energy technology-industrial update," presented at *Power and Energy Society General Meeting, 2011 IEEE*, San Diego, CA, 2011, pp.1, 5.

[3] "Wind turbines." [Online] Available: http://commons.wikimedia.org/w/index.php?title=Special:Search&limit=20&offset=20&redirs=0&profile=default&search=wind+turbine

[4] D.MacPhee, "Recent advances in rotor design of vertical axis wind turbines," *Wind Engineering*, vol. 36, no. 6, pp. 647-666, Dec. 2013.

[5] F. Balduzzi, A. Bianchini, E. Carnevale, L Ferrari, S. Magnani, "Feasibility analysis of a Darrieus vertical-axis wind turbine installation in the rooftop of a building," *Applied Energy*, vol.97, pp. 921-929, Dec. 2011.

[6] M. Mukinovic, G. Brenner, A. Rahimi, "Aerodynamic Study of Vertical Axis Wind Turbines," *Lectures Notes in Computational Science and Engineering*, vol. 74, pp. 43-49, 2011.

[7] F Scheurich, R Brown, " Modeling the aerodynamics of vertical-axis wind turbines in unsteady wind conditions," *Wind Energy*, vol.16, pp. 91-107, 2013.

[8] H.C. Davis, "Wind-electric ice making for developing world villages," M.S. thesis, Dept. Mech. Eng., Univ. Colorado, Boulder, CO, 1994.

[9] "Monterey Peninsula Airport in Monterey, CA." [Online] Available: http://www.city-data.com/airports/Monterey-Peninsula-Airport-Monterey-California.html

[10] "Monterey, CA." [Online] Available: https://maps.google.com/

[11] D. Ramsuar, Private communication, *Fleet Numerical Meteorology and Oceanography Center*, 2012.

[12] G. Hobson, Private communication, *Naval Postgraduate School*, 2013.

[13] "NACA 0012 Airfoils." [Online] Available: http://airfoiltools.com/airfoil/details?airfoil=n0012-il

[14] S. Ghatage, J. Joshi, “Optimisation of vertical axis wind turbine: CFD simulations and experimental measurements,” *The Canadian Journal of Chemical Engineering*, pp. 1186-1201, 2012.

[15] F. M. White, *Fluid Mechanics*, 7th ed. New York: McGraw Hill, 2011

[16] “Picture Gallery.” [Online] Available: http://www.urbangreenenergy.com/products/picture-gallery

[17] “UGE 4K Specification Sheet.” [Online] Available: http://www.urbangreenenergy.com/products/uge-4k/downloads

[18] L. Olsen, “An initial investigation of a novel thermal storage concept as part of a renewable energy system,” M.S. Thesis, Dept. Mech. Eng., Naval Postgraduate School, Monterey, CA, 2013.

[19] L. Deshun, L. Rennian, Y. Congxin, W. Xiuyong, X. Wang, “Numerical Simulation in the Wake of a Horizontal Axis Wind Turbine,” *Power and Energy Engineering Conference*, vol., pp. 1,4,25-28, March 2011.

[20] “Picture Gallery.” [Online] Available: http://www.urbangreenenergy.com/products/picture-gallery

[21] “Technical Documentation: Load Specifications for UGE 4k.” [Online] Available: http://www.urbangreenenergy.com/sites/default/files/UGE-4K%20Load%20Specifications.pdf

[22] “I-beam Definitions.” [Online] Available: http://commons.wikimedia.org/w/index.php?title=Special%3ASearch&profile=default&search=i+beam+dimensions&fulltext=Search&uselang=en

[23] “Hurricane Categories.” [Online] Available: http://geography.about.com/od/lists/a/hurrcategories.htm

[24] C. Wagner, Private communication, *Turbopropulsion Laboratory intern*, 2013.

INITIAL DISTRIBUTION LIST

1. Defense Technical Information Center
   Ft. Belvoir, Virginia

2. Dudley Knox Library
   Naval Postgraduate School
   Monterey, California